Electronic Supplementary Information for

Synthesis of covalent organic frameworks using sustinable solvents and machine learning

Sushil Kumar, Gergo Ignacz and Gyorgy Szekely*

Advanced Membranes and Porous Materials Center, Physical Science and Engineering Division (PSE), King Abdullah University of Science and Technology (KAUST), Thuwal 23955-6900, Saudi Arabia. E-mail: *gyorgy.szekely@kaust.edu.sa; www.szekelygroup.com; Tel: +966128082769

Table of Contents

Section S1: Materials, Methods, and Instrumentation

S1.1. Materials

The precursor material 1,3,5-triformylphloroglucinol (**Tp**)[1] was synthesized using a previously reported literature protocol. All other commercially available diamine reagents, i.e., 1,4-phenylenediamine (**Pa1**), 2,5-dimethylphenylenediamine (**Pa2**), benzidine (**BD**), 4,4'-diamino azobenzene (**Azo**), 2,6-diaminoanthraquinone (**Anq**), 1,3,5-tris(4-aminophenyl)benzene (**Tab**), 1,3,5-tris(4-aminophenyl)triazine (**Tta**), and solvents purchased from Sigma-Aldrich, TCI chemicals, and Fisher Scientific chemical suppliers were used as received. The following green solvents were used: dimethyl carbonate (**DC**), propylene carbonate (**PC**), *γ*-butyrolactone (**GBL**), 1,2-ethylenesulfite (**ES**), 1,3-propylenesulfite (**PS**), Cyrene (**Cyr)**, isosorbide dimethyl ether (**IDE**), 2,5-dimethylfuran (**DF**), 2-methyl-1-propanol (**MP**), Terpineol (**Tn**), *para*-Cymene (**Cym**), and Rhodiasolv polar clean (**PCl**). The reactions were performed in an oven-dried glassware under ambient atmosphere.

S1.2. General instrumentation and methods

Powder X-ray diffraction (PXRD) data were collected using Bruker D8 ADVANCE with a high-intensity microfocus rotating anode X-ray generator. All the COFs were recorded in the 2θ range between 5–40°, and the data were collected using the Diffrac Plus XRD commander software. The radiation used was Cu Kα (α = 1.54 Å) with a Ni filter, and the data collection was performed using a Quartz holder at a scan speed of 1° min^{-1} and a step size of 0.01°.

Fourier-transform infrared (FTIR) spectra were obtained using a ThermoScientific Nicolet iS10 spectrometer with a universal Zn-Se attenuated total reflection accessory. FTIR spectroscopic data were reported on a wavenumber (cm^{-1}) scale.

Thermogravimetric analyses (TGA) were performed on a TGA 209 F1 analyzer (Netzsch) under N_2 atmosphere at a heating rate of 10 ºC min^{-1} within a temperature range of 30−900 °C. Prior to the measurement, the samples were dried under high vacuum for 12 h and then activated by heating at 100 ºC for ~1 h.

Solid-state ^{13}C cross-polarization magic angle Spinning (CP-MAS) NMR were measured on a Bruker Avance III 400 MHz widebore instrument.

SEM measurements were performed with a Magellan FEI 400 scanning electron microscope. The samples were prepared simply by casting a drop of COFs dispersed in isopropanol on a clean unit of a silicon wafer.

To avoid charging during the SEM analyses, we coated all the samples with a 3-nm-thick layer of iridium by Q150T S sputter Coater prior to the analyses.

Nitrogen adsorption analyses were performed at 77 K using a liquid nitrogen bath (77 K) on a Micromeritics ASAP 2420 BET instrument. All the samples were degassed for 12 h at 140 °C under vacuum prior to the gas adsorption studies. The surface areas were evaluated using a Brunauer–Emmett–Teller (BET) model applied between P/P_0 values in the range of 0.05–0.3 for COFs. The pore size distributions were calculated using the non-localized density functional theory (NLDFT) method.

S1.3. Method used for calculating yields of the prepared COFs

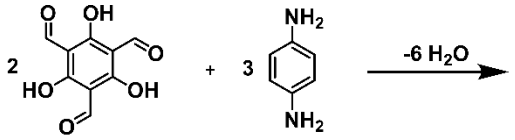

Molecular weight	210.14	108.14	
Weight	(2 x 210.14)	(3 x 108.14)	(420.28 + 324.42) - (6 x 18)
	= 420.28 mg	= 324.42 mg	= 636.70 mg

Theoretical yield:

420.28 mg of aldehyde reacts to give 636.70 mg of TpPa COF

60 mg of aldehyde reacts to give (636.70 / 420.28) × 60 mg of TpPa COF

= 90.89 mg

Experimental yield from 60 mg of aldehyde is 68.02 mg

Yield (wt/wt) = (Experimental yield / Theoretical yield) × 100 %

= (68.02 / 90.89) × 100 %

= 74.83 %

Similar procedure was followed for calculating the yields of other COFs. We tried to scale up the synthesis of the COFs, and on performing the synthesis on a large scale was found to hamper the crystallinity as well as the porosity of the respective COFs.

S1.4. Machine learning algorithms

Molecular descriptors. The used molecular descriptors clustered into categories are depicted in Table S1.

Table S1. List of 2D and 3D molecular descriptors used in this work clustered into categories and subcategories.

Descriptor name	Number of descriptors	Descriptor name	Number of descriptors
2D		2D	
ABCIndex	2	McGowanVolume	1
AcidBase	2	MoeType	53
AdjacencyMatrix	13	MolecularDistanceEdge	19
Aromatic	2	MolecularId	12
AtomCount	16	PathCount	21
Autocorrelation	606	Polarizability	2
BCUT	24	RingCount	138
BalabanJ	1	RotatableBonda	2
BaryszMatrix	104	SLogP	2
BertzCT	1	TopoPSA	2
BondCount	9	TopologicalCharge	21
CarbonTypes	10	TopologicalIndex	4
Chi	56	VdwVolumeABC	1
Constitutional	16	VertexAdjacencyInformation	1
DetourMatrix	14	WalkCount	21
DistanceMatrix	13	Weight	2
EState	316	WienerIndex	2
EccentricConnectivityIndex	1	ZagrebIndex	4
ExtendedTopochemicalAtom	45	*3D*	
FragmentComplexity	1	CPSA	43
Framework	1	GeometricalIndex	4
HydrogenBonda	2	GravitationalIndex	4
InformationContent	42	MoRSE	160
KappaShapeIndex	3	MomentOfInertia	3
Lipinski	2		

PLS regression variable importance list. The list of the variables here are displayed in decreasing importance order, comma separated.

[C1SP2,BCUTdv1l,EState_VSA1,MATS4d,MATS4v,AATSC4d,AATSC4v,GATS4d,ETA_shape_y,PEOE_VSA10,ATSC1s,AATSC1s,PEOE_VSA3,SlogP_VSA10,PEOE_VSA2,MATS4p,AATSC3s,AATSC1are,VSA_EState2,AATSC1pe,AATSC2p,GATS4pe.1,GATS4v,GATS4are.1,AATSC4are.1,GATS3v,

GATS4se.1,MATS4i,MATS4se.1,AATSC0i.1,VSA_EState1,AATSC4i,MATS4c.1,GATS4dv.1,AATSC4se.1,AATS4d,GATS1dv,ATSC1are,JGI1,ATSC3c.1,EState_VSA2,ATSC4d,nBondsKD, MDEN11, AATSC4pe.1,ATSC3Z,ATSC7c,MATS1are,ATSC7se,SdsN.1,VSA_EState3.1,SMR_VSA4.1,PEOE_VSA4.1,NdsN.1,PEOE_VSA9.1,GATS4s.1,BCUTi1h.1,Xch7d,ATSC3m,GATS4c.1,EState_VSA7,AATSC0d,BCUTc1l,AATSC2v,EState_VSA9,ATSC7are,PEOE_VSA8,ATSC5i,BIC4.1,BIC5.1,BIC3.1,MATS4are.1,MATS2p,MATS2v,ETA_beta_ns,AATSC2m,AETA_dBeta,GATS4s,SIC2,SIC4.1,SIC5.1,SIC3.1,GATS2se.1,AATSC2Z,ATSC7pe,AATSC3m,ATSC2are.1,ATSC2pe.1,NdssC,NsssCH,SdO,AATSC3Z,EState_VSA3,MATS1se.1,GATS2c.1,AATS2se.1,ATSC4v.1,JGT10,TopoShapeIndex.1,AATS2are.1,NdO, GATS4i.1,AATS3Z,BIC2,ATSC1are.1,ATSC1pe.1,AATS3se.1,PetitjeanIndex.1,GATS4v.1,AATS3are.1,AETA_beta_ns,AATSC4p,ATSC3i.1,GATS2s.1,AATSC3d,ZMIC5,AATS1pe.1,ATSC4se.1,MATS1are.1,GATS1are,BCUTp1l.1,ETA_dBeta,ZMIC4,SIC2.1,ATSC5d,ATSC2i.1,MATS3v,ATSC4are.1,ATSC1se.1,AATSC2i,AATS2pe.1,CIC2,GATS4p.1,BCUTdv1h.1,CIC5.1,CIC4.1,CIC3.1,SIC3,ZMIC2,AATS2m,AATSC3v,MATS4s.1,ZMIC3,AATS4se.1,AATSC4c.1,AATS3pe.1,AATS1are.1,GATS4p,AATS2Z, MATS4pe.1,AETA_eta_BR,AATS4m,AATSC4s.1,GATS4i,BIC2.1,AATS3p,MID_h.1,AATS4Z,nBondsD.1,AATS3v,MATS1pe.1,JGI7.1,GATS1se.1,AATSC1dv.1,AATSC1v.1,MATS1s,AATS2se,AATS4are.1,nHBDon,NsOH,VSA_EState3,SsOH,ATSC5p,CIC3,Xch6dv,GATS1are.1,MATS2i,ETA_dPsi_B,IC0.1,ATSC1pe,GGI3,Mare.1,AMID_h.1,JGI10.1,BCUTc1l.1,ETA_dEpsilon_C.1,MATS1pe,AATS0are.1,BCUTpe1h.1,ATSC3se.1,ETA_dEpsilon_A.1,ATSC4p.1,EState_VSA4.1,SMR_VSA9.1,SlogP_VSA8.1,G

ATS1se,Xpc-6d]

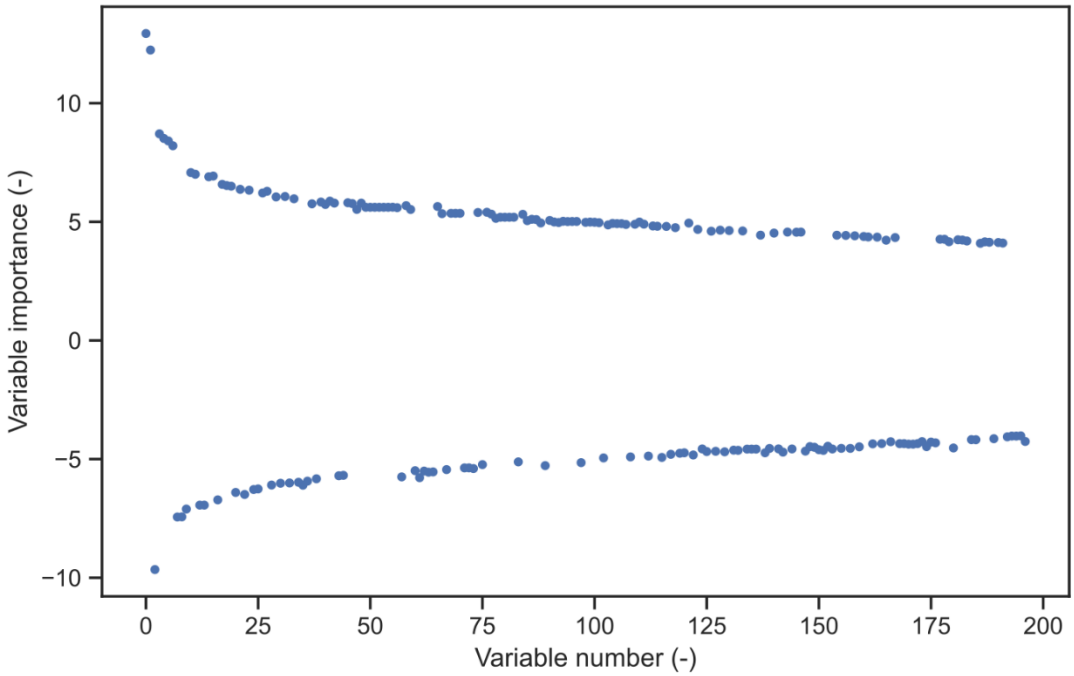

Figure S1. Variable importance score with respect to variable number. The variable scores are in absolute decreasing order.

PLS regression. The PLS regressor data are detailed in Table S2. The PLS linear regressor does not have a range limit, indicating that the model can predict negative surface area values that are undefined. Therefore, the datasets were preprocessed where three negative results were set to zero.

Table S2. Results of the PLS regression analysis for Figure 4a). The raw data were generated from PLS_Toolbox and displayed after the negative results were set to zero.

Cal/Test Samples	Scores on LV 1 (39.86%)	Scores on LV 2 (11.24%)	Scores on LV 3 (12.73%)	Q Residuals (36.17%)	Hotelling T^2 (63.83%)	Q Residuals Reduced (p=0.950) (36.17%)	Hotelling T^2 Reduced (p=0.950) (63.83%)	KNN Score Distance (k=3)	Y Measured 1 BET	Y Predicted 1 BET	Y Residual 1 BET	Y Stdnt Residual 1 BET	Y Error Est. 1 BET
Calibration	-1.3584	1.4861	-2.1753	132.5893	0.2226	0.4879	0.0233	0.1775	473	459.6051	-13.3949	-0.1058	162.4284
Calibration	0.0138	6.7482	3.5497	169.0784	1.8266	0.6222	0.1915	0.2947	888	755.7740	-132.2260	-1.0743	166.8265
Calibration	-2.8368	-1.6071	-6.2387	158.4677	1.2639	0.5832	0.1325	0.2008	113	254.0642	141.0642	1.1344	165.2970
Calibration	-1.3397	1.1467	-1.2685	128.3352	0.1045	0.4723	0.0110	0.1570	518	459.9560	-58.0440	-0.4573	162.0998
Calibration	-2.7687	-4.7270	-7.3399	73.8280	2.3230	0.2717	0.2435	0.1320	207	136.7988	-70.2012	-0.5757	168.1644
Calibration	-2.5575	-5.0142	-6.2550	85.7978	1.9833	0.3157	0.2079	0.1616	197	147.6633	-49.3367	-0.4020	167.2499
Calibration	-2.9513	-4.8152	-8.1737	78.3533	2.7277	0.2883	0.2860	0.1618	163	117.2760	-45.7240	-0.3778	169.2473
Calibration	-1.1514	0.8552	0.7958	172.9141	0.0536	0.6363	0.0056	0.2385	480	482.0306	2.0306	0.0160	161.9581
Calibration	-2.1808	10.6069	7.8570	67.0201	5.4267	0.2466	0.5689	0.5061	1046	865.7019	-180.2981	-1.5728	176.2992
Calibration	-4.9634	-0.8683	-3.0326	104.2640	0.5099	0.3837	0.0535	0.2246	36	246.7267	210.7267	1.6721	163.2249
Calibration	-3.3460	4.7139	5.1031	127.9883	1.5591	0.4710	0.1634	0.2502	718	591.9584	-126.0416	-1.0191	166.1012
Calibration	16.1813	5.9227	-5.2131	222.6045	4.2844	0.8192	0.4492	0.3224	399	1167.7203	768.7203	6.0458	173.3496
Calibration	17.0883	8.7248	-2.3944	61.9828	5.2717	0.2281	0.5527	0.5911	1562	1328.5626	-233.4374	-1.8359	175.9018
Calibration	18.4605	13.9869	3.3305	32.9259	9.7205	0.1212	1.0190	1.0000	1674	1624.7315	-49.2685	-0.4752	186.9703
Calibration	15.6780	2.5117	-7.5590	74.7468	4.0637	0.2751	0.4260	0.0733	885	1005.7562	120.7562	1.0242	172.7740
Calibration	15.8892	2.2245	-6.4741	83.0347	3.6473	0.3056	0.3824	0.1123	1065	1016.6208	-48.3792	-0.4069	171.6825
Calibration	15.4954	2.4235	-8.3929	84.4881	4.3764	0.3109	0.4588	0.0926	879	986.2335	107.2335	0.9153	173.5891
Calibration	15.4395	1.5630	-7.8691	83.6512	4.0078	0.3078	0.4201	0.0892	1118	961.6119	-156.3881	-1.3249	172.6277
Calibration	17.2953	8.0939	0.5767	103.2687	4.8407	0.3800	0.5075	0.6373	1077	1350.9880	273.9880	2.1549	174.7922
Calibration	15.9854	-7.5040	10.8742	43.0808	7.5030	0.1585	0.7866	0.6668	785	904.5844	119.5844	1.0924	181.5377
Calibration	14.7864	-14.0043	6.7945	20.8792	9.6236	0.0768	1.0089	0.8778	573	592.6426	19.6426	0.1890	186.7363
Calibration	16.1924	-8.1349	13.8453	31.7404	9.9714	0.1168	1.0453	0.7570	1000	927.0099	-72.9901	-0.7087	187.5753
Calibration	-9.7452	2.9941	4.8307	57.7382	1.8164	0.2125	0.1904	0.1540	102	313.0645	211.0645	1.7145	166.7988
Calibration	-8.3730	8.2562	10.5557	53.5798	6.0053	0.1972	0.6296	0.4817	288	609.2334	321.2334	2.5264	177.7743

Calibration	-11.2236	-0.0991	0.7673	117.6257	1.1622	0.4329	0.1218	0.2025	144	107.5236	-36.4764	-0.2928	165.0191
Calibration	-10.9230	-0.1208	2.0331	78.0155	1.2027	0.2871	0.1261	0.2146	217	132.6737	-84.3263	-0.6774	165.1298
Calibration	-9.7265	2.6547	5.7376	64.6345	2.0240	0.2379	0.2122	0.1817	166	313.4154	147.4154	1.2021	167.3597
Calibration	-11.1555	-3.2190	-0.3339	88.5808	1.4685	0.3260	0.1540	0.0733	190	-9.7418	-199.7418	-1.6123	165.8548
Calibration	-10.9443	-3.5062	0.7510	99.6226	1.5012	0.3666	0.1574	0.1123	42	1.1227	-40.8773	-0.3301	165.9438
Calibration	-10.2180	3.1508	3.5163	113.3661	1.6210	0.4172	0.1699	0.1797	84	286.0512	202.0512	1.6355	166.2693
Calibration	-11.3381	-3.3072	-1.1677	95.2282	1.5600	0.3504	0.1635	0.0926	63	-29.2646	-92.2646	-0.7460	166.1037
Calibration	-11.3940	-4.1677	-0.6439	95.6538	1.7520	0.3520	0.1837	0.0892	30	-53.8862	-83.8862	-0.6806	166.6245
Calibration	-9.5382	2.3632	7.8018	103.8945	2.7391	0.3823	0.2871	0.2294	1036	335.4900	-700.5100	-5.5094	169.2776
Calibration	-2.2654	-1.3160	-4.9940	252.3012	0.8121	0.9285	0.0851	0.1924	247	298.7629	51.7629	0.4129	164.0585
Calibration	-3.5530	5.3448	2.1321	79.2616	1.1650	0.2917	0.1221	0.2547	363	569.5330	206.5330	1.6580	165.0267
Test	-3.0072	-5.6757	-7.6500	70.2598	2.7859	0.2586	0.2921	0.0892	197	92.6544	-104.3456	-0.8207	169.4025
Test	-5.1459	-0.9565	-3.8664	110.4748	0.6956	0.4066	0.0729	0.1363	69	227.2039	158.2039	1.2442	163.7376
Test	16.6155	8.8815	-3.7088	120.8398	5.4441	0.4447	0.5707	0.5728	1418	1301.5493	-116.4507	-0.9159	176.3435
Test	-2.5362	-1.6288	-4.9730	114.2438	0.8477	0.4204	0.0889	0.1001	109	279.2143	170.2143	1.3387	164.1564
Test	-1.8312	1.6428	-3.4897	179.0258	0.4640	0.6588	0.0486	0.1660	354	432.5918	78.5918	0.6181	163.0978
Test	14.5751	-13.7172	5.7096	45.4442	8.9246	0.1672	0.9356	0.4741	717	581.7781	-135.2219	-1.0635	185.0389
Test	14.3366	-14.6659	5.3996	43.5500	9.6320	0.1603	1.0098	0.5301	1033	537.6337	-495.3663	-3.8959	186.7566
Test	-10.6522	0.1920	2.0121	202.7396	1.1479	0.7461	0.1203	0.1250	77	152.2223	75.2223	0.5916	164.9799

Binary classification machine learning algorithms

The algorithms were run as a python script using scikit-learn and matplotlib packages.[2,3] The Y-scrambling contained 200 iterations per algorithm, and the average accuracy score was noted.

Accuracy. The set of labels predicted for a sample x_i must *exactly* match the corresponding y_i. $accuracy = \frac{number\ of\ correct\ predictions}{total\ number\ of\ predictions}$

K-nearest neighbor (KNN)[4] is a non-parametric classification method based on the closest training examples in the dataset. In our case, the output is a class of 0 or 1 corresponding to the non-crystalline and crystalline COFs, respectively. Parameters: n_neighbors = 5; all other parameters were retained as default values.

Support vector machines (SVM)[5] are statistical machine learning frameworks, and in our case, belonging to the non-probabilistic binary classification methods. SVM optimizes and finds the best hyperplane with the largest distance across the training examples. This hyperplane (maximum-margin classifier) is then used to predict the new input data. Parameters of Sigmoid SVM: kernel="sigmoid", C=0.025. Parameters for RBF SVM: kernel= "rbf", gamma=0.02, C=1. Parameters for Poly SVM: kernel= "poly," C=0.04).

Gaussian processes classifier (GPC)[6] is a statistical modeling tool based on the normal distribution.

Decision tree classification (classification tree)[7] is a non-parametric supervised machine learning approach based on decision trees. The model works by learning decision rules inferred from the training data. Parameters: max_depth = 5.

Random forest classification[7] is a decision tree-based ensemble (combination of multiple learning algorithms) machine learning approach. Random forest combines several decision trees, therefore offering deeper learning capabilities; however, it requires a larger dataset and deeper training. Parameters: max_depth = 7, n_estimators = 5, max_features = 2.

Artificial neural network (ANN, neural net)[8] refers to a simple (shallow) neural network used for binary classification based on the multilayer perceptron model (MLP classification). In our case, the ANN learns a function to target y,

$$g(x): R^m \rightarrow R^o \mid X = x_1, x_2, \ldots x_m$$

where m and o are the training and target dimensions, respectively; and x_i is the ith target value. Parameters: alpha=0.01, max_iter=1000, solver='lbfgs'.

Adaptive Boosting algorithm (AdaBoost)[9] is a boosting technique used in ensemble machine learning problems where the weights are re-assigned to each instance having larger weights to incorrectly classified instances. AdaBoost combines multiple weak classifiers (decision stumps) into one classifier method. Parameters left default.

Naïve Bayes method[10] refers to an ensemble supervised machine learning algorithm based on the Bayes' theorem with conditionally independent features. Herein, the naïve Bayes function maps the following equation across the training examples:

$$\hat{y} = arg \underbrace{max}_{y} P(y \prod_{i=1}^{n} P(x_i|y)$$

where y is the class variable, x is the feature vector, and $P(x \mid y)$ is the conditional probability. Parameters were left default.

Quadratic Discriminant Analysis (QDA)[11] The QDA classifier optimizes a quadratic decision boundary on the class conditional densities. QDA is also based on Bayes' theorem. Parameters were left default.

Section S2: Synthetic Procedures

S2.1 Synthesis of 1,3,5-triformylphloroglucinol (Tp). In a two-neck, 1 L, round-bottom flask, hexamethylenetetramine, **HMTA** (25 g, 180 mmol) was added and subjected to high vacuum for 2 h to remove any moisture present in it. Then, 150 mL of trifluoroacetic acid (TFA) on an ice bath was added to dissolve it and stirred for 15 min. Phloroglucinol (10 g, 80 mmol) was slowly added to avoid the formation of lumps. The reaction mixture was then subjected to 110 °C with constant stirring for 3 h. Then, 500 mL of hydrochloric acid (3M) was added and further stirred at the same temperature for 1 h. The reaction mixture was then filtered through a celite pad and allowed to cool to 25 °C. The filtrate was then extracted with dichloromethane. The organic phase was subsequently washed with water, saturated sodium bicarbonate, and brine solution. After drying the organic phase over magnesium sulfate, it was filtered. The solvent was removed under vacuum to give an orange-colored crude solid product. The product was purified by washing with hot ethanol. Yield 2.5 g (15%). ^{1}H NMR (400 MHz, DMSO-d_6) δ 12.29 (s, 3H, -OH), 10.02 (s, 3H, -CHO) ppm. ^{13}C NMR (101 MHz, DMSO-d_6) δ 192.08 (-CHO), 173.50 (>C-OH)), 103.52 (aromatic) ppm. FTIR (ATR, cm^{-1}) 3312 (ν_{OH}), 3200, 1673 ($\nu_{C=O}$), 1606, 1319, 1119, 936.

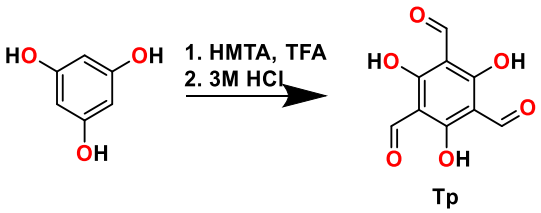

Scheme S1. Synthetic procedure of Tp.

S2.2 General procedure for the synthesis of covalent organic frameworks (COFs). The COFs were synthesized by following the method reported literature.[12] In a typical synthesis, a Pyrex tube (outer diameter × inner diameter = 20 mm × 18 mm, and length 25 cm) is charged with 0.3 mmol of Tp, 0.45 mmol of the corresponding diamine or 0.3 mmol of triamine, 3 mL of green solvent, and 0.2 mL of acetic acid. After sonication for 15 min, the mixture is subjected to three consecutive freeze–pump–thaw cycles under liquid nitrogen (77 K). The Pyrex tube was sealed under vacuum and heated in an oven maintained at 120 °C for 72 h. The resulting solid material was then purified by immersing in hot water followed by solvent exchange or soxhlet extraction method with hot ethanol/isopropanol for several days. Finally, the obtained COFs were dried at 100 °C in a vacuum oven to isolate crystalline porous COFs.

Table S3. Isolated yield (%) of five series of COFs synthesized in green solvents.

COFs	Yield (%)	COFs	Yield (%)	COFs	Yield (%)
TpPa-DC	74	TpBD-Tn	13	TpAnq-PCl	47
TpPa-PC	79	TpBD-PCl	56	TpTab-DC	23
TpPa-GBL	96	TpAzo-DC	69	TpTab-PC	56
TpPa-ES	94	TpAzo-PC	82	TpTab-GBL	67
TpPa-PS	93	TpAzo-GBL	44	TpTab-ES	75
TpPa-Cyr	71	TpAzo-IDE	64	TpTab-PS	73
TpPa-IDE	70	TpAzo-DF	58	TpTab-Cyr	48
TpPa-DF	44	TpAzo-MP	54	TpTab-IDE	80
TpPa-MP	26	TpAzo-Tn	44	TpTab-DF	58
TpPa-Tn	20	TpAzo-Cym	46	TpTab-MP	20
TpPa-Cym	59	TpAzo-PCl	58	TpTab-Tn	89
TpPa-PCl	64	TpAnq-PC	43	TpTab-Cym	53
TpBD-PC	82	TpAnq-IDE	55	TpTab-PCl	68
TpBD-GBL	56	TpAnq-DF	30		
TpBD-IDE	74	TpAnq-Cym	47		

Section S3: NMR characterizations of Tp

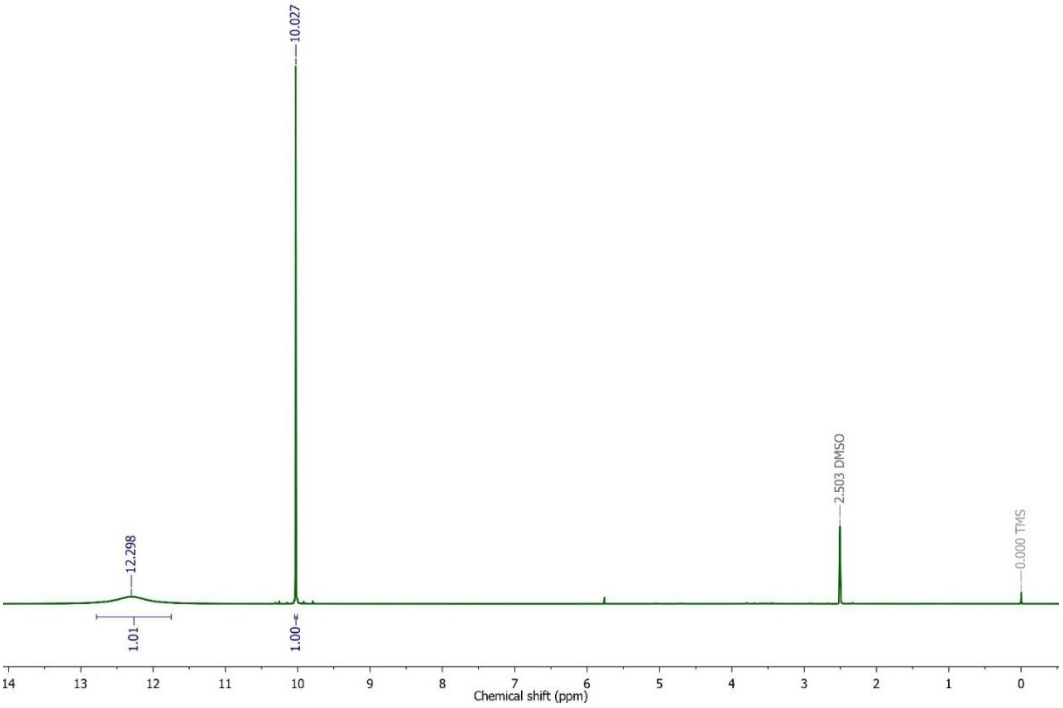

Figure S2. ^{1}H NMR spectrum of Tp recorded in DMSO-d$_6$.

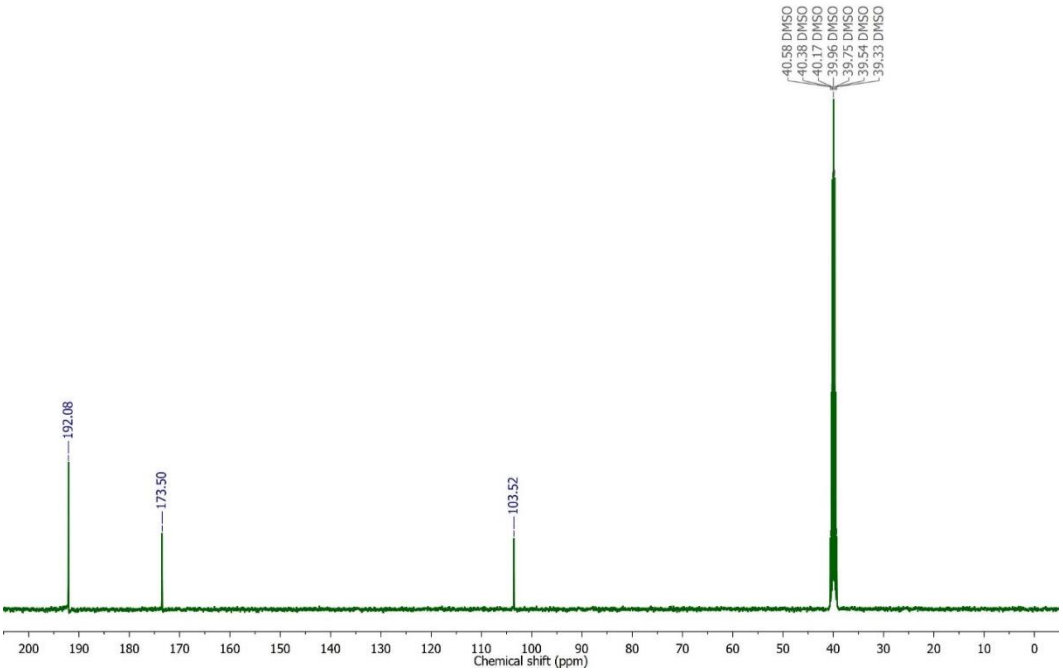

Figure S3. ^{13}C NMR spectrum of Tp recorded in DMSO-d$_6$.

Section S4: PXRD patterns and Scherrer analysis of as-synthesized COFs

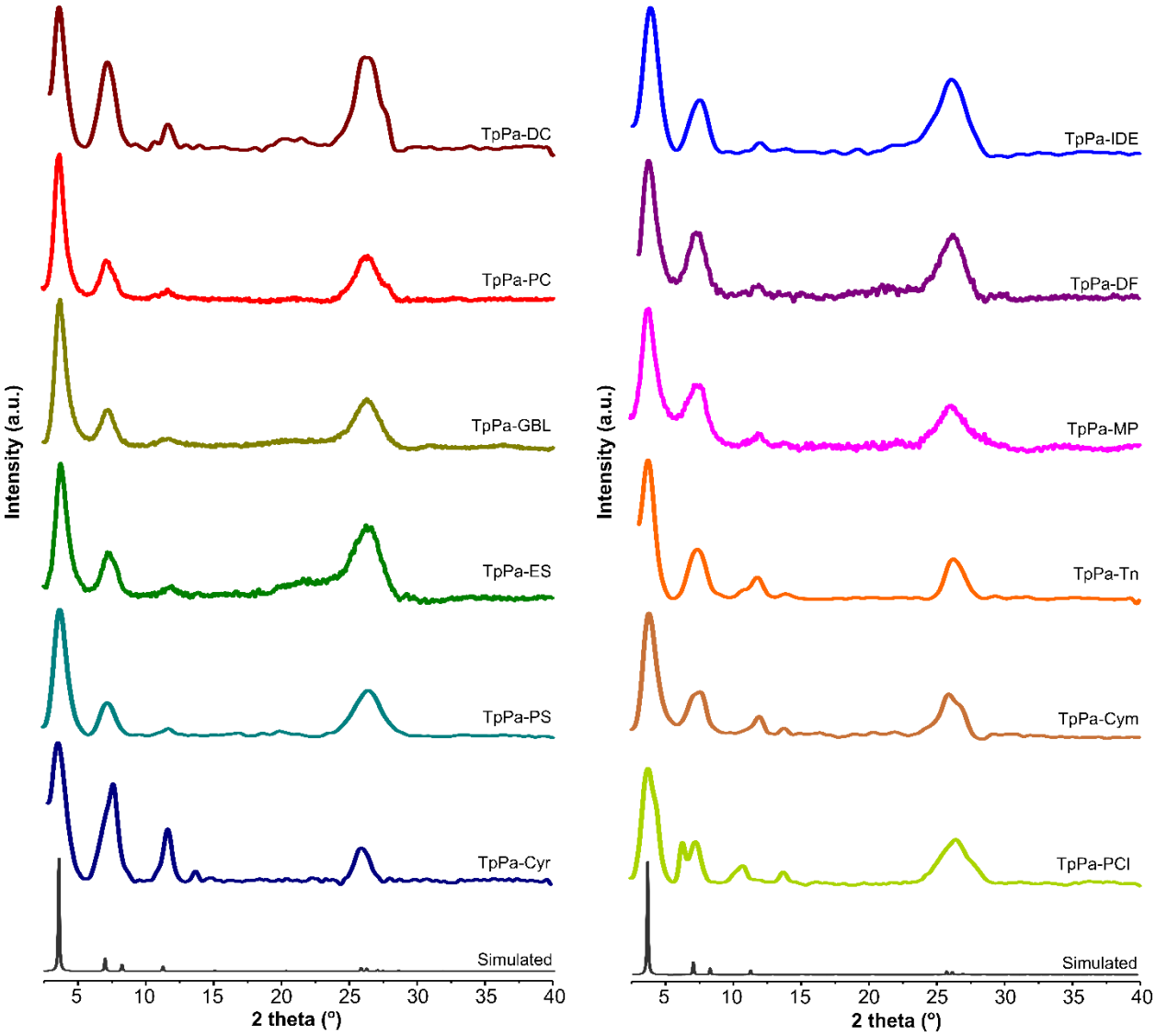

Figure S4. PXRD patterns for as-synthesized TpPa COFs. Twelve green solvents were used to prepare the COFs, which resulted in varying crystallinities of the COFs. Experimental PXRD patterns were compared with the simulated PXRD patterns. The first peak corresponds to the [100] plane, where the peak at 2theta ≈ 27° is assigned to the [001] plane.

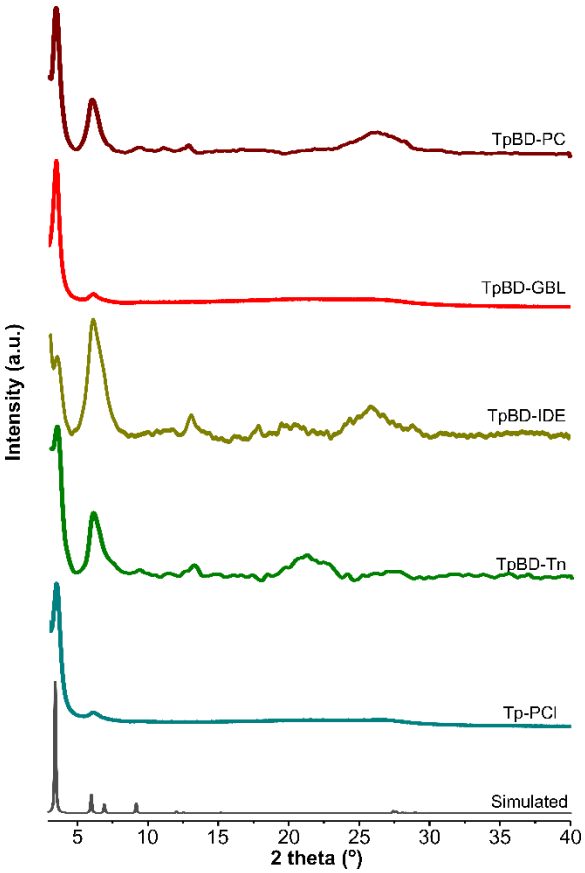

Figure S5. PXRD patterns for as-synthesized TpBD COFs. Twelve green solvents were used to prepare the COFs, which resulted in the varying crystallinities of the COFs. Experimental PXRD patterns were compared with the simulated PXRD patterns. The first peak corresponds to the [100] plane where the peak at 2theta ≈ 27° is assigned to the [001] plane.

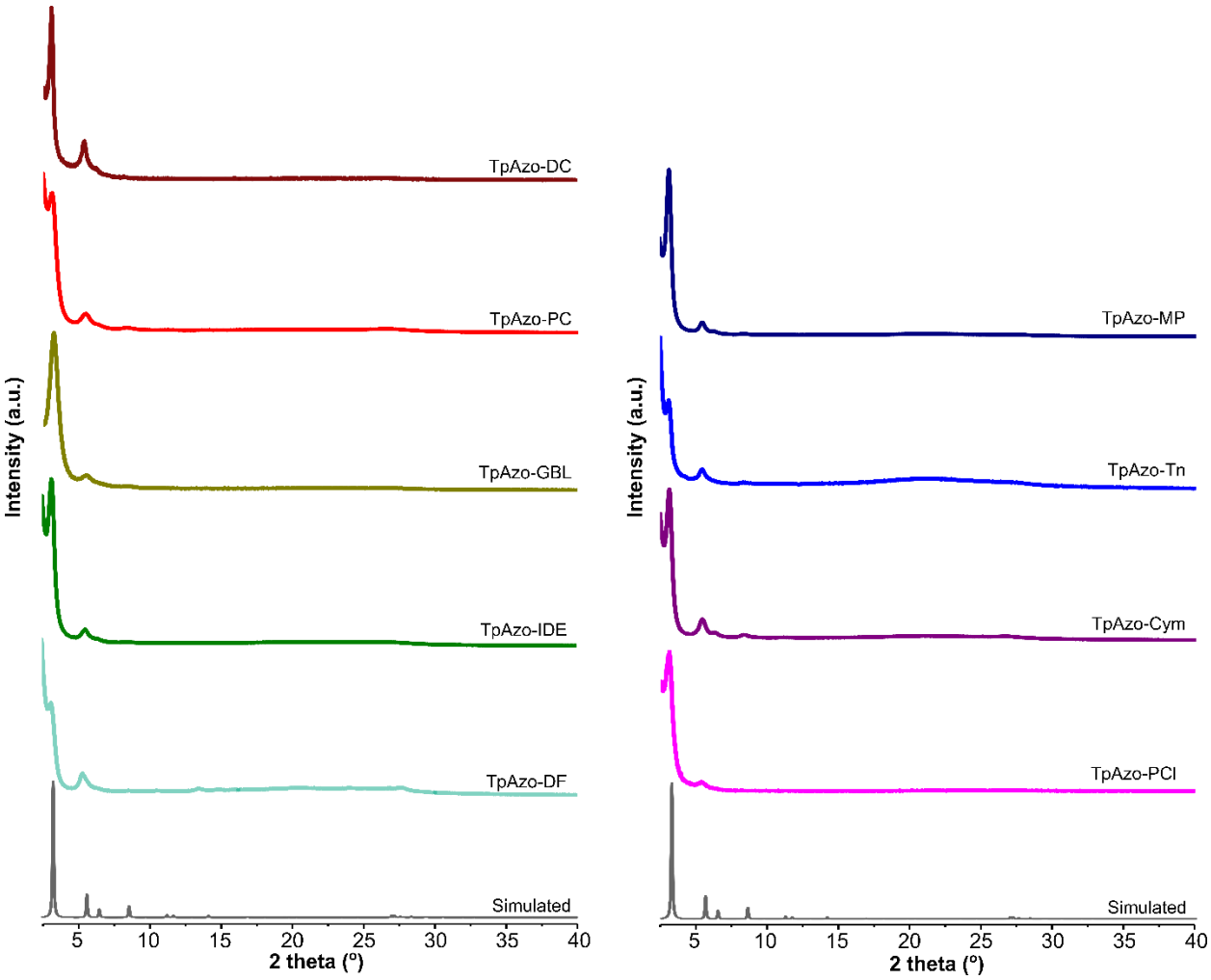

Figure S6. PXRD patterns for as-synthesized TpAzo COFs. Twelve green solvents were used to prepare the COFs, which resulted in the varying crystallinities of the COFs. Experimental PXRD patterns were compared with the simulated PXRD patterns. The first peak corresponds to the [100] plane where the peak at 2theta ≈ 27° is assigned to the [001] plane.

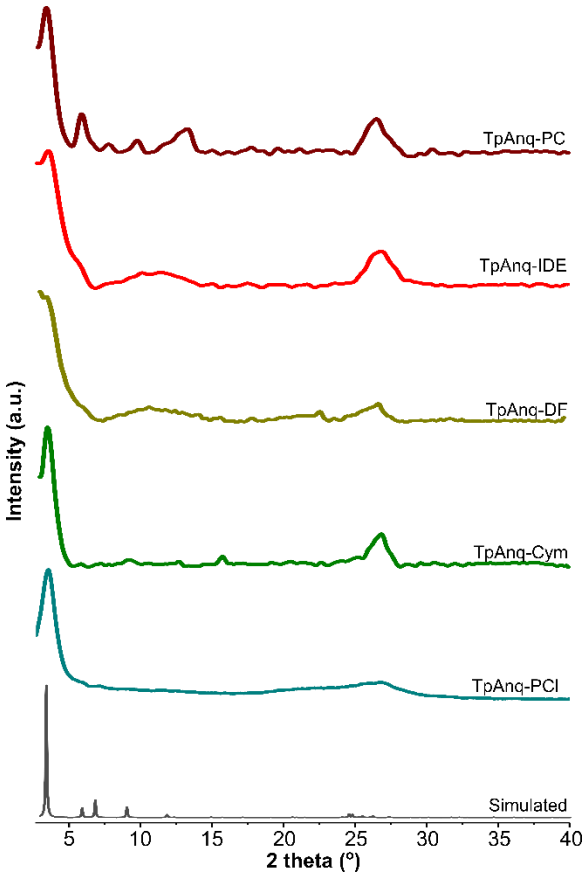

Figure S7. PXRD patterns for as-synthesized TpAnq COFs. Twelve green solvents were used to prepare the COFs, which resulted in the varying crystallinity of the COFs. Experimental PXRD patterns were compared with the simulated PXRD patterns. The first peak corresponds to the [100] plane where the peak at 2theta ≈ 27° is assigned to the [001] plane.

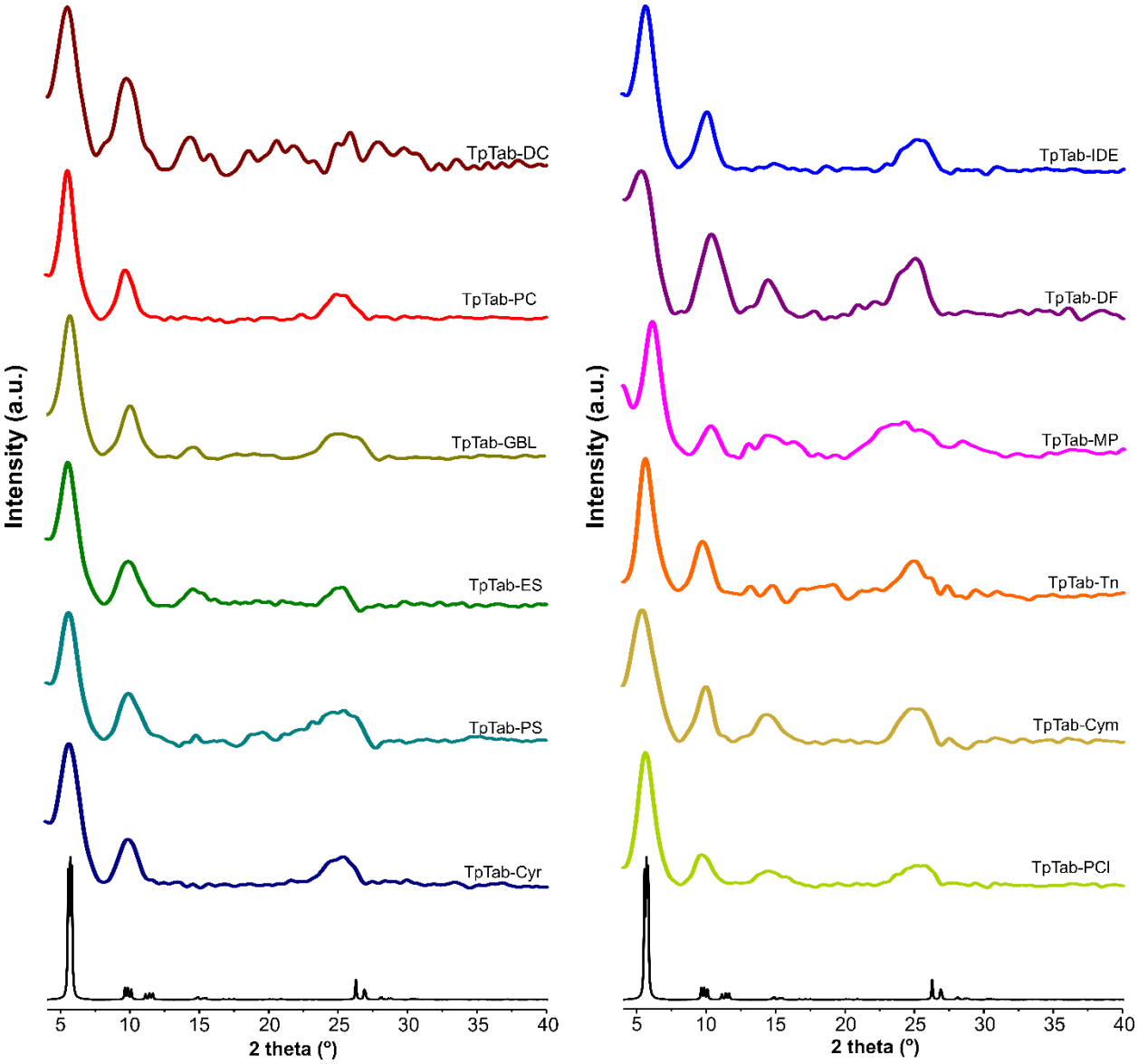

Figure S8. PXRD patterns for as-synthesized TpTab COFs. Twelve green solvents were used to prepare the COFs, which resulted in the varying crystallinities of the COFs. Experimental PXRD patterns were compared with the simulated PXRD patterns. The first peak corresponds to the [100] plane where the peak at 2theta ≈ 27° is assigned to the [001] plane.

In the PXRD patterns, the first diffraction peak corresponding to the [100] plane has been selected to determine the crystallinity of the as-synthesized COFs (Table S3). For example, in case of **TpPa**, the intensity count in its PXRD pattern varies with a green solvent employed. An intensity count of 3786 clearly indicates that **TpPa-Tn** (synthesized in terpineol solvent) has the highest crystallinity, whereas **TpPa-DC** (synthesized in dimethyl carbonate) with a value of 1500 has the least crystallinity.

Table S4. PXRD peak intensity count for [100] plane of all the as-synthesized COFs in different green solvents.

COFs	Peak intensity (a.u.)	COFs	Peak intensity (a.u.)	COFs	Peak intensity (a.u.)	COF	Peak intensity (a.u.)	COFs	Peak intensity (a.u.)
TpPa-DC	1500	-	-	TpAzo-DC	5529	-	-	TpTab-DC	634
TpPa-PC	2700	TpBD-PC	2502	TpAzo-PC	127692	TpAnq-PC	2233	TpTab-PC	3434
TpPa-GBL	3441	TpBD-GBL	51177	TpAzo-GBL	15657	-	-	TpTab-GBL	3992
TpPa-ES	1749	-	-	-	-	-	-	TpTab-ES	2106
TpPa-PS	2485	-	-	-	-	-	-	TpTab-PS	2530
TpPa-Cyr	3024	-	-	-	-	-	-	TpTab-Cyr	3054
TpPa-IDE	3384	TpBD-IDE	2528	TpAzo-IDE	112813	TpAnq-IDE	4708	TpTab-IDE	3562
TpPa-DF	2218	-	-	TpAzo-DF	36168	TpAnq-DF	4882	TpTab-DF	1144
TpPa-MP	2914	-	-	TpAzo-MP	375039	-	-	TpTab-MP	1652
TpPa-Tn	3786	TpBD-Tn	2708	TpAzo-Tn	19500	-	-	TpTab-Tn	936
TpPa-Cym	1751	-	-	TpAzo-Cym	88024	TpAnq-Cym	4538	TpTab-Cym	1464
TpPa-PCl	3367	TpBD-PCl	71760	TpAzo-PCl	4435	TpAnq-PCl	837	TpTab-PCl	2248

The domain size of the COF crystallites in the form of powder were calculated using Scherrer equation. This equation is generally used to correlate the size of crystallites in a solid to the broadening of the peak in the PXRD pattern. The calculation of integral breadth (β) was performed through Gaussian fitting of the high-intensity first peak that corresponds to the [100] plane. According to our findings, the size of the COF crystallites varies when the synthesis is performed using different green solvents.

The Scherrer equation can be written as:

$$\tau = \frac{K\lambda}{\beta cos\theta} \qquad \text{(eq. 1)}$$

where

τ is the size of the ordered (crystalline) domains, and K is a dimensionless shape factor with a value close to the unity. The shape factor varies with the actual shape of the crystallite. Herein we considered the shape factor value 0.94 in our calculations.

λ is the X-ray wavelength (1.54178 Å) used for the measurement of the PXRD diffraction pattern of the COFs,

β is the line broadening at half of the maximum intensity,

θ is the Bragg angle.

The relative crystallinity is calculated by dividing the experimental integral breadth (β_{exp}) of the first intensity peak (corresponding to diffraction from [100] planes) of the experimental PXRD pattern of the sample with the COF exhibiting the highest integral breadth (β_{hexp}). It can be expressed as:[13]

$$\text{Relative crystallinity} = \frac{\beta_{exp}}{\beta_{hexp}} \qquad \text{(eq. 2)}$$

Table S5. Domain size of the COF crystallites (Å) synthesized in different green solvents.

COFs	COF crystallite size (Å)	COFs	COF crystallite size (Å)	COFs	COF crystallite size (Å)	COF	COF crystallite size (Å)	COFs	COF crystallite size (Å)
TpPa-DC	9.73	-	-	TpAzo-DC	28.42	-	-	TpTab-DC	4.35
TpPa-PC	9.70	TpBD-PC	18.00	TpAzo-PC	19.40	TpAnq-PC	10.11	TpTab-PC	5.25
TpPa-GBL	9.25	TpBD-GBL	18.50	TpAzo-GBL	13.32	-	-	TpTab-GBL	6.01
TpPa-ES	8.33	-	-	-	-	-	-	TpTab-ES	6.01
TpPa-PS	8.30	-	-	-	-	-	-	TpTab-PS	6.27
TpPa-Cyr	8.84	-	-	-	-	-	-	TpTab-Cyr	5.54
TpPa-IDE	8.19	TpBD-IDE	20.05	TpAzo-IDE	22.46	TpAnq-IDE	8.83	TpTab-IDE	5.78
TpPa-DF	8.98	-	-	TpAzo-DF	23.91	TpAnq-DF	9.25	TpTab-DF	4.84
TpPa-MP	7.43	-	-	TpAzo-MP	23.66	-	-	TpTab-MP	6.43
TpPa-Tn	7.01	TpBD-Tn	21.31	TpAzo-Tn	27.70	-	-	TpTab-Tn	5.76
TpPa-Cym	7.51	-	-	TpAzo-Cym	23.72	TpAnq-Cym	11.29	TpTab-Cym	4.60
TpPa-PCl	7.51	TpBD-PCl	18.85	TpAzo-PCl	19.88	TpAnq-PCl	10.56	TpTab-PCl	5.34

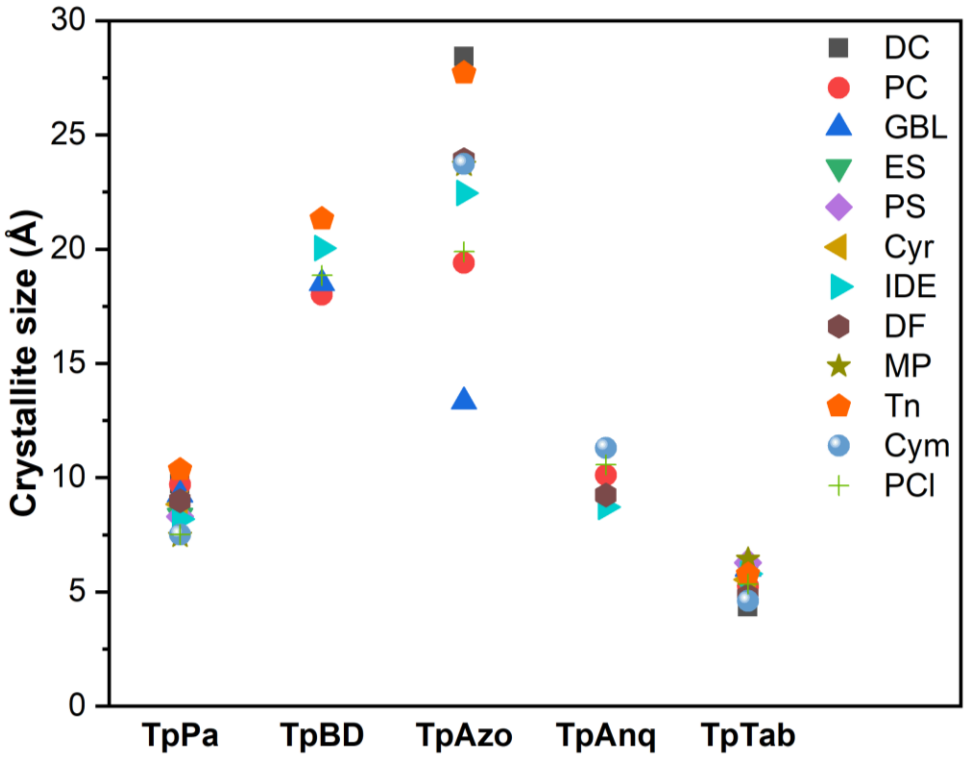

Figure S9. Crystallite size (Å) of the as-synthesized COFs in different solvents. The crystallite domain size of COF crystallites in the form of powder were calculated using Scherrer equation. The size of all the COF crystallites was found to fall in a certain range, as shown in Table S3. However, in case of the **TpAzo** series, the range of variation in the size of the crystallites is large as compared to other series of the COFs synthesized.

According to the results shown in Table S3, the large size of the COF crystallites (**TpPa**, **TpBD**, and **TpAzo**) are produced in terpineol, Cymene (**TpAnq**), and propylene carbonate (**TpTab**) solvents. However, in case of **TpAzo,** the size of the COF crystallites was found to vary in different solvents. For example, the size of the **TpAzo-GBL** crystallite is relatively smaller although it exhibits the highest surface area among all the COFs synthesized in this work.

Section S5: Pawley refinement and fractional atomic coordinates of the as-synthesized COFs

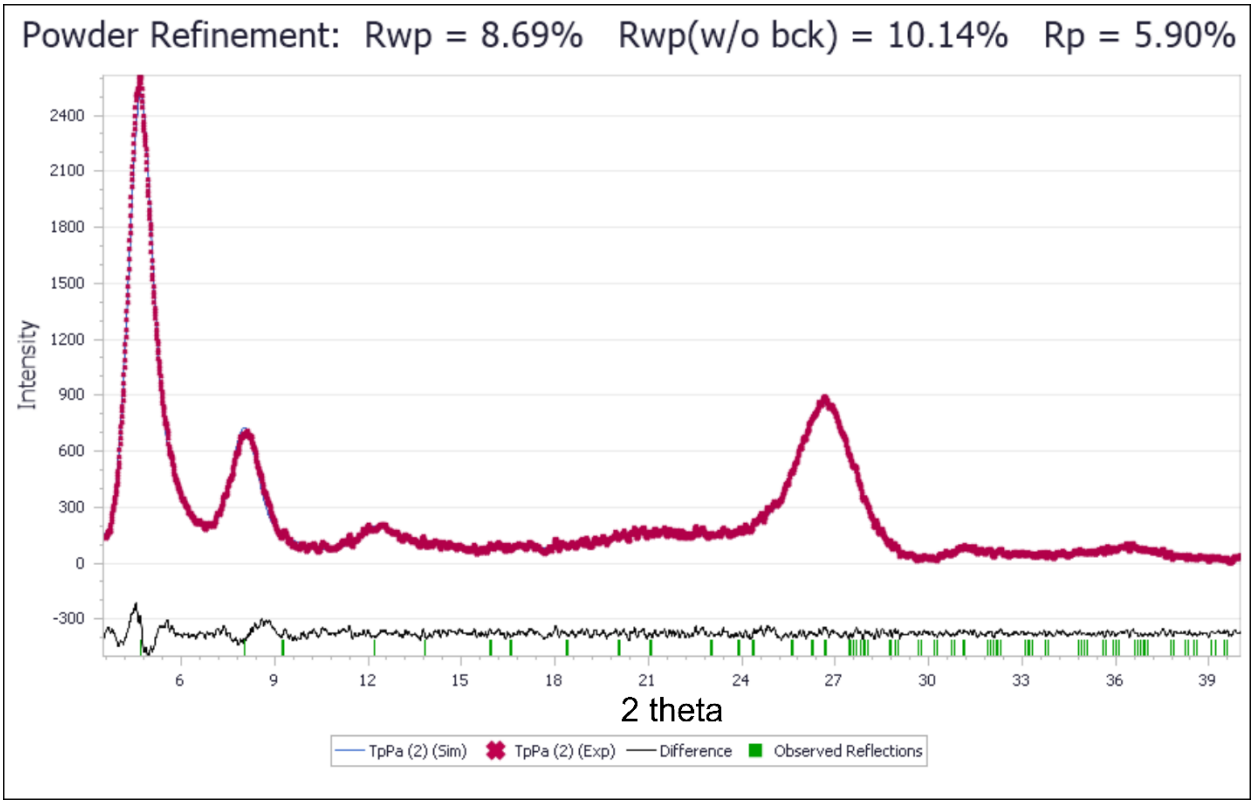

Figure S10. Pawley refinement for TpPa COF. Pawley refinement suggests that the simulated and experimental PXRD patterns are in good agreement.

Table S6. Fractional atomic coordinates for the unit cell of the TpPa COF.

TpPa in eclipsed AA model (Space group *P*6/m)			
a = b = 29.60 Å, c = 3.58 Å			
α = β = 90º, γ = 120º			
Atoms	x	y	z
O	0.28355	0.52709	0.5
N	0.41129	0.55212	0.5
C	0.30695	0.59146	0.5
C1	0.38113	0.64063	0.5
C5	0.42797	0.61784	0.5
C6	0.45481	0.52704	0.5
C7	0.42936	0.4559	0.5
C8	0.52674	0.57065	0.5
H	0.37353	0.42043	0.5
H1	0.4837	0.65597	0.5
H1#	0.54893	0.62685	0.5
H17	0.35757	0.51744	0.5

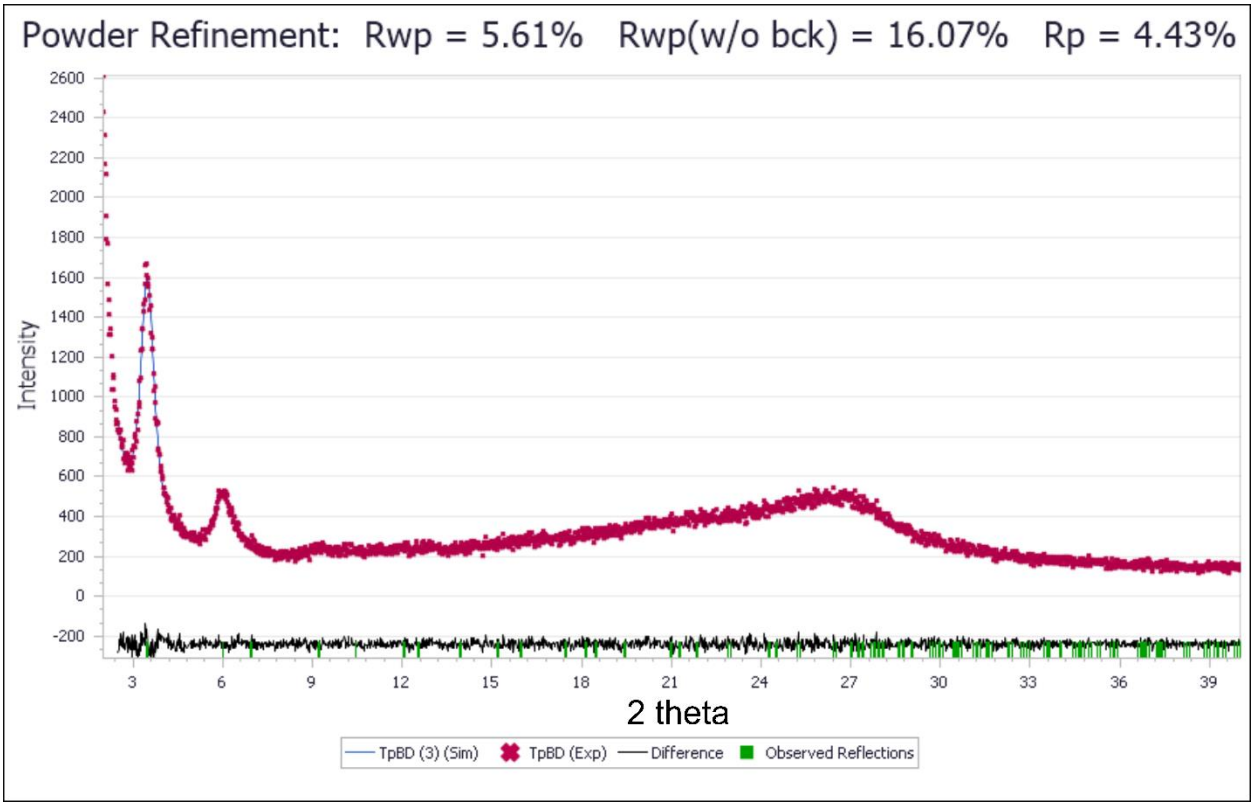

Figure S11. Pawley refinement for TpBD COF. Pawley refinement suggests that the simulated and experimental PXRD patterns are in good agreement.

Table S7. Fractional atomic coordinates for the unit cell of the TpBD COF.

TpBD in eclipsed AA model (Space group *P*6/m)			
a = b = 29.36 Å, c = 3.30 Å			
α = β = 90º, γ = 120º			
Atom	x	y	z
O1	0.2956	0.5612	0
N2	0.3872	0.5781	0
C3	0.3135	0.6107	0
C4	0.4039	0.6298	0
C5	0.4195	0.5569	0
C6	0.4739	0.5883	0
C7	0.5046	0.5656	0
C8	0.4829	0.5112	0
C9	0.4281	0.4803	0
C10	0.3968	0.5027	0
C11	0.3684	0.6472	0
H12	0.4458	0.6592	0
H13	0.4926	0.6314	0
H14	0.3442	0.5557	0

H15	0.3534	0.4783	0
H16	0.5476	0.5916	0
H17	0.4091	0.4372	0

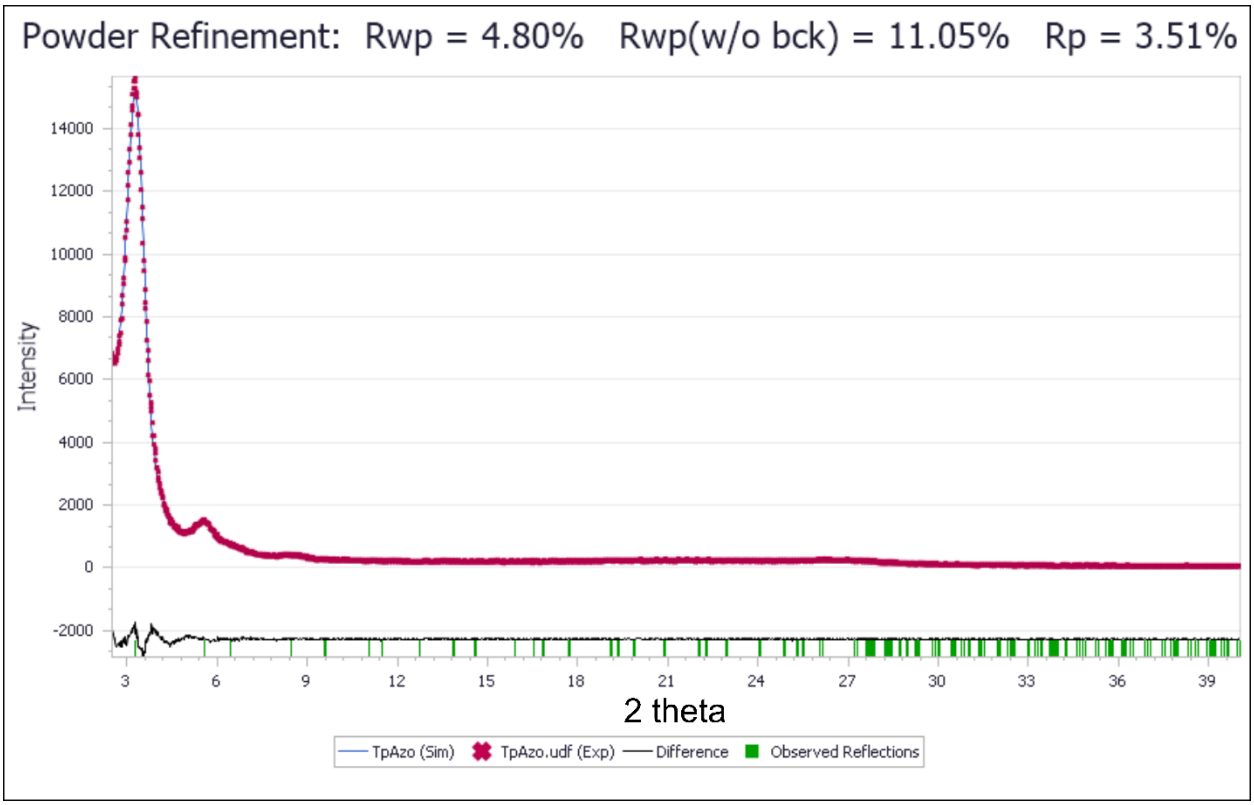

Figure S12. Pawley refinement for TpAzo COF. Pawley refinement suggests that the simulated and experimental PXRD patterns are in good agreement.

Table S8. Fractional atomic coordinates for the unit cell of the TpAzo COF.

TpAzo in eclipsed AA model (Space group *P*6/m)			
a = b = 32.38 Å, c = 3.23 Å			
α = β = 90º, γ = 120º			
Atoms	x	y	z
O1	0.29695	0.57697	0
N2	0.38245	0.58505	0
C3	0.31382	0.61757	0
C4	0.39342	0.63145	0
C5	0.41468	0.5699	0
C6	0.46145	0.59947	0
C7	0.49111	0.58277	0
C8	0.47494	0.53664	0

C9	0.42853	0.50701	0
C10	0.39878	0.52354	0
C11	0.36359	0.64675	0
H12	0.42849	0.65656	0
H13	0.47589	0.63531	0
H14	0.34922	0.55946	0
H15	0.36308	0.50007	0
H16	0.52692	0.60571	0
H17	0.41558	0.4712	0
N1	0.50627	0.52081	0

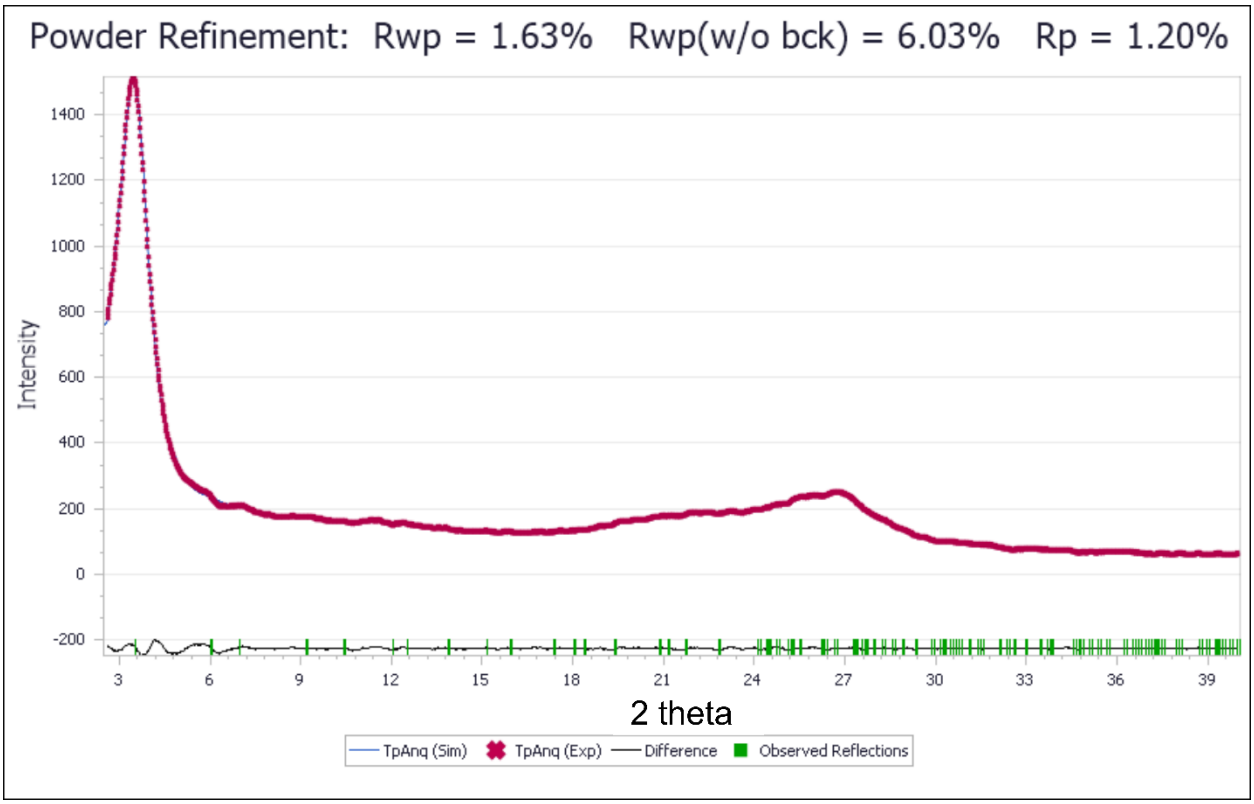

Figure S13. Pawley refinement for TpAnq COF. Pawley refinement suggests that the simulated and experimental PXRD patterns are in good agreement.

Table S9. Fractional atomic coordinates for the unit cell of the TpAnq COF.

TpAnq in eclipsed AA model (Space group *P*6/m)			
a = b = 29.54 Å, c = 3.63 Å			
α = β = 90º, γ = 120º			
Atoms	x	y	z
C1	0.68317	0.38629	0
C2	0.62934	0.3502	0

C3	0.59309	0.3624	0
N4	0.60004	0.41163	0
C5	0.56079	0.42318	0
C6	0.51053	0.38683	0
C7	0.44994	0.4632	0
C8	0.4867	0.44984	0
C9	0.53695	0.48675	0
C10	0.47409	0.40005	0
C11	0.57332	0.4729	0
O12	0.40658	0.43128	0
O13	0.6976	0.43014	0
H14	0.55564	0.33232	0
H15	0.49823	0.34804	0
H16	0.43561	0.37126	0
H17	0.6119	0.50121	0
H18	0.63518	0.44226	0

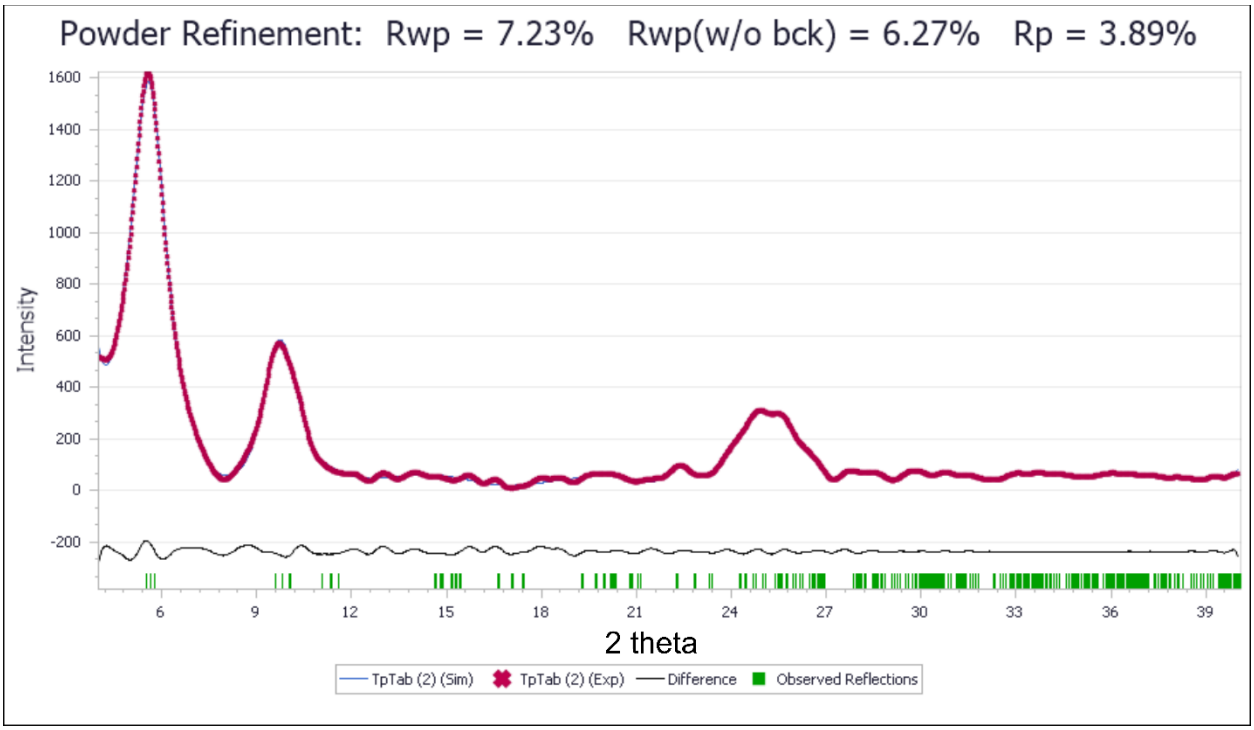

Figure S14. Pawley refinement for TpTab COF. Pawley refinement suggests that the simulated and experimental PXRD patterns are in good agreement.

Table S10. Fractional atomic coordinates for the unit cell of the TpTab COF.

TpTab in eclipsed AA model (Space group *P*1)
a = 18.38 Å, b = 17.56 Å, c = 3.39 Å

α = 89.50º, β = 90.38º, γ = 119.91º			
Atoms	x	y	z
O1	0.22808	0.53994	0.48279
N2	0.38116	0.56198	0.4825
C3	0.26054	0.61917	0.48265
C4	0.352	0.67554	0.48244
C5	0.40577	0.64342	0.48238
H6	0.4785	0.69417	0.48221
H7	0.3105	0.5126	0.50265
O8	0.46921	0.81445	0.48209
N9	0.44977	0.94937	0.48209
C10	0.38998	0.76768	0.48227
C11	0.33361	0.80277	0.48233
C12	0.36574	0.88866	0.48219
H13	0.31354	0.90871	0.48216
H14	0.50051	0.93009	0.45229
C15	0.24148	0.74861	0.48255
O16	0.1947	0.78107	0.48259
N17	0.06366	0.62799	0.48298
C18	0.20639	0.65716	0.4827
C19	0.12049	0.60339	0.48291
H20	0.09852	0.53066	0.48303
H21	0.08436	0.6979	0.43416
C22	0.6864	0.34918	0.47275
C23	0.67353	0.46712	0.48935
C24	0.72017	0.43167	0.48599
C25	0.55565	0.33617	0.4841
C26	0.60365	0.30251	0.48092
C27	0.59154	0.41867	0.48132
C28	0.80217	0.4789	0.49373
C29	0.84124	0.56468	0.50784
C30	0.9273	0.61243	0.52894
C31	0.97793	0.5768	0.53772
C32	0.93764	0.4905	0.52678
C33	0.85232	0.44118	0.49695
C34	0.56487	0.21305	0.48126
C35	0.4794	0.16273	0.49056
C36	0.44313	0.07679	0.50581
C37	0.49039	0.03747	0.51328
C38	0.5762	0.08898	0.50722
C39	0.61431	0.17456	0.48327
C40	0.53659	0.4558	0.48359
C41	0.44972	0.40529	0.47752
C42	0.3997	0.44169	0.46801

C43	0.57043	0.54236	0.4759
C44	0.51779	0.57578	0.46642
C45	0.43253	0.52655	0.46019
H46	0.41862	0.33102	0.48051
H47	0.32541	0.39869	0.46644
H48	0.64444	0.58745	0.47748
H49	0.54652	0.64976	0.46345
H50	0.80075	0.59869	0.50191
H51	0.96036	0.68683	0.54024
H52	0.97717	0.45557	0.54349
H53	0.82062	0.36702	0.47388
H54	0.43567	0.1932	0.48548
H55	0.36885	0.03388	0.51299
H56	0.62073	0.0595	0.52313
H57	0.6886	0.21625	0.46427
H58	0.73021	0.31892	0.45406
H59	0.70563	0.54146	0.49945
H60	0.48144	0.29254	0.48937
N9	0.44977	-0.05063	0.48209
N17	1.06366	0.62799	0.48298
C31	-0.02207	0.5768	0.53772
C37	0.49039	1.03747	0.51328

Section S6: FTIR spectroscopic characterizations of as-synthesized COFs

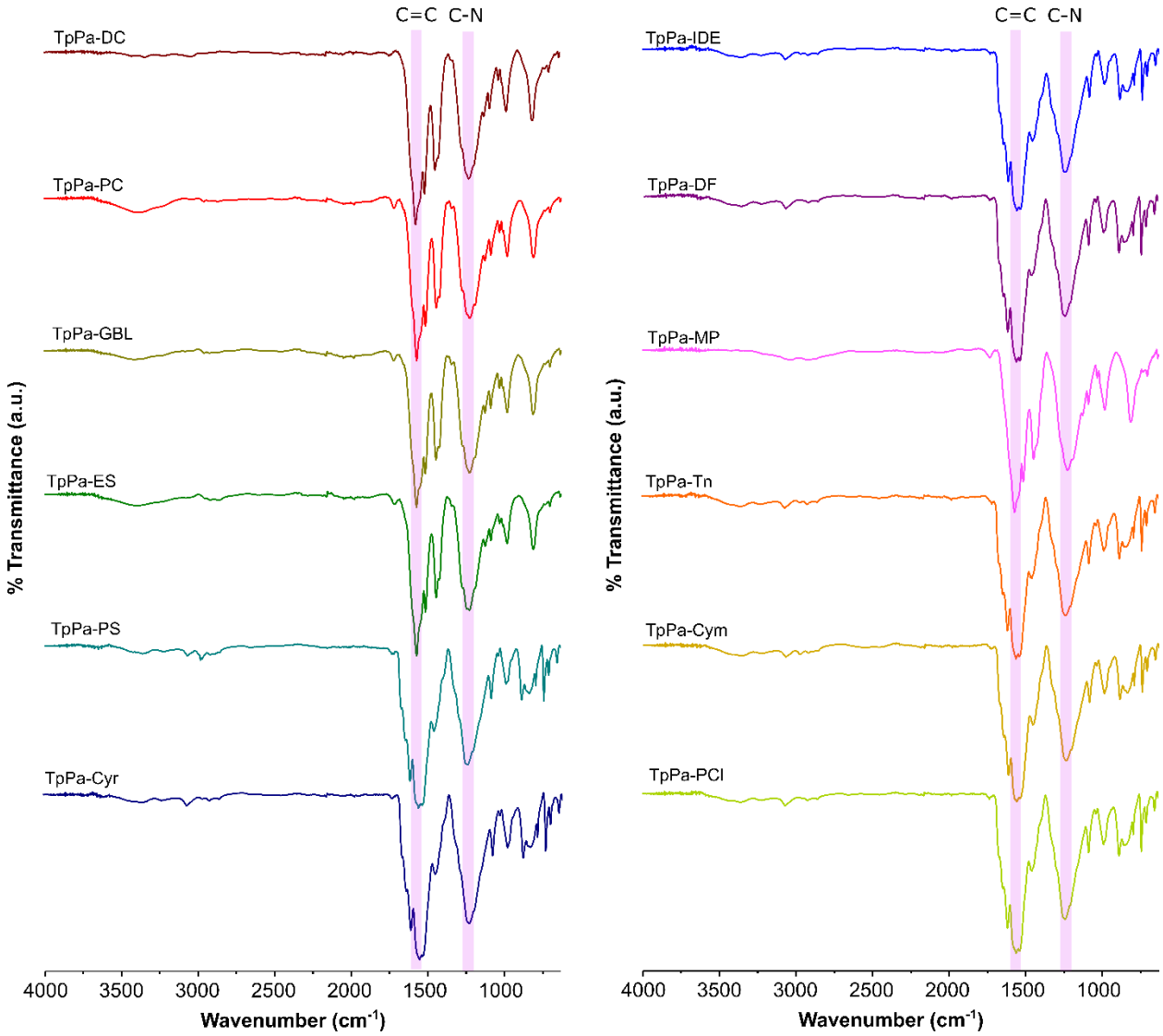

Figure S15. FTIR spectra of the TpPa COFs synthesized in green solvent media. FTIR spectra of the as-synthesized COFs exhibit characteristic stretches corresponding to the β-ketoenamine-linked framework structures. Both C=C and C-N peaks have been highlighted for ready reference.

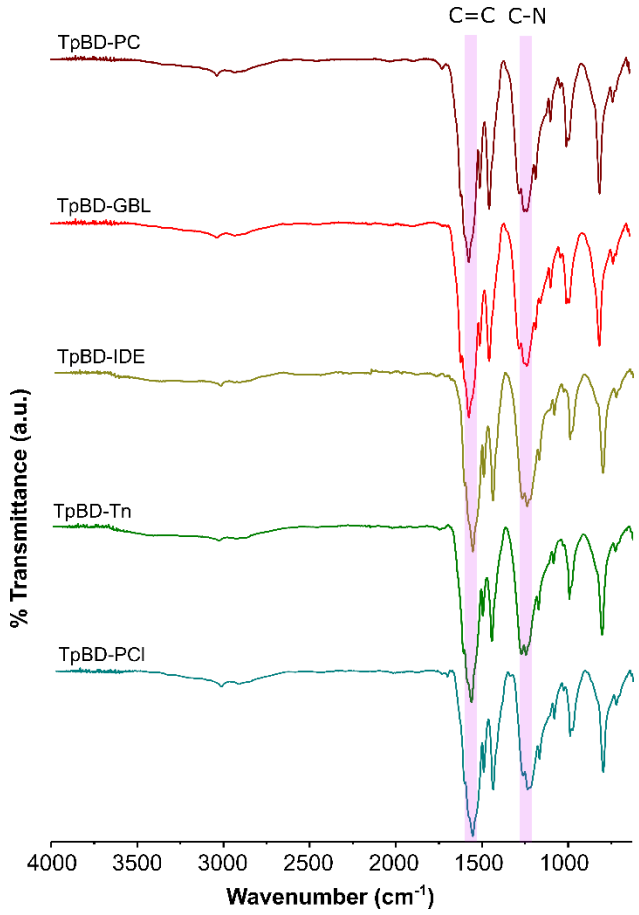

Figure S16. FTIR spectra of the TpBD COFs synthesized in green solvent media. FTIR spectra of the as-synthesized COFs exhibit characteristic stretches corresponding to the β-ketoenamine-linked framework structures. Both C=C and C-N peaks have been highlighted for ready reference.

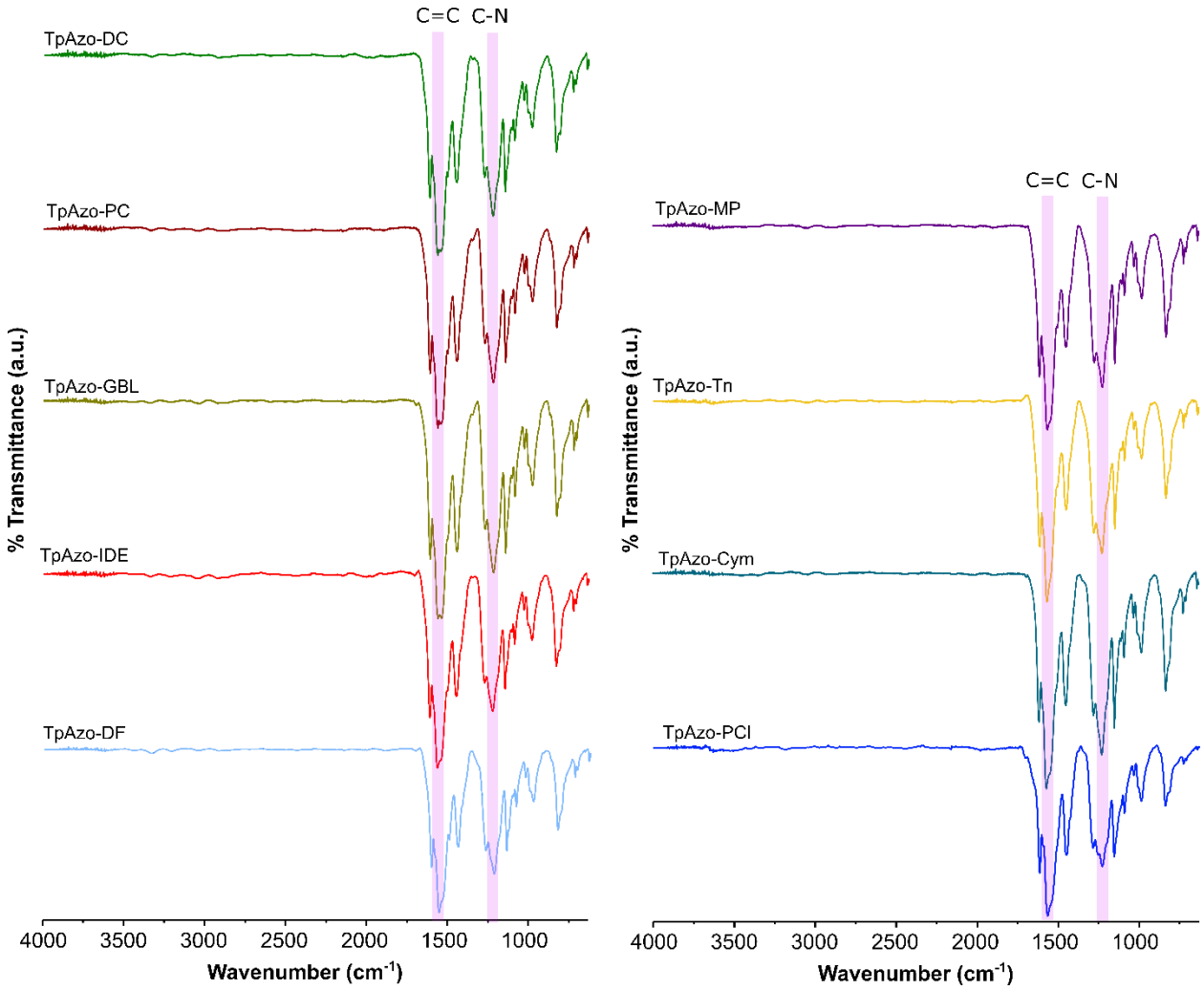

Figure S17. FTIR spectra of TpAzo COFs synthesized in green solvent media. FTIR spectra of the as-synthesized COFs exhibit characteristic stretches corresponding to the β-ketoenamine-linked framework structures. Both C=C and C-N peaks have been highlighted for ready reference.

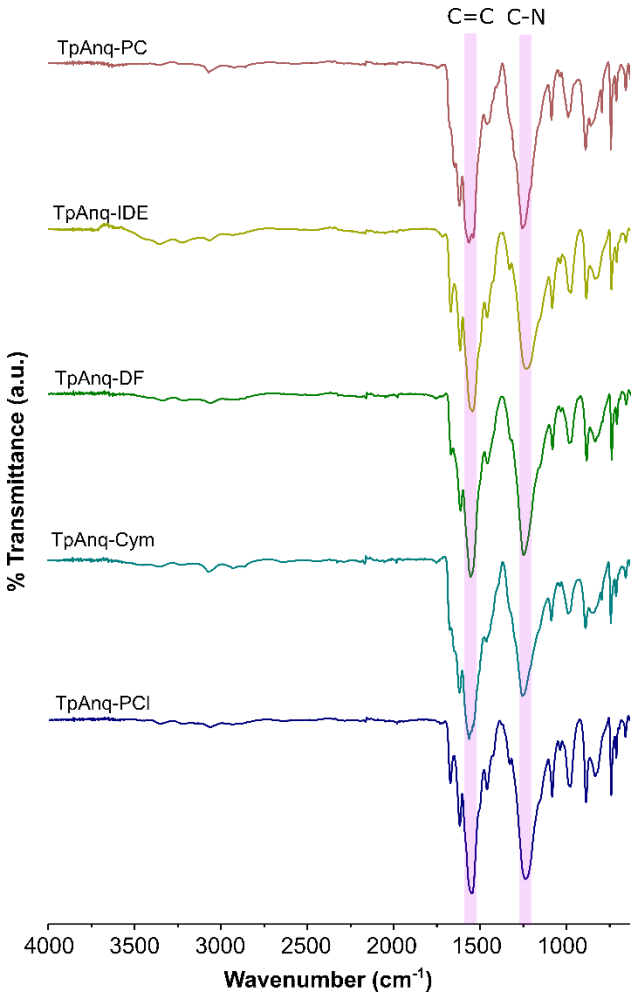

Figure S18. FTIR spectra of the TpAnq COFs synthesized in green solvent media. FTIR spectra of the as-synthesized COFs exhibit characteristic stretches corresponding to the β-ketoenamine-linked framework structures. Both C=C and C-N peaks have been highlighted for ready reference.

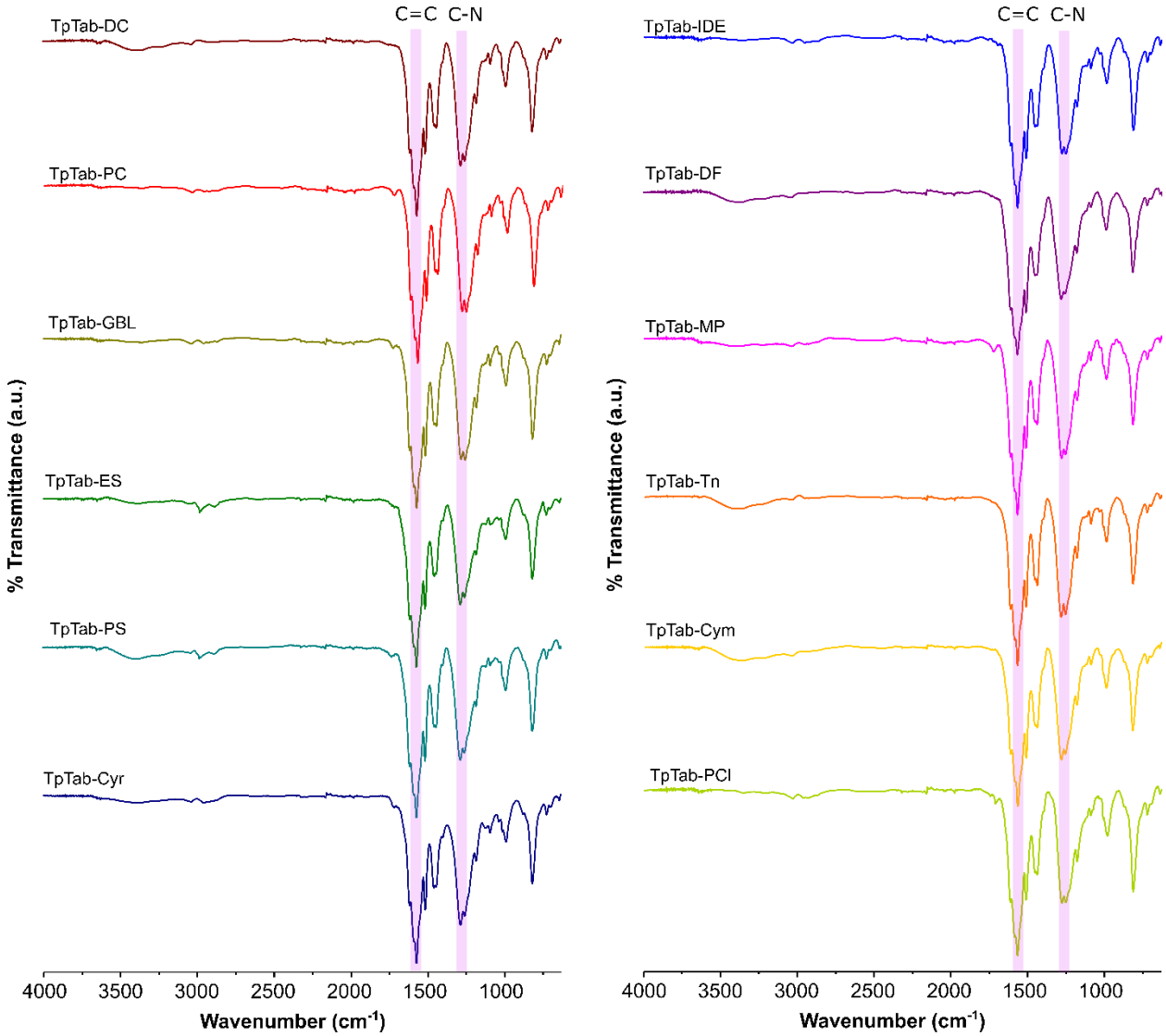

Figure S19. FTIR spectra of TpTab COFs synthesized in green solvent media. FTIR spectra of the as-synthesized COFs exhibit characteristic stretches corresponding to the β-ketoenamine-linked framework structures. Both C=C and C-N peaks have been highlighted for ready reference.

Section S7: Analysis of solid state ^{13}C CP-MAS NMR spectra of as-synthesized COFs

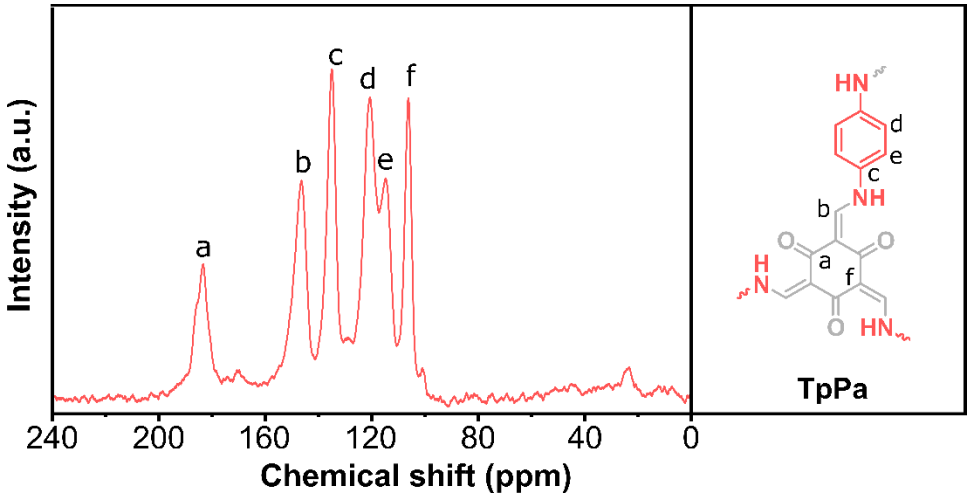

Figure S20. Solid-state ^{13}C CP-MAS NMR spectrum. Analysis of the solid-state ^{13}C CP-MAS NMR spectrum of the TpPa COF showing the characteristic carbonyl (C=O) peak and other carbon peaks corresponding to the formation of the *β*-ketoenamine framework structure.

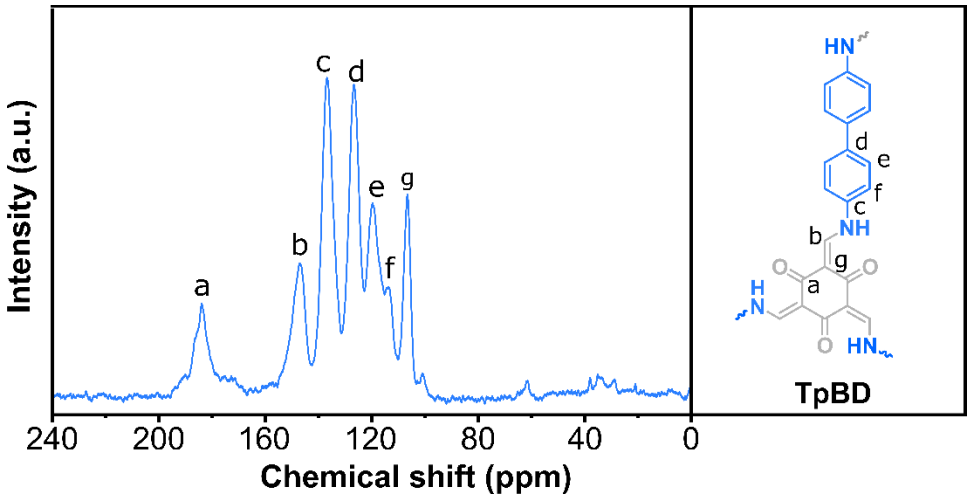

Figure S21. Solid-state ^{13}C CP-MAS NMR spectrum. Analysis of the solid-state ^{13}C CP-MAS NMR spectrum of the TpBD COF showing the characteristic carbonyl (C=O) peak and other carbon peaks corresponding to the formation of the *β*-ketoenamine framework structure.

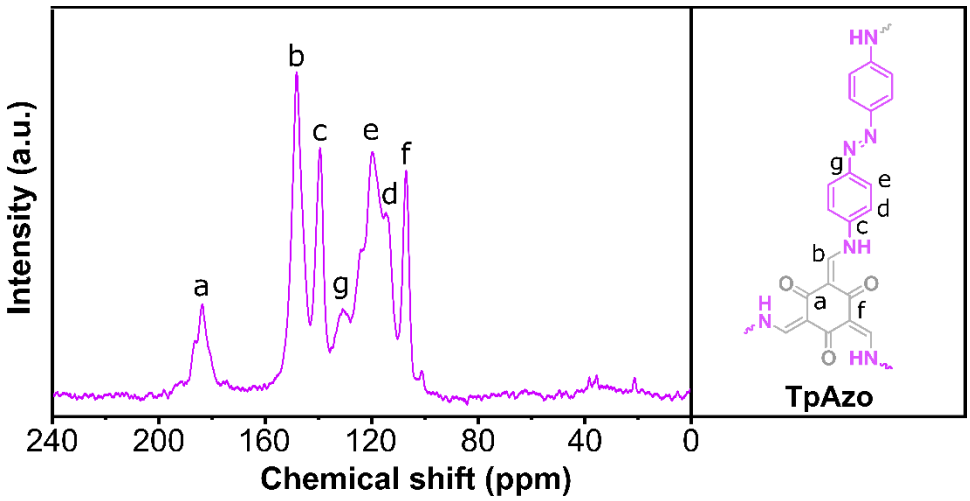

Figure S22. Solid-state ^{13}C CP-MAS NMR spectrum. Analysis of the solid-state ^{13}C CP-MAS NMR spectrum of the TpAzo COF showing the characteristic carbonyl (C=O) peak and other carbon peaks corresponding to the formation of the *β*-ketoenamine framework structure.

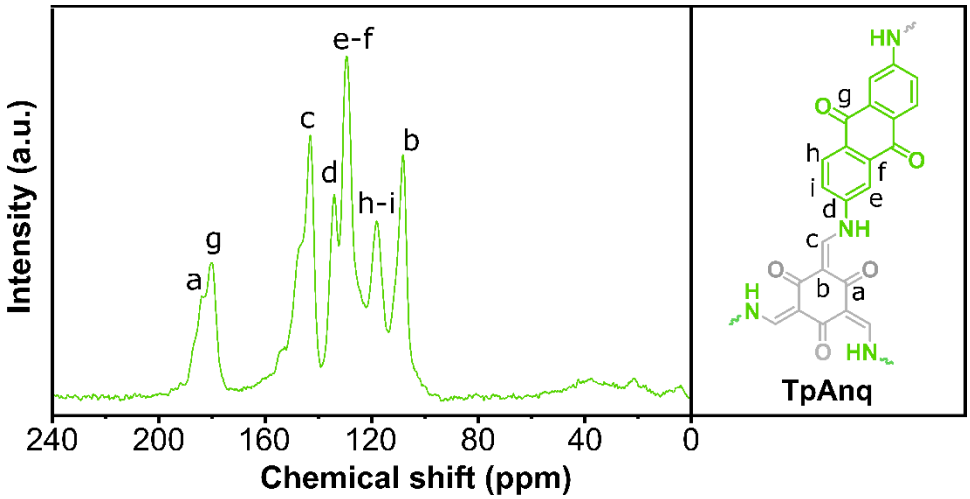

Figure S23. Solid-state ^{13}C CP-MAS NMR spectrum. Analysis of the solid-state ^{13}C CP-MAS NMR spectrum of the TpAnq COF showing the characteristic carbonyl (C=O) peak and other carbon peaks corresponding to the formation of the *β*-ketoenamine framework structure.

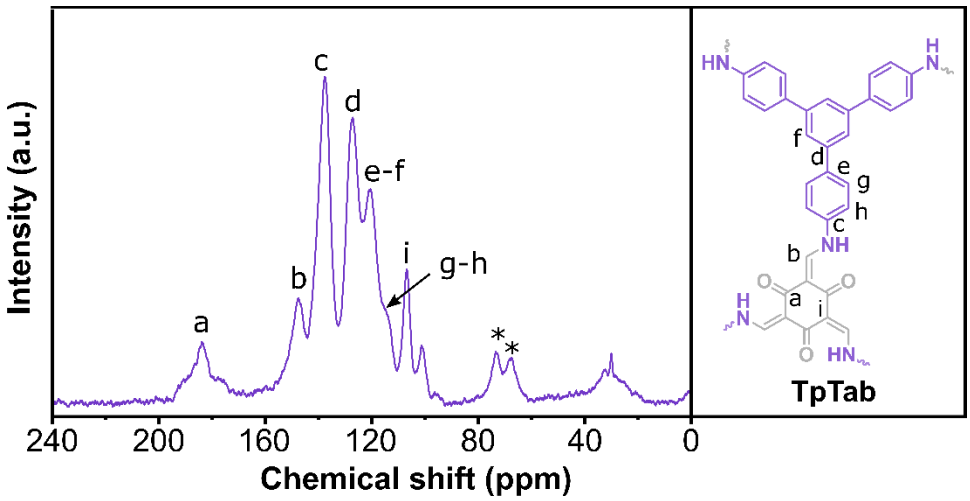

Figure S24. Solid state ^{13}C CP-MAS NMR spectrum. Analysis of the solid-state ^{13}C CP-MAS NMR spectrum of the TpTab COF showing the characteristic carbonyl (C=O) peak and other carbon peaks corresponding to the formation of the *β*-ketoenamine framework structure.

Section S8: XPS profiles of as-synthesized COFs

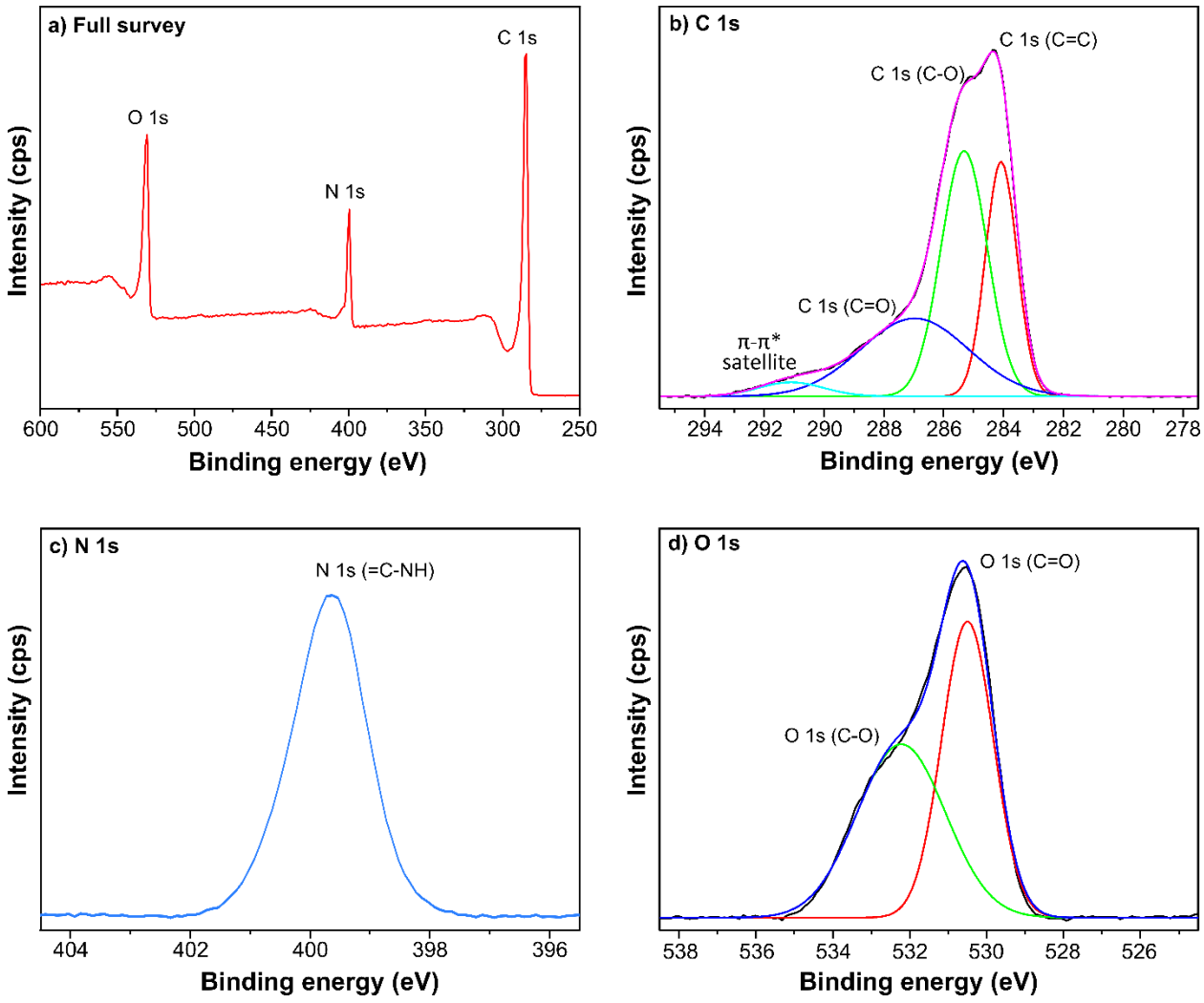

Figure S25. X-ray photoelectron spectroscopy (XPS) profile of the representative TpPa COF. a) Full-survey XPS profile shows three peaks at 284.62 (for C 1s), 399.63 (for N 1s), and 530.62 eV (for O 1s). b) In the deconvoluted XPS profile for C 1s, 284.13 eV is assigned to C=C of the aromatic ring system, and the shoulders appearing at 285.36 and 287.01 eV are assigned to the C-O and C=O bonds, respectively. c) For the N 1s XPS profile, only one peak is appears at 399.63 eV and is assigned to the =C-NH bond of the framework. d) Analysis of the O 1s XPS profile shows one peak at 530.49 and a shoulder at 532.21 eV, which are assigned to the C=O and C-O bonds of the framework, respectively.

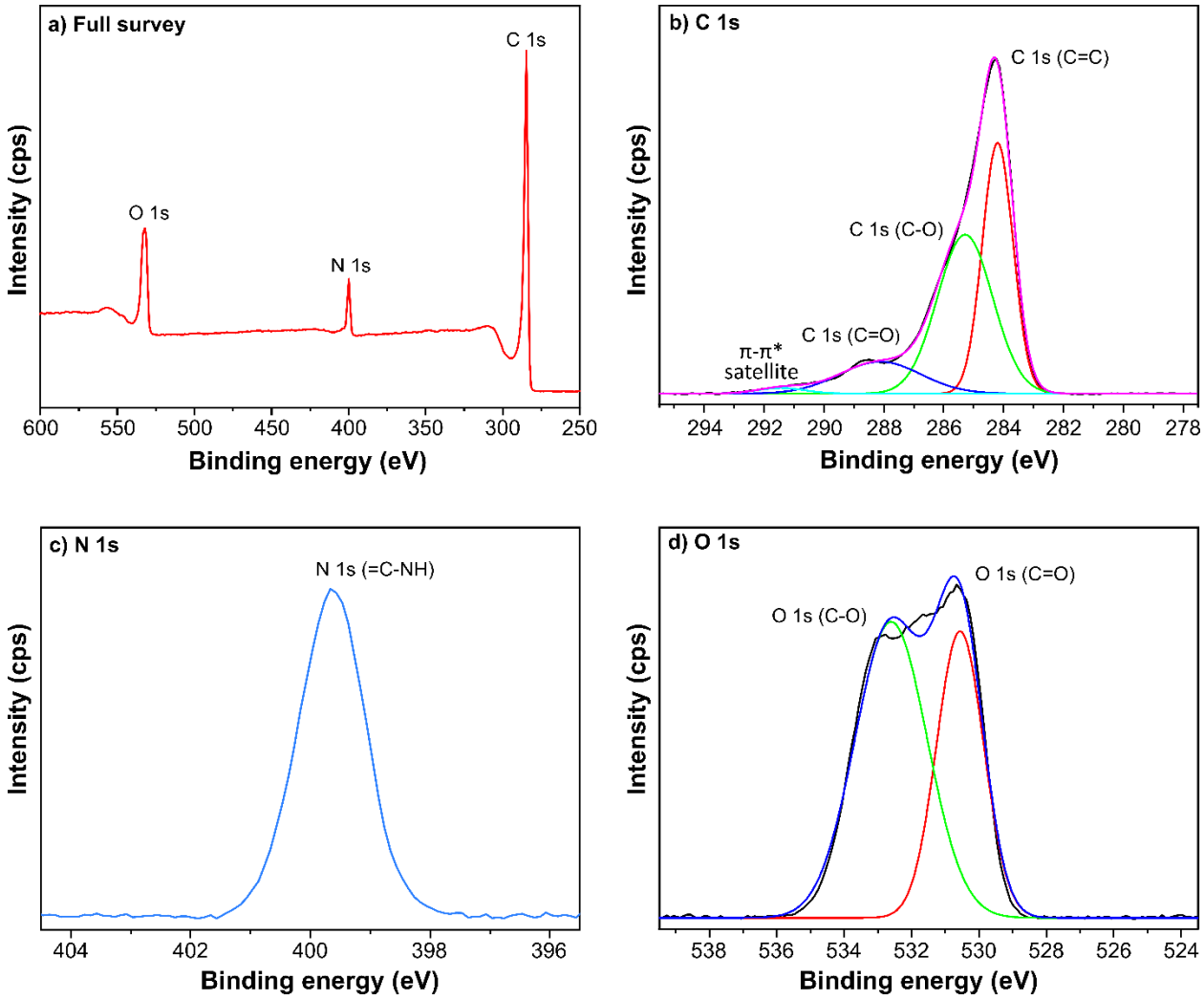

Figure S26. X-ray photoelectron spectroscopy (XPS) profile of the representative TpBD COF. a) Full-survey XPS profile shows three peaks at 284.76 (for C 1s), 399.76 (for N 1s), and 531.76 eV (for O 1s). In addition, a satellite peak is observed at 291.47 eV, which arises from the π-π* transitions. b) In the deconvoluted XPS profile for C 1s, 284.32 eV is assigned to C=C of the aromatic ring system, and shoulders appearing at 285.39 and 288.20 eV are assigned to C-O and C=O bonds, respectively. c) For the N 1s XPS profile, only one peak appears at 399.63 eV and is assigned to the =C-NH bond of the framework. d) Analysis of the O 1s XPS profile shows one peak at 530.56 and a shoulder at 532.60 eV, which are assigned to the C=O and C-O bonds of the framework, respectively.

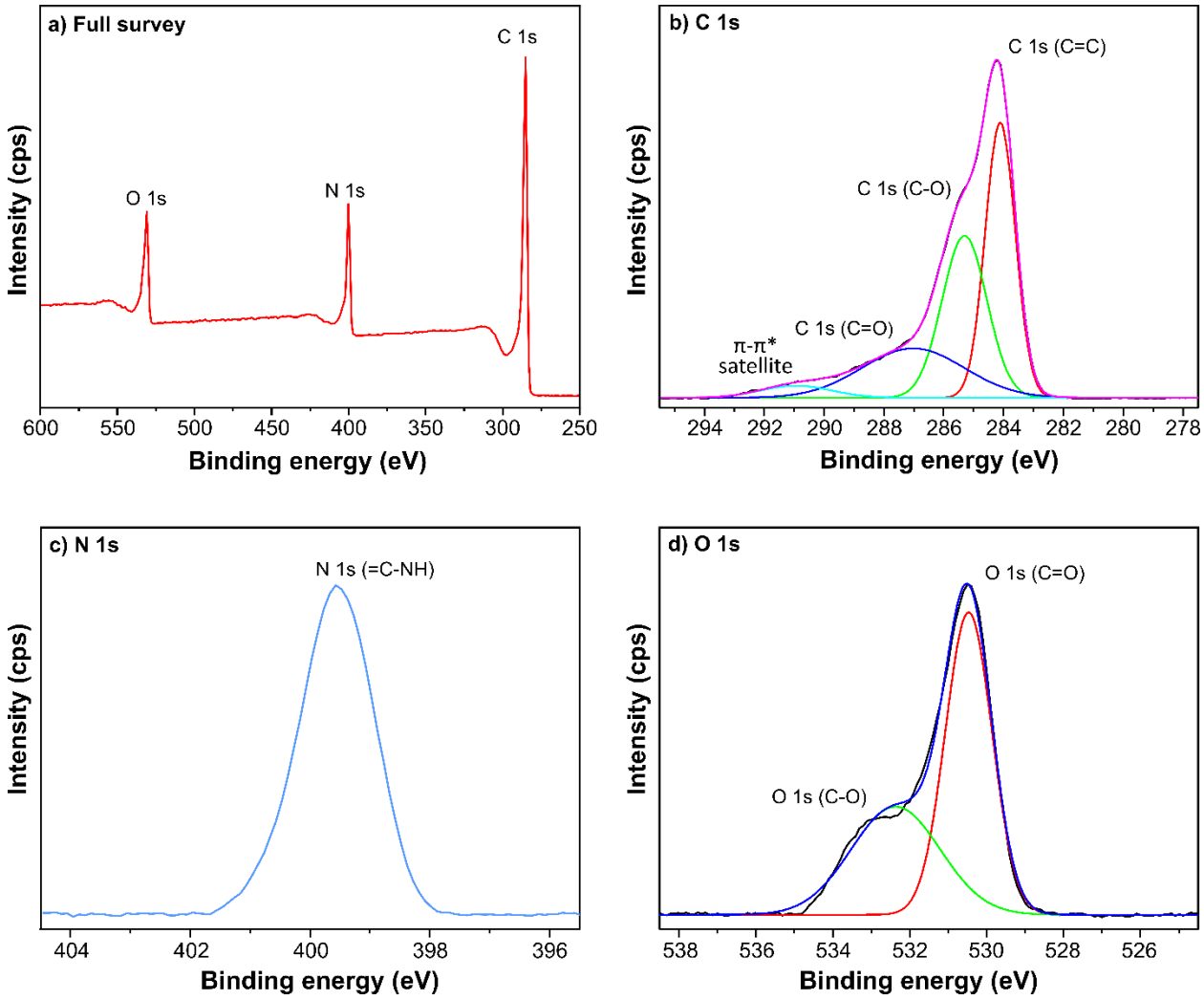

Figure S27. X-ray photoelectron spectroscopy (XPS) profile of the representative TpAzo COF. a) Full-survey XPS profile shows three peaks at 284.78 (for C 1s), 399.78 (for N 1s), and 530.78 eV (for O 1s). In addition, a satellite peak is observed at 291.02 eV, which arises from the π-π* transitions. b) In the deconvoluted XPS profile for C 1s, 284.29 eV is assigned to C=C of the aromatic ring system, and the shoulders appearing at 285.47 and 287.17 are assigned to C-O and C=O bonds, respectively. c) For the N 1s XPS profile, only one peak appears at 399.57 eV and is assigned to the =C-NH bond of the framework. d) Analysis of the O 1s XPS profile shows one peak at 530.45 and a shoulder at 532.34 eV, which are assigned to the C=O and C-O bonds of the framework, respectively.

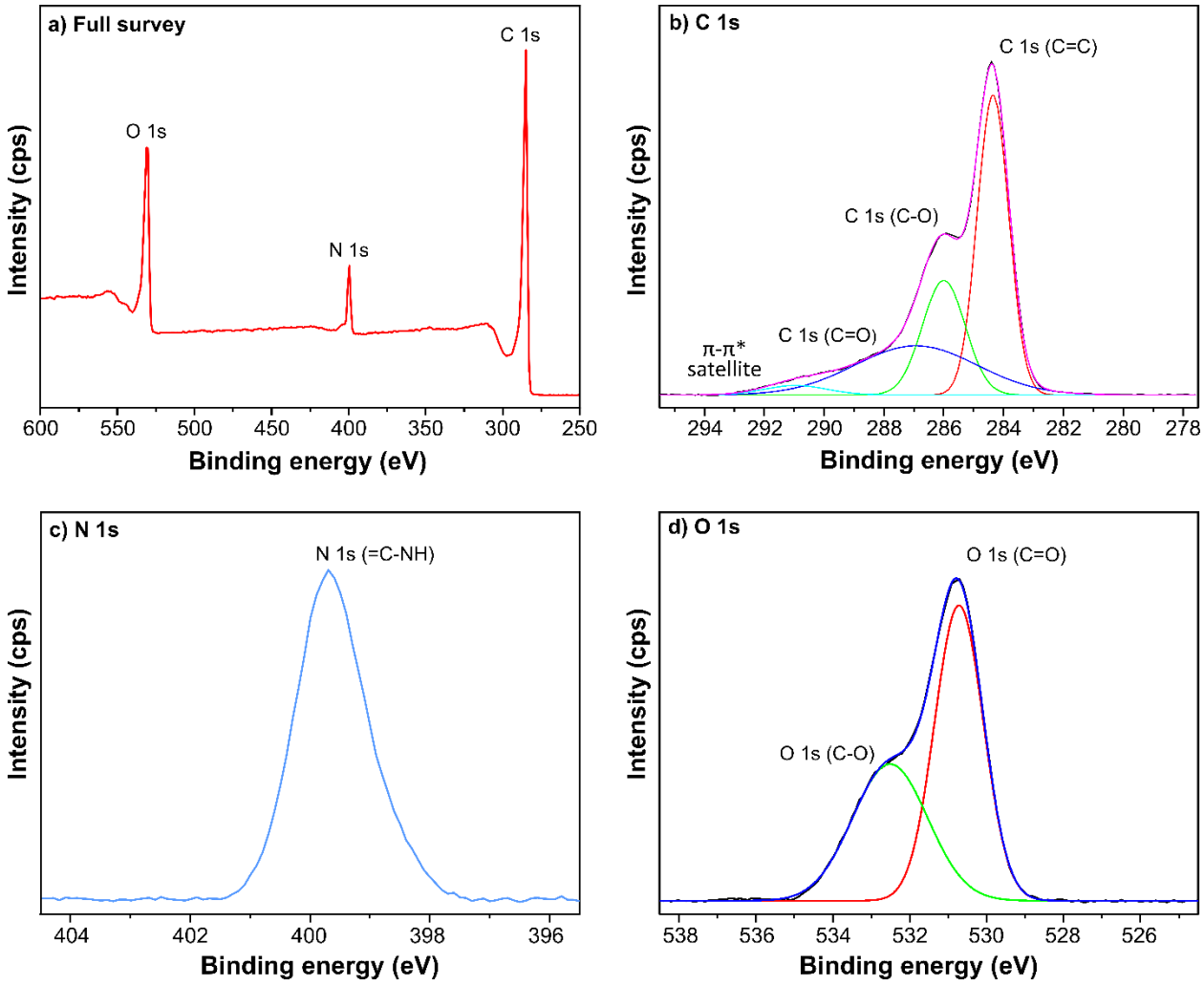

Figure S28. X-ray photoelectron spectroscopy (XPS) profile of the representative TpAnq COF. a) Full-survey XPS profile shows three peaks at 284.60 (for C 1s), 399.60 (for N 1s), and 531.60 eV (for O 1s). In addition, a satellite peak is observed at 290.94 eV, which arises from the π-π* transitions. b) In the deconvoluted XPS profile for C 1s, 284.34 eV is assigned to C=C of the aromatic ring system, and the shoulders appearing at 285.99 and 286.92 are assigned to C-O and C=O bonds, respectively. c) For the N 1s XPS profile, only one peak appears at 399.64 eV and is assigned to the =C-NH bond of the framework. d) Analysis of the O 1s XPS profile shows one peak at 530.71 and a shoulder at 532.50 eV, which are assigned to the C=O and C-O bonds of the framework, respectively.

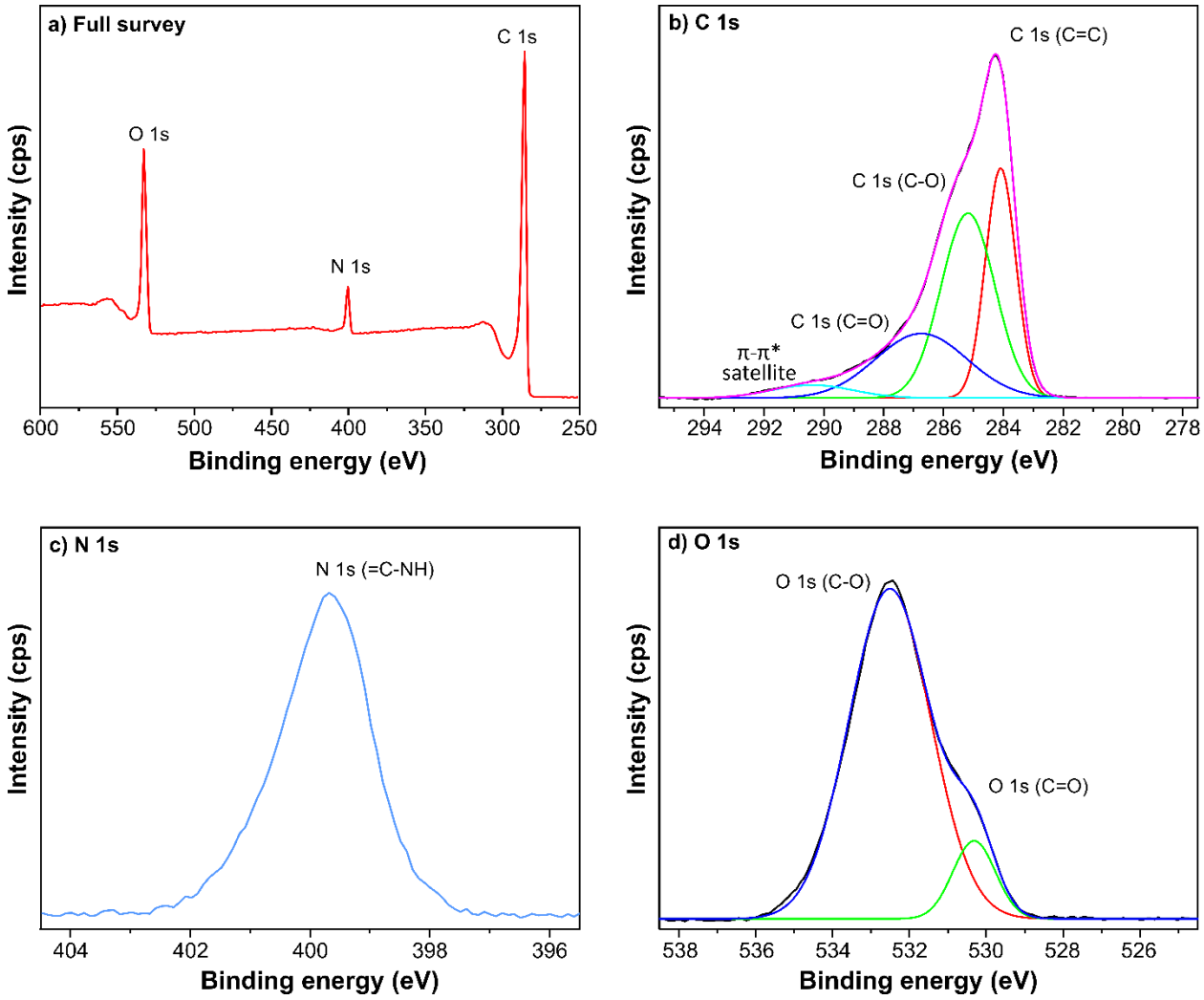

Figure S29. X-ray photoelectron spectroscopy (XPS) profile of the representative TpTab COF. a) Full-survey XPS profile shows three peaks at 284.63 (for C 1s), 399.63 (for N 1s), and 532.63 eV (for O 1s). In addition, a satellite peak is observed at 290.42 eV, which arises from the π-π* transitions. b) In the deconvoluted XPS profile for C 1s, 284.20 eV is assigned to C=C of the aromatic ring system, and the shoulders appearing at 285.28 and 286.82 are assigned to C-O and C=O bonds, respectively. c) For the N 1s XPS profile, only one peak appears at 399.65 eV and is assigned to the =C-NH bond of the framework. d) Analysis of the O 1s XPS profile shows one shoulder at 530.31 and a peak at 532.50 eV, which are assigned to the C=O and C-O bonds of the framework.

Section S9. Thermal gravimetric analysis

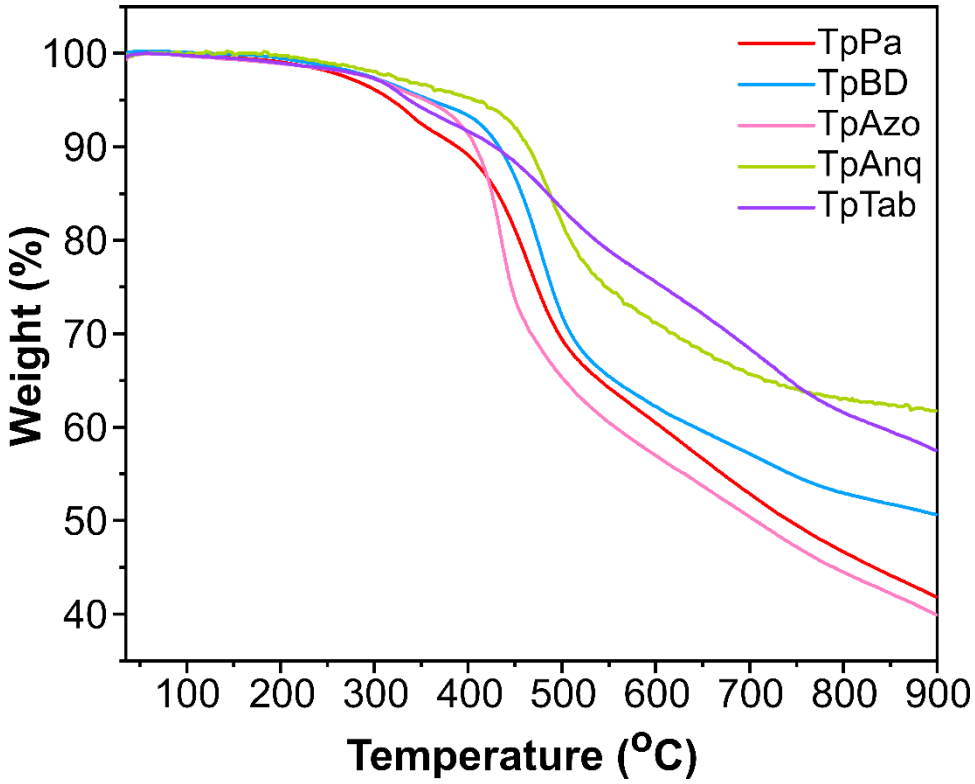

Figure S30. Thermal gravimetric analysis (TGA) profile of the as-synthesized COFs shows the thermal stability up to ~320 °C.

Section S10: SEM images of as-synthesized COFs

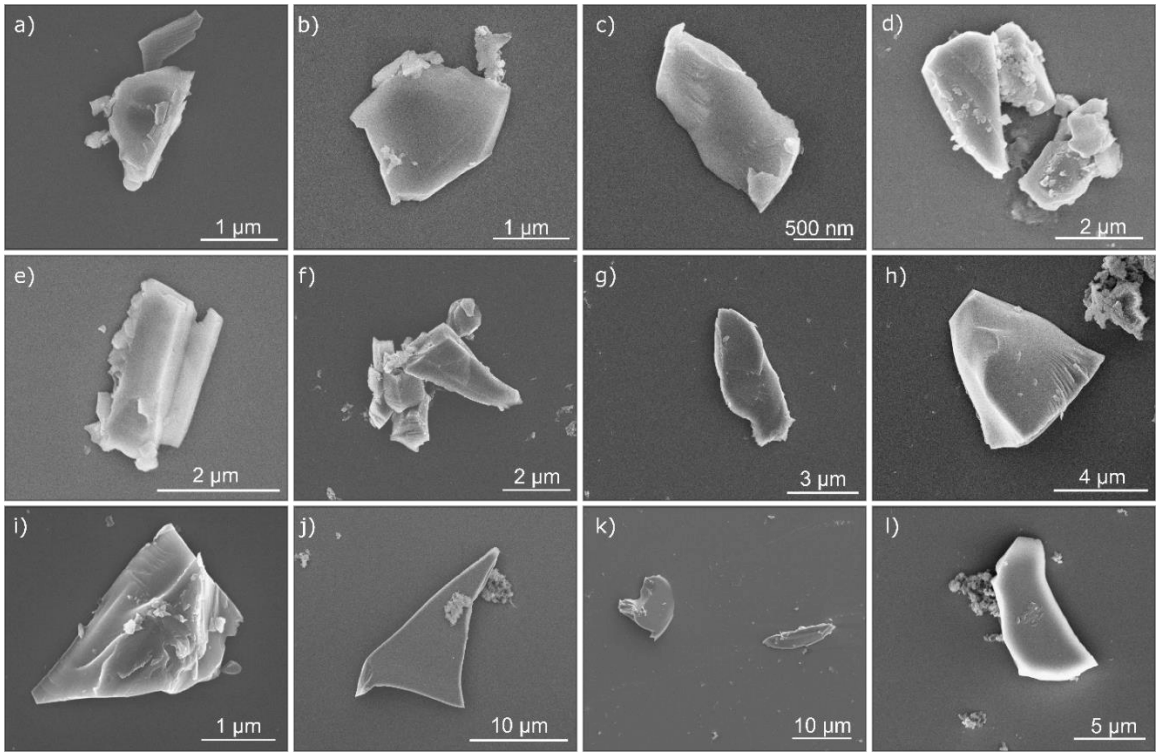

Figure S31. SEM analyses of COFs. SEM images show sheet-like morphology for the series of TpPa COFs prepared in a green solvent: a) TpPa-DC, b) TpPa-PC, c) TpPa-GBL, d) TpPa-ES, e) TpPa-PS, f) TpPa-Cyr, g) TpPa-IDE, h) TpPa-DF, i) TpPa-MP, j) TpPa-Tn, k) TpPa-Cym, and l) TpPa-PCl.

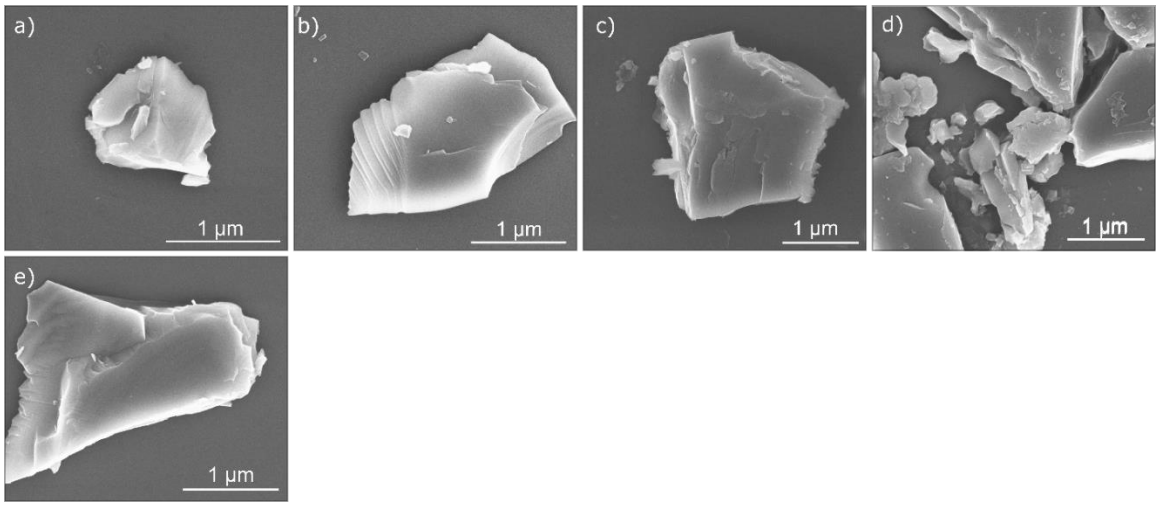

Figure S32. SEM analyses of COFs. SEM images show sheet-like morphology for the series of TpBD COFs prepared in a green solvent: a) TpBD-PC, b) TpBD-GBL, c) TpBD-IDE, d) TpBD-Tn, and e) TpBD-PCl.

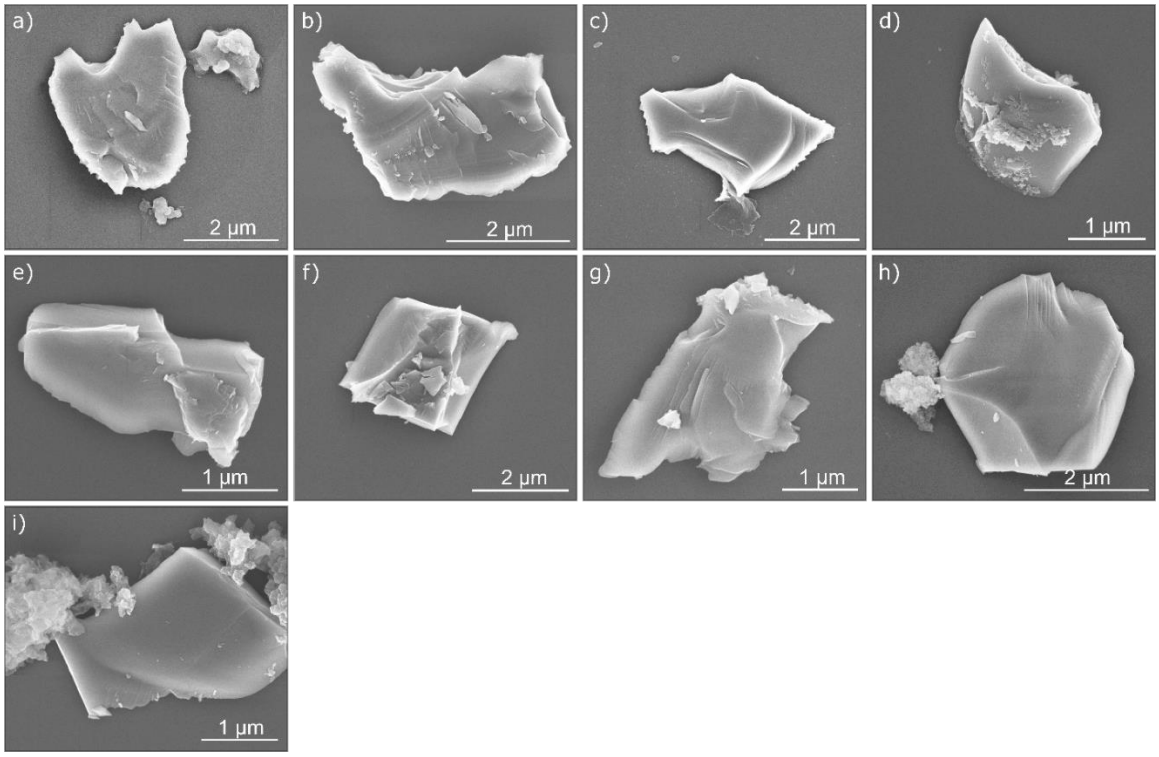

Figure S33. SEM analyses of COFs. SEM images show sheet-like morphology for the series of TpAzo COFs prepared in a green solvent: a) TpAzo-DC, b) TpAzo-PC, c) TpAzo-GBL, d) TpAzo-IDE, e) TpAzo-DF, f) TpAzo-MP, g) TpAzo-Cym, h) TpAzo-Tn, and i) TpAzo-PCl.

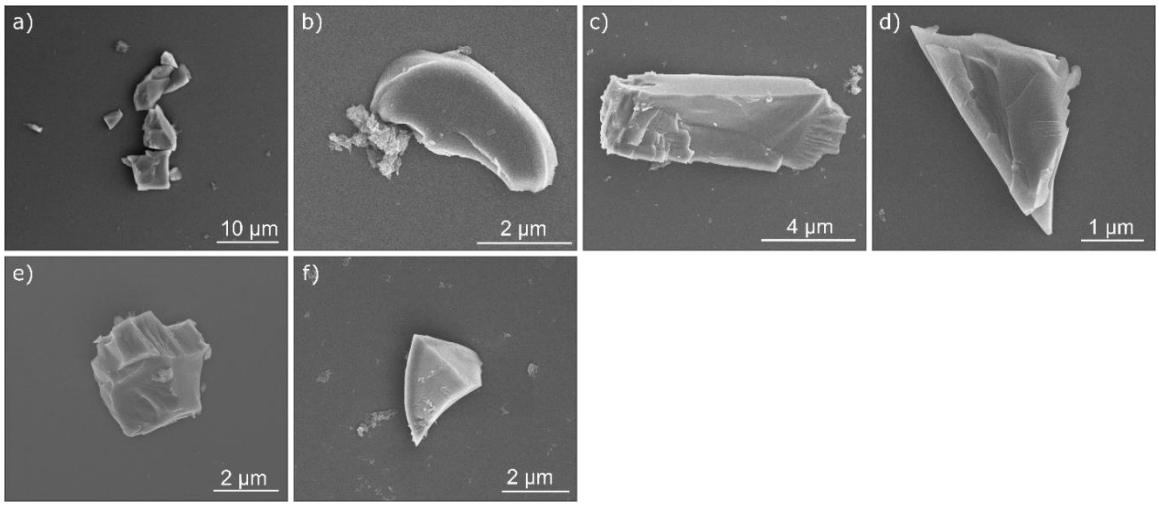

Figure S34. SEM analyses of COFs. SEM images show sheet-like morphology for the series of TpAnq COFs prepared in a green solvent: a) TpAnq-PC, b) TpAnq-GBL, c) TpAnq-IDE, d) TpAnq-DF, e) TpAnq-Cym, and f) TpAnq-PCl.

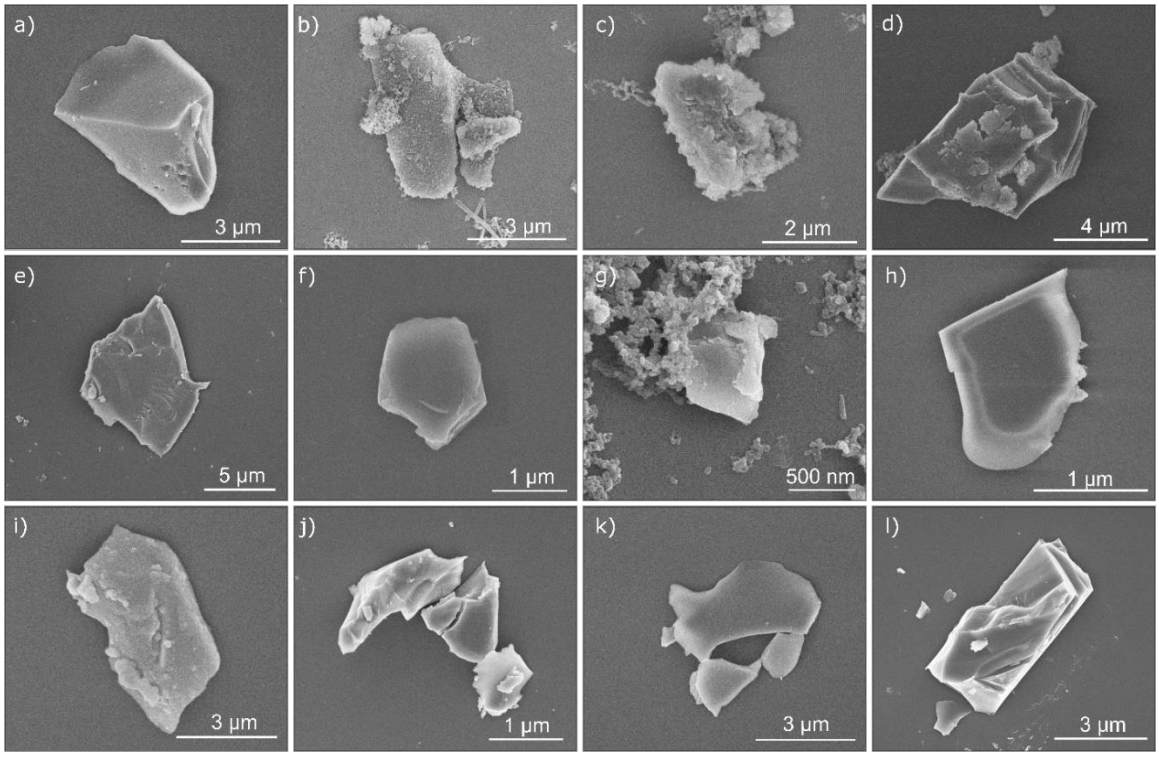

Figure S35. SEM analyses of COFs. SEM images show sheet-like morphology for the series of TpTab COFs prepared in a green solvent: a) TpTab-DC, b) TpTab-PC, c) TpTab-GBL, d) TpTab-ES, e) TpTab-PS, f) TpTab-Cyr, g) TpTab-IDE, h) TpTab-DF, i) TpTab-MP, j) TpTab-Tn, k) TpTab-Cym, and l) TpTab-PCl.

Section S11: Digital pictures of as-synthesized COFs

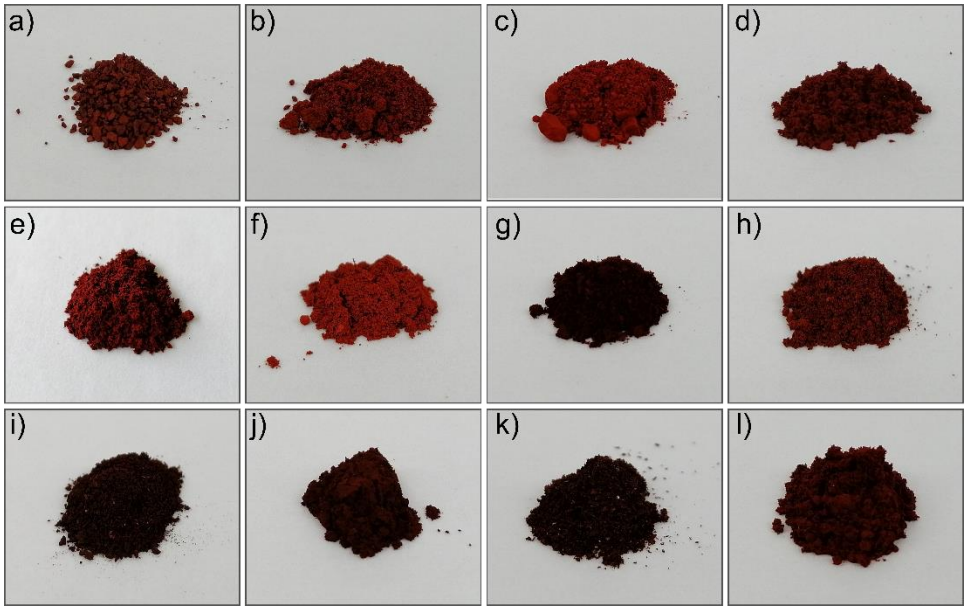

Figure S36. Digital images of the series of TpPa COFs synthesized in green solvents: a) TpPa-DC, b) TpPa-PC, c) TpPa-GBL, d) TpPa-ES, e) TpPa-PS, f) TpPa-Cyr, g) TpPa-IDE, h) TpPa-DF, i) TpPa-MP, j) TpPa-Tn, k) TpPa-Cym, and l) TpPa-PCl.

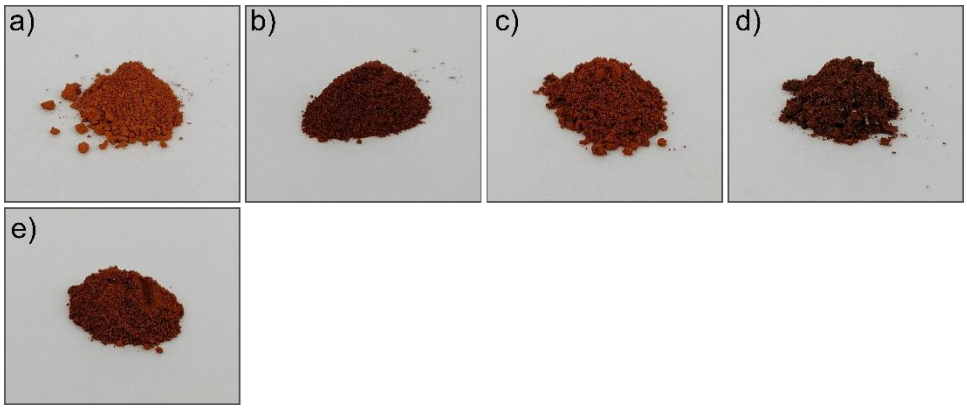

Figure S37. Digital images of the series of TpBD COFs prepared in a green solvent: a) TpBD-PC, b) TpBD-GBL, c) TpBD-IDE, d) TpBD-Tn, and e) TpBD-PCl.

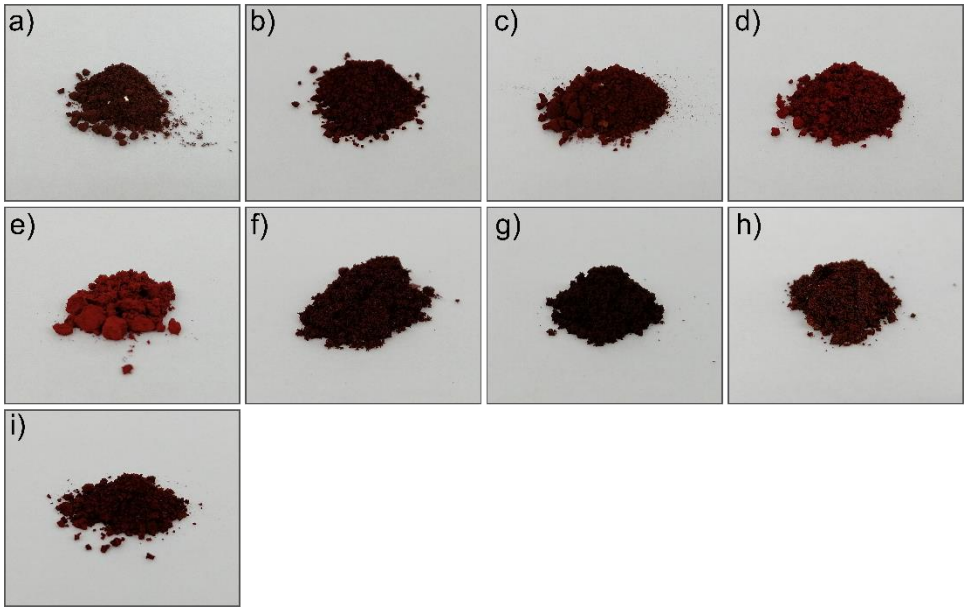

Figure S38. Digital images of the series of TpAzo COFs prepared in a green solvent: a) TpAzo-DC, b) TpAzo-PC, c) TpAzo-GBL, d) TpAzo-IDE, e) TpAzo-DF, f) TpAzo-MP, g) TpAzo-Cym, h) TpAzo-Tn, and i) TpAzo-PCl.

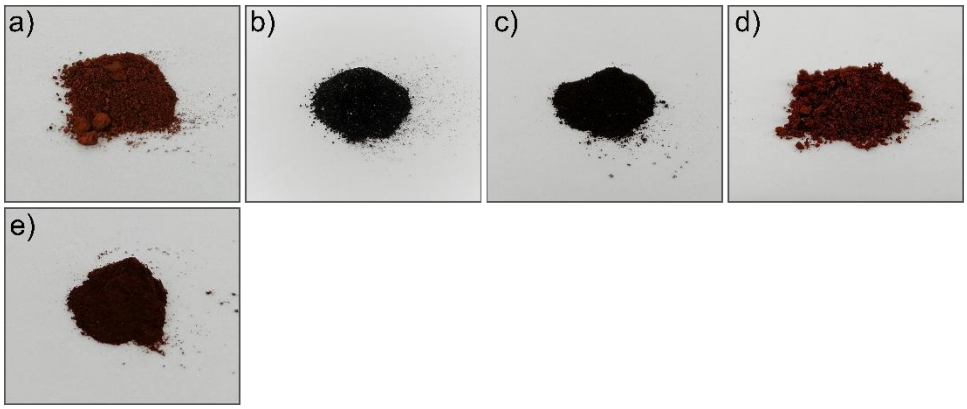

Figure S39. Digital images of the series of TpAnq COFs prepared in a green solvent: a) TpAnq-PC, b) TpAnq-GBL, c) TpAnq-IDE, d) TpAnq-DF, e) TpAnq-Cym, and f) TpAnq-PCl.

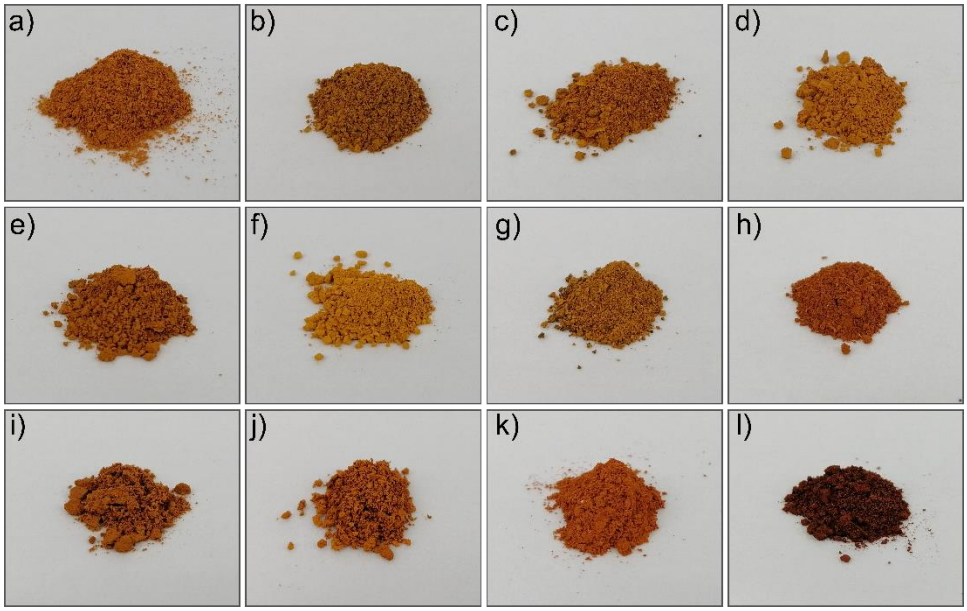

Figure S40. Digital images of the series of TpTab COFs prepared in a green solvent: a) TpTab-DC, b) TpTab-PC, c) TpTab-GBL, d) TpTab-ES, e) TpTab-PS, f) TpTab-Cyr, g) TpTab-IDE, h) TpTab-DF, i) TpTab-MP, j) TpTab-Tn, k) TpTab-Cym, and l) TpTab-PCl.

Section S12: Analysis of nitrogen gas uptake BET isotherms of as-synthesized COFs

BET theory is an extension of Langmuir theory, which is widely used to determine the adsorption of gas molecules forming a monolayer on a solid surface; monolayer formation is related to the physical adsorption of gas molecules on a solid surface. BET equation describes the relationship between the number of gas molecules adsorbed at a given relative pressure. Therefore, it serves as the basis for the measurement of the specific surface area of a material.

The BET equation is

$$\frac{1}{v[(p_o/p)-1]} = \frac{c-1}{v_m c}\left(\frac{p}{p_o}\right) + \frac{1}{v_m c}$$

where p and p_o are the equilibrium and saturation pressure of adsorbents at the adsorption temperature; v is the adsorbed gas quantity (for example, in volume units); and v_m is the adsorbed gas quantity on the monolayer; c is the BET constant.

Table S11. Correlation coefficient (r) values of all the as-synthesized COFs.

COF series	COF	Solvent used	Correlation coefficient (r)
TpPa	TpPa-DC	Dimethyl carbonate	0.9999
	TpPa-PC	Propylene carbonate	0.9999
	TpPa-GBL	γ-butyrolactone	0.9994
	TpPa-ES	1,2-ethylenesulfite	0.9998
	TpPa-PS	1,3-propylenesulfite	0.9998
	TpPa-Cyr	Cyrene	0.9999
	TpPa-IDE	Isosorbide dimethyl ether	0.9997
	TpPa-DF	2,5-dimethylfuran	0.9998
	TpPa-MP	2-methyl-1-propanol	0.9999
	TpPa-Tn	Terpineol	0.9999
	TpPa-Cym	Para-Cymene	0.9999
	TpPa-PCl	Rhodiasolv polar clean	0.9999
TpBD	TpBD-PC	Propylene carbonate	0.9996
	TpBD-GBL	γ-butyrolactone	0.9997
	TpBD-IDE	Isosorbide dimethyl ether	0.9999
	TpBD-Tn	Terpineol	0.9993

	TpBD-PCl	Rhodiasolv polar clean	0.9996
TpAzo	TpAzo-DC	Dimethyl carbonate	0.9995
	TpAzo-PC	Propylene carbonate	0.9996
	TpAzo-GBL	γ-butyrolactone	0.9997
	TpAzo-IDE	Isosorbide dimethyl ether	0.9996
	TpAzo-DF	2,5-dimethylfuran	0.9999
	TpAzo-MP	2-methyl-1-propanol	0.9999
	TpAzo-Tn	Terpineol	0.9997
	TpAzo-Cym	Para-Cymene	0.9942
	TpAzo-PCl	Rhodiasolv polar clean	0.9998
TpAnq	TpAnq-PC	Propylene carbonate	0.9999
	TpAnq-IDE	Isosorbide dimethyl ether	0.9999
	TpAnq-DF	2,5-dimethylfuran	0.9999
	TpAnq-Cym	Para-Cymene	0.9999
	TpAnq-PCl	Rhodiasolv polar clean	0.9999
TpTab	TpTab-DC	Dimethyl carbonate	0.9999
	TpTab-PC	Propylene carbonate	0.9999
	TpTab-GBL	γ-butyrolactone	0.9999
	TpTab-ES	1,2-ethylenesulfite	0.9999
	TpTab-PS	1,3-propylenesulfite	0.9999
	TpTab-Cyr	Cyrene	0.9997
	TpTab-IDE	Isosorbide dimethyl ether	0.9999
	TpTab-DF	2,5-dimethylfuran	0.9991
	TpTab-MP	2-methyl-1-propanol	0.9999
	TpTab-Tn	Terpineol	0.9996
	TpTab-Cym	Para-Cymene	0.9997
	TpTab-PCl	Rhodiasolv polar clean	0.9999

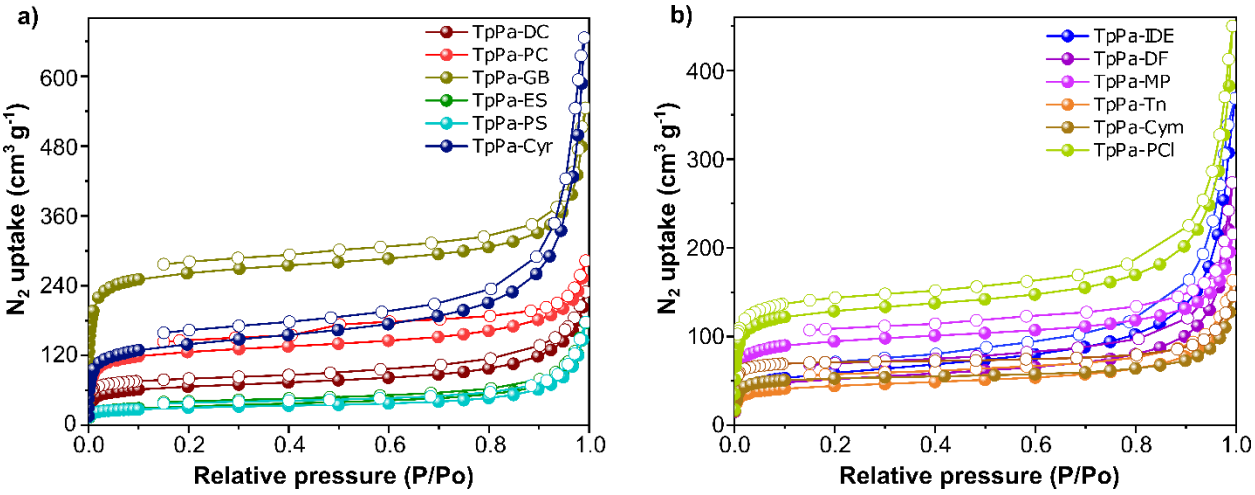

Figure S41. Nitrogen gas uptake BET isotherms. TpPa COFs synthesized in various green solvents resulted in different surface areas, which reflected in their respective nitrogen gas adsorption isotherms.

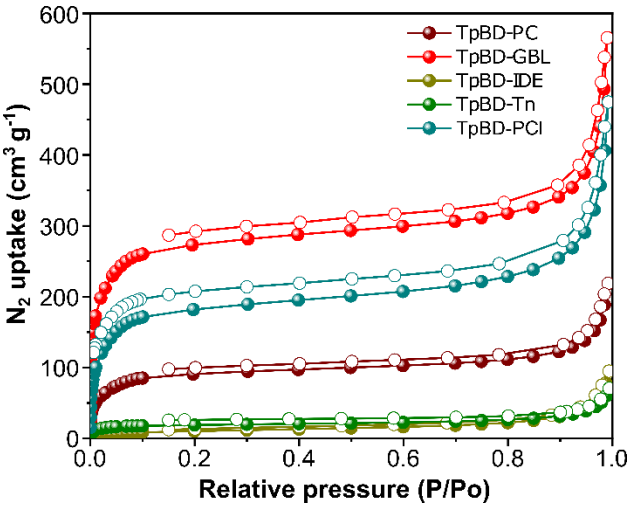

Figure S42. Nitrogen gas uptake BET isotherms. TpBD COFs synthesized in various green solvents resulted in different surface areas, which reflected in their respective nitrogen gas adsorption isotherms.

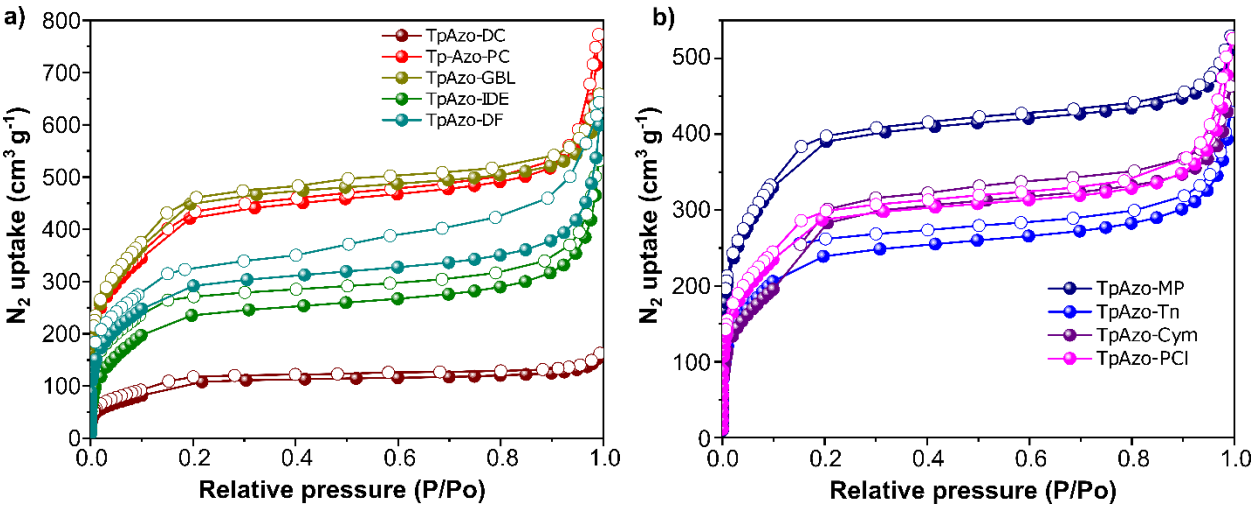

Figure S43. Nitrogen gas uptake BET isotherms. TpAzo COFs synthesized in various green solvents resulted in different surface areas, which reflected in their respective nitrogen gas adsorption isotherms.

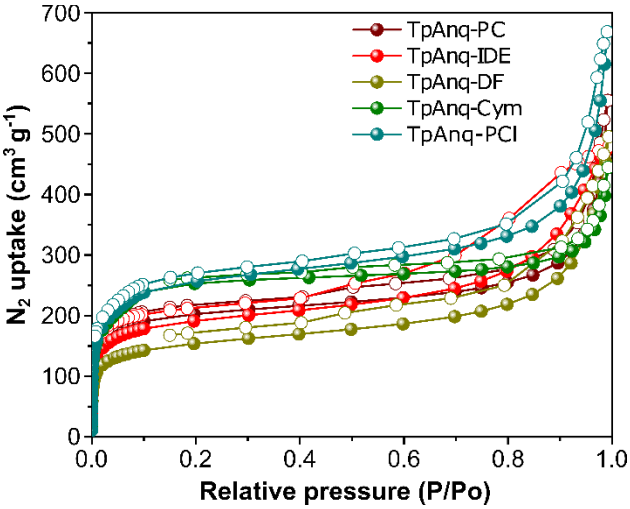

Figure S44. Nitrogen gas uptake BET isotherms. TpAnq COFs synthesized in various green solvents resulted in different surface areas, which reflected in their respective nitrogen gas adsorption isotherms.

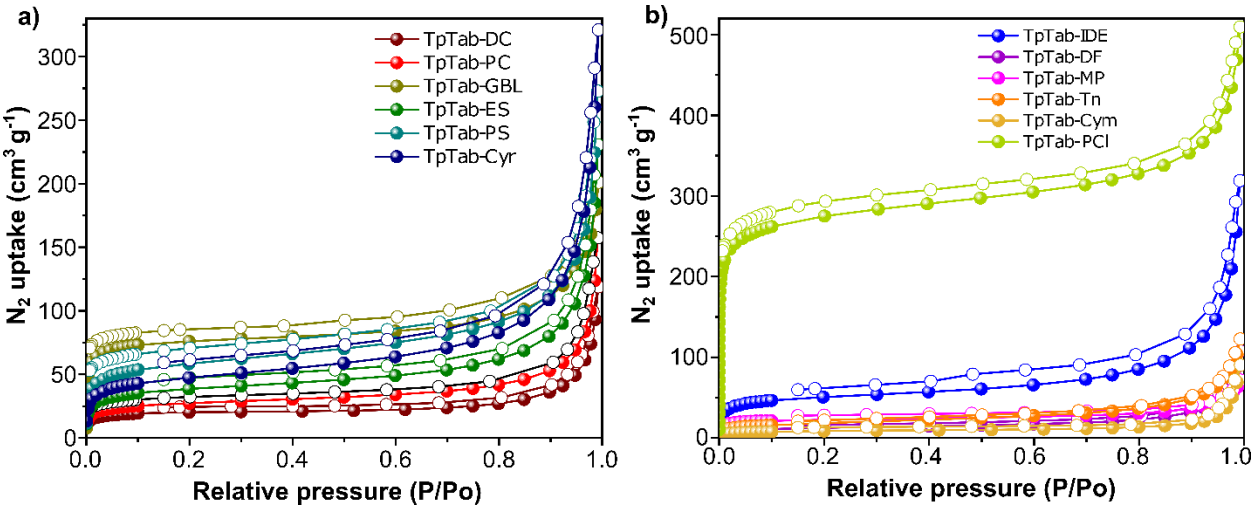

Figure S45. Nitrogen gas uptake BET isotherms. TpTab COFs synthesized in various green solvents resulted in different surface areas, which reflected in their respective nitrogen gas adsorption isotherms.

Table S12. Nitrogen gas uptake values for the prepared series of COFs.

COFs	**BET ($m^2 g^{-1}$)**	**COFs**	**BET ($m^2 g^{-1}$)**	**COFs**	**BET ($m^2 g^{-1}$)**	**COFs**	**BET ($m^2 g^{-1}$)**	**COFs**	**BET ($m^2 g^{-1}$)**
TpPa-DC	247	-	-	TpAzo-DC	399	-	-	TpTab-DC	77
TpPa-PC	473	TpBD-PC	363	TpAzo-PC	1562	TpAnq-PC	785	TpTab-PC	102
TpPa-GBL	888	TpBD-GBL	1046	TpAzo-GBL	1674	-	-	TpTab-GBL	288
TpPa-ES	113	-	-	-	-	-	-	TpTab-ES	144
TpPa-PS	109	-	-	-	-	-	-	TpTab-PS	217
TpPa-Cyr	518	-	-	-	-	-	-	TpTab-Cyr	166
TpPa-IDE	207	TpBD-IDE	36	TpAzo-IDE	885	TpAnq-IDE	717	TpTab-IDE	190
TpPa-DF	197	-	-	TpAzo-DF	1065	TpAnq-DF	573	TpTab-DF	42
TpPa-MP	354	-	-	TpAzo-MP	1418	-	-	TpTab-MP	84
TpPa-Tn	163	TpBD-Tn	69	TpAzo-Tn	879	-	-	TpTab-Tn	63
TpPa-Cym	197	-	-	TpAzo-Cym	1118	TpAnq-Cym	1033	TpTab-Cym	30
TpPa-PCl	480	TpBD-PCl	718	TpAzo-PCl	1077	TpAnq-PCl	1000	TpTab-PCl	1036
TpPa[a]	535[14]	TpBD[a]	537[14]	TpAzo[b]	1328[12]	TpAnq[c]	435[15]	TpTab[d]	567[16]

Solvent used: [a]Mesitylene and Dioxane, [b]N,N-dimethylacetamide and 1,2-dichlorobenzene, [c]N,N-dimethylacetamide, [d]dioxane

Section S13: Pore size distribution profiles of as-synthesized COFs

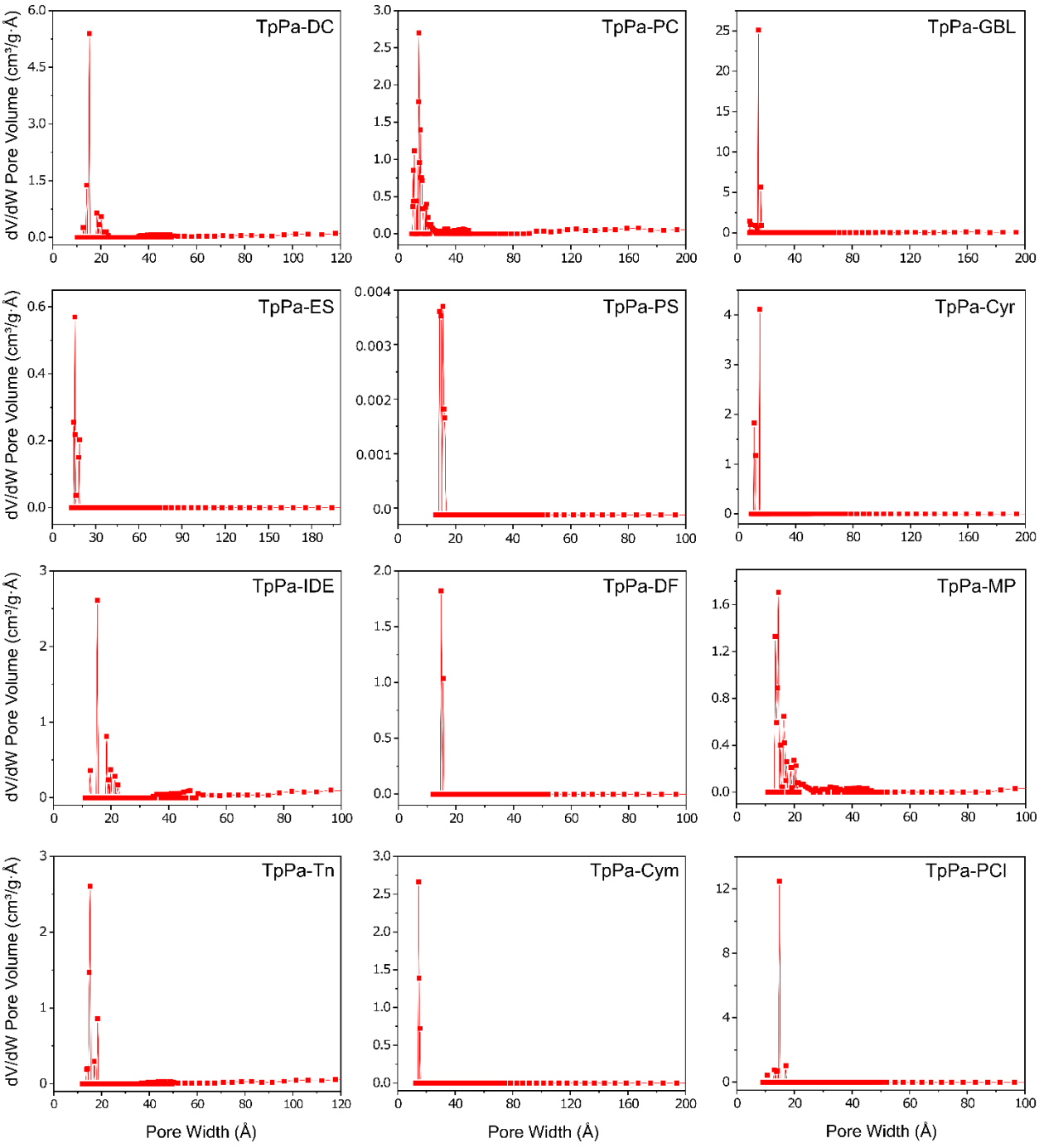

Figure S46. Pore size distribution of COFs. Pore size distribution curves of a series of **TpPa** COFs calculated using non-local density functional theory (NLDFT) show similar pore size distribution for all the COFs synthesized from various green solvents.

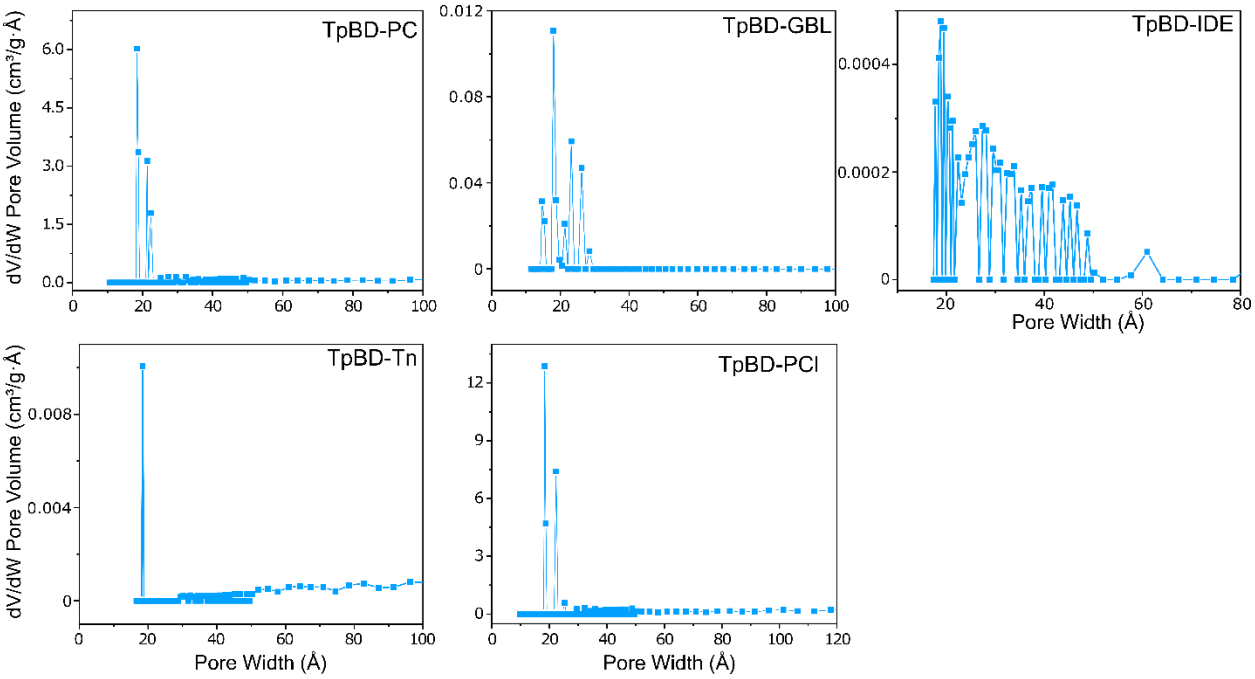

Figure S47. Pore size distribution of COFs. Pore size distribution curves of series of **TpBD** COFs calculated using non-local density functional theory (NLDFT) show similar pore size distribution for all the COFs synthesized from various green solvents.

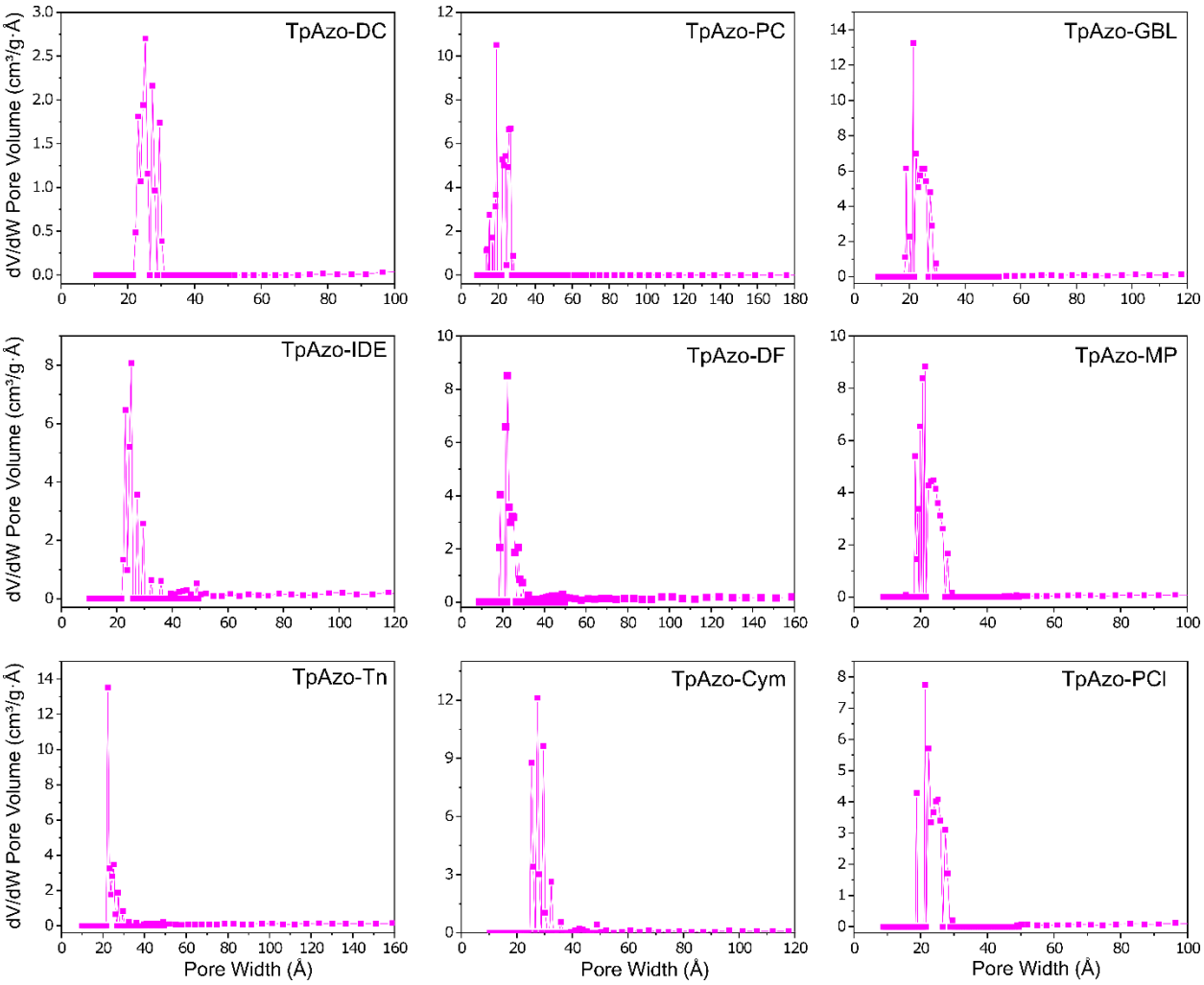

Figure S48. Pore size distribution of COFs. Pore size distribution curves of series of **TpAzo** COFs calculated using non-local density functional theory (NLDFT) show similar pore size distribution for all the COFs synthesized from various green solvents.

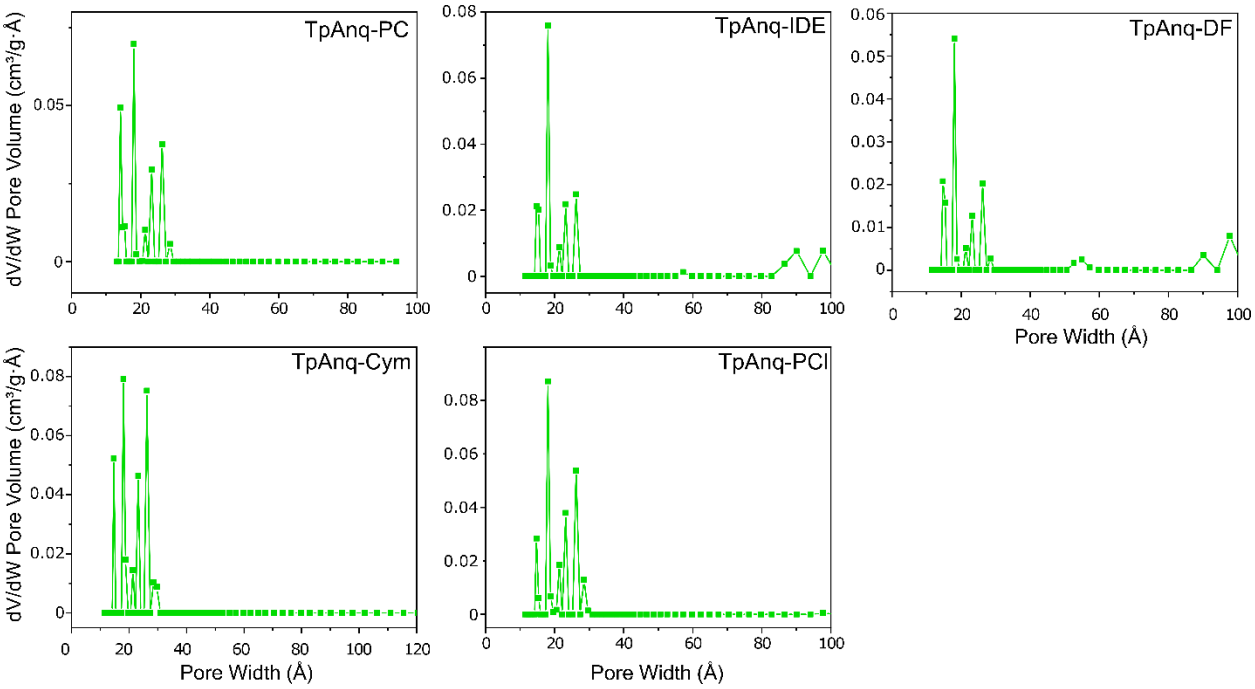

Figure S49. Pore size distribution of COFs. Pore size distribution curves of series of **TpAnq** COFs calculated using non-local density functional theory (NLDFT) show similar pore size distribution for all the COFs synthesized from various green solvents.

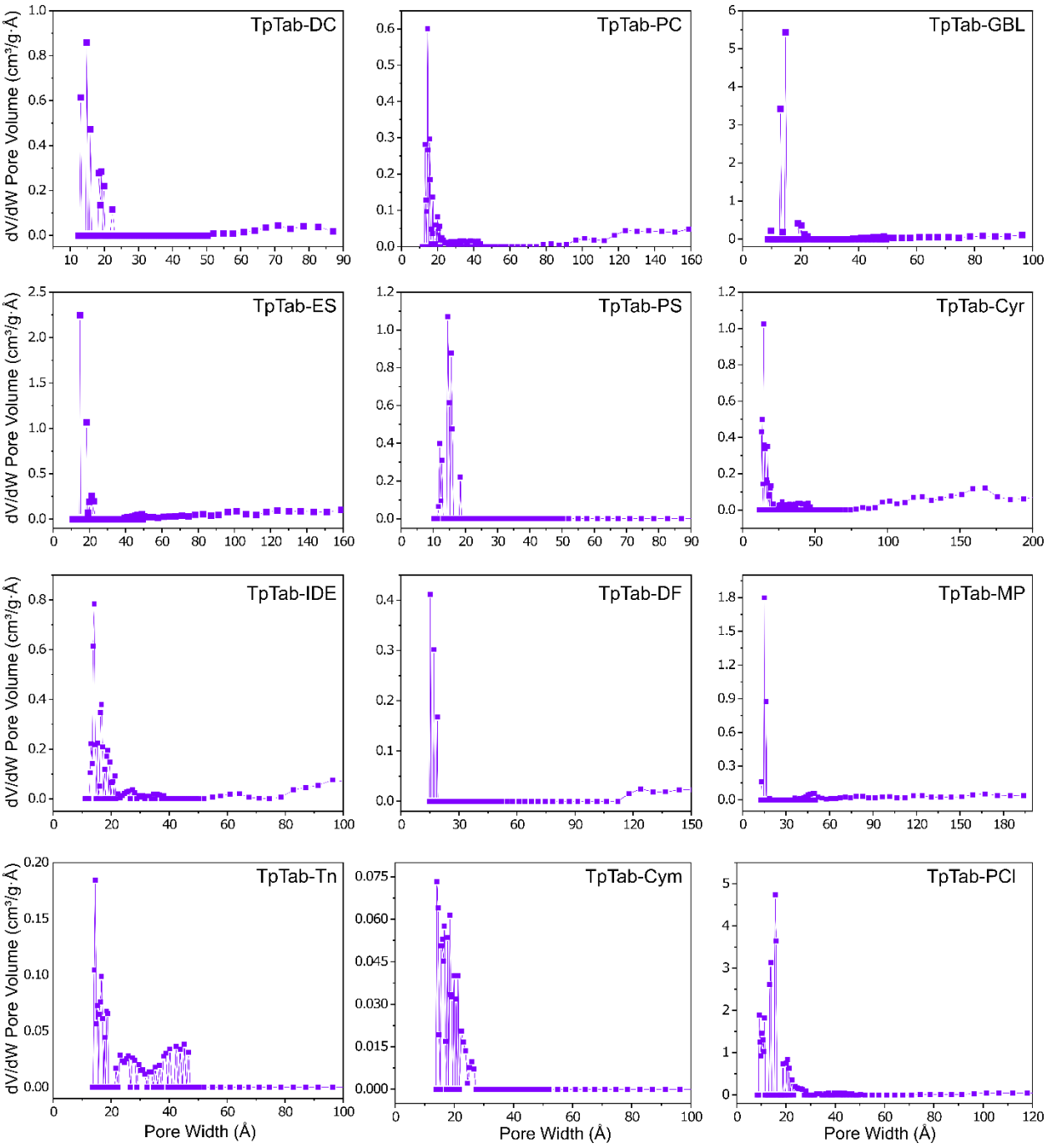

Figure S50. Pore size distribution of COFs. Pore size distribution curves of series of **TpTab** COFs calculated using non-local density functional theory (NLDFT) show similar pore size distribution for all the COFs synthesized from various green solvents.

Table S13. Pore widths (Å) of the prepared series of COFs.

COFs	Pore width (Å)	COFs	Pore width (Å)	COFs	Pore width (Å)	COFs	Pore width (Å)	COFs	Pore width (Å)
TpPa-DC	15.22	-	-	TpAzo-DC	25.23	-	-	TpTab-DC	14.87
TpPa-PC	14.51	TpBD-PC	18.44	TpAzo-PC	22.37	TpAnq-PC	18.07	TpTab-PC	14.51
TpPa-GBL	14.87	TpBD-GBL	18.07	TpAzo-GBL	22.37	-	-	TpTab-GBL	14.87
TpPa-ES	15.58	-	-	-	-	-	-	TpTab-ES	14.87
TpPa-PS	15.58	-	-	-	-	-	-	TpTab-PS	14.51
TpPa-Cyr	14.87	-	-	-	-	-	-	TpTab-Cyr	14.51
TpPa-IDE	15.22	TpBD-IDE	18.80	TpAzo-IDE	25.23	TpAnq-IDE	18.07	TpTab-IDE	14.15
TpPa-DF	14.87	-	-	TpAzo-DF	22.37	TpAnq-DF	18.07	TpTab-DF	15.22
TpPa-MP	14.51	-	-	TpAzo-MP	21.3	-	-	TpTab-MP	14.87
TpPa-Tn	15.22	TpBD-Tn	18.44	TpAzo-Tn	22.37	-	-	TpTab-Tn	14.51
TpPa-Cym	14.51	-	-	TpAzo-Cym	25.23	TpAnq-Cym	18.07	TpTab-Cym	14.15
TpPa-PCl	14.87	TpBD-PCl	18.44	TpAzo-PCl	21.3	TpAnq-PCl	18.07	TpTab-PCl	15.58

Section S14: Classification and color coding for different properties of green solvents

According to the literature,[17] the COFs have been synthesized using a wide range of solvents, either in a sole or mixtures, at different temperature conditions. Herein, the green solvents used for the synthesis of the COFs are shown in table S13–S17. The selected solvents represent various chemical classes such as carbonates, esters, ethers, sulfites, alcohols, aromatics, and dipolar aprotic solvents. A color coding system was introduced in the GlaxoSmithKline and CHEM21 solvent selection guides, which were successfully utilized for the description of the sustainable synthesis of UiO-66.[18] The solvents were coded as red, green, and yellow, corresponding to the extent of their greenness. We followed the same color-coding system in this study. The properties of the solvents, such as boiling point and viscosity, and the corresponding COFs, such as characteristic peaks from the (100) plane and BET surface area, are color-coded according to a certain range criteria shown in Table S12.

Table S14. Ranking of boiling point (°C), viscosity (mPa s), surface area (m^2 g^{-1}), and COFs formation.

Color	Boiling point (°C)	Viscosity (η, mPa s)	Presence of characteristic peak (100) plane	SA_{BET} (m^2 g^{-1})
Green	50 <bp< 100	$\eta \geq 2$	Yes/crystalline	≥ 800
Yellow	100 <bp< 200	$5 \geq \eta \geq 2$	low crystalline	$800 < SA < 200$
Red	200 <bp< 300	$\eta > 5$	No reaction/amorphous	$SA < 200$

Besides the color code already in the literature for the assessment of greenness of a solvent, we incorporated a color code for the classification of the prepared COFs based on the presence of characteristic first peak in the PXRD patterns that correspond to the diffraction of the COFs from (100) planes. The conventional solvents reported for the synthesis of the COFs were also included as a reference for comparison. To synthesize thermodynamically stable crystalline *β*-ketoenamine-based COFs, the temperature at which the synthesis is conducted plays a crucial role in navigating the reversibility of the covalent bond formation and succeeding the network augmentation. Under ambient conditions, kinetically disordered, amorphous polymer products are often formed. In fact, the reversible covalent bond formation and extension demand energy of 50–110 kcal mol^{-1} can be easily achieved at high temperature and pressure.[19] Despite performing the synthesis in nearly identical conditions, some of the screened solvents were incompetent. In such cases,

the resulting COFs are either amorphous or no reaction occurred; hence, such cases are coded red (table S13–S17).

Table S15. Assessment of the green solvents used in the synthesis of TpPa COFs. The color coding is adapted from Venturi et al.[18]

Classification	Solvent	Overall green assessment	Boiling point (°C)	Viscosity (η, mPa s)	COF	Presence of characteristic peak (100) plane	BET surface area ($m^2 g^{-1}$)	Default rank	Ranking after discussion
Carbonate	DC		90	0.7	TpPa–DC	Yes	247		
	PC		242	5.4	TpPa–PC	Yes	473		
Ester	GBL		204	1.8	TpPa–GBL	Yes	888		
Sulfite	ES		159.1	1.6	TpPa–ES	Yes	113		
	PS		211-217	1.5	TpPa–PS	Yes	109		
Ether	Cyr		226	3.4	TpPa–Cyr	Yes	518		
	IDE		93-95	2.8	TpPa–IDE	Yes	207		
	DF		93.5	0.7	TpPa–DF	Yes	197		
Alcohol	MP		108	1.2	TpPa–MP	Yes	354		
	Tn		214-217	4.8	TpPa–Tn	Yes	163		
Aromatic	Cym		177	1.2	TpPa–Cym	Yes	197		
Aprotic	PCl		281.9	24.2	TpPa–PCl	Yes	480		
	M/D*[14]		-	-		Yes	535		
	Water[20]		100	9.1		Yes	633		

*M = Mesitylene, and D = 1,4-Dioxane

According to the results shown in table S13, all the twelve green solvents used in the synthesis resulted in the formation of **TpPa** COFs, suggesting the compatibility of the solvents with the reaction conditions. The resulting COFs were characterized by PXRD patterns. Analysis of the PXRD patterns indicates the presence of the characteristic peak corresponding to the diffraction from (100) planes; hence, the COFs exhibiting this property are coded green. Furthermore, the BET surface areas of the COFs are color-coded based on whether their respective values are high or low. For example, the highest surface area of 888 $m^2 g^{-1}$ observed in **TpPa-GBL** is coded green, whereas the lowest surface area (113 $m^2 g^{-1}$) observed for **TpPa-ES** is coded red. The color code in the column 'Default rank' is basically adapted from the column defining the surface area of the as-synthesized COFs. The color code in the column 'Rank after discussion' is defined according to the overall assessment of the solvent properties as well as the COFs features. As per the classification mentioned in the table S12, the column basically provides the information on the efficiency of the respective green solvents in producing crystalline and porous COFs. The reason for such color coding is to identify the solvents that are most suitable for the preparation of the COFs with improved surface area. For example, the GBL solvent, which is green-coded in the "Overall green assessment" column, is efficient in delivering crystalline (this information is deduced from relative crystallinity plot) and porous COFs (this information is deduced from SA_{BET} column). Therefore, the GBL solvent in the "Rank after discussion" column has been green-coded. Although the quality of the COFs prepared in typical solvents such as N, N-Dimethylacetamide (DMAc) is comparable, it is still listed as "not recommended" for their reproving toxicological behavior.

Table S16. Assessment of the green solvents used in the synthesis of TpBD COFs. The color coding is adapted from Venturi et al.[18]

Classification	Solvent	Overall green assessment	Boiling point (°C)	Viscosity (η, mPa s)	COF	Presence of characteristic peak (100) plane	BET surface area (m^2 g^{-1})	Default rank	Ranking after discussion
Carbonate	DC		90	0.7	TpBD–DC	NR	-		
	PC		242	5.4	TpBD–PC	Yes	363		
Ester	GBL		204	1.8	TpBD–GBL	Yes	1046		
Sulfite	ES		159.1	1.6	TpBD–ES	NR	-		
	PS		211-217	1.5	TpBD–PS	NR	-		
Ether	Cyr		226	3.4	TpBD–Cyr	NR	-		
	IDE		93-95	2.8	TpBD–IDE	Yes	36		
	DF		93.5	0.7	TpBD–DF	NR	-		
Alcohol	MP		108	1.2	TpBD–MP	NR	-		
	Tn		214-217	4.8	TpBD–Tn	Yes	69		
Aromatic	Cym		177	1.2	TpBD–Cym	NR	-		
Aprotic	PCl		281.9	24.2	TpBD–PCl	Yes	718		
	M/D*[14]		-	-		Yes	537		
	Water[20]		100	9.1		Yes	601		

*M = Mesitylene, and D = 1,4-Dioxane; NR = No reaction

According to the results shown in table S14, five out of the twelve green solvents used in the synthesis resulted in the formation of **TpBD** COFs, suggesting the compatibility of the solvents with the reaction conditions. The resulting COFs were characterized by their PXRD patterns. Analysis of the PXRD patterns indicates the presence of the characteristic peak corresponding to the diffraction from (100) planes; hence, the COFs exhibiting this property are coded green. Formation of no COFs or amorphous polymers are coded red. The BET surface areas of the COFs are color-coded as described earlier. That is, the highest surface area of 1046 m^2 g^{-1} observed for **TpBD-GBL** is coded green, whereas the lowest one (36 m^2 g^{-1}) observed for **TpBD-IDE** is coded red. The color code in the column 'Default rank' are basically adapted from the column defining the surface area of the as-synthesized COFs. The color code in the column 'Rank after discussion' are defined based on the overall assessment of the solvent properties as well as the COFs features. As per classification mentioned in the table S12, the column basically provides the information on the efficiency of the respective green solvents in the synthesis of crystalline and porous COFs. For example, the GBL solvent, coded green in the "Overall green assessment" column, is efficient in delivering the formation of crystalline (this information is deduced from relative crystallinity plot) and porous COFs (this information is deduced from SA_{BET} column. Therefore, the GBL in the "Rank after discussion" column is assigned the green code. In addition, **TpBD-PCl** synthesized in PolarClean also shows an SA_{BET} of 718 m^2 g^{-1}, which is relatively high compared to the rest of the solvents. Considering this, it is coded yellow in the "Rank after discussion" column. It is worth mentioning that the **TpBD** COFs synthesized in the GBL solvent exhibits an improved SA_{BET} value when compared to the those synthesized in a conventional organic solvent mesitylene : dioxane mixture and in water, which are reported in the literature.[17,20] This

clearly suggests high efficiency of the green solvents over conventional organic solvents in delivering crystalline and porous COFs.

Table S17. Assessment of the green solvents used in the synthesis of TpAzo COFs. The color coding is adapted from Venturi et al.[18]

Classification	Solvent	Overall green assessment	Boiling point (°C)	Viscosity (η, mPa s)	COF	Presence of characteristic peak (100) plane	BET surface area ($m^2 g^{-1}$)	Default rank	Ranking after discussion
Carbonate	DC		90	0.7	TpAzo–DC	Yes	400		
	PC		242	5.4	TpAzo–PC	Yes	1562		
Ester	GBL		204	1.8	TpAzo–GBL	Yes	1674		
Sulfite	ES		159.1	1.6	TpAzo–ES	NR	-		
	PS		211-217	1.5	TpAzo–PS	NR	-		
Ether	Cyr		226	3.4	TpAzo–Cyr	NR	-		
	IDE		93-95	2.8	TpAzo–IDE	Yes	885		
	DF		93.5	0.7	TpAzo–DF	Yes	1065		
Alcohol	MP		108	1.2	TpAzo–MP	Yes	1418		
	Tn		214-217	4.8	TpAzo–Tn	Yes	879		
Aromatic	Cym		177	1.2	TpAzo–Cym	Yes	1118		
Aprotic	PCl		281.9	24.2	TpAzo–PCl	Yes	1077		
	DMAc/o-DCB*[12]					Yes	1328		

*DMAc = N,N-Dimethylacetamide, and o-DCB = 1,2-Dichlorobenzene

According to the results shown in table S14, nine out of the twelve green solvents employed in the synthesis resulted in the formation of **TpAzo** COFs, suggesting the compatibility of the solvents with the reaction conditions. The resulted COFs were characterized by their PXRD patterns. Analysis of the PXRD patterns indicates the presence of the characteristic peak corresponding to the diffraction from (100) planes; hence, the COFs exhibiting this property are coded green. Formation of no COFs or amorphous polymers are coded red. The SA_{BET} values of the COFs, which suggest their high porous nature, are color-coded as described earlier. For example, the highest surface area of 1674 $m^2 g^{-1}$ observed for **TpBD-GBL** is coded green, whereas the lowest one (400 $m^2 g^{-1}$) observed for **TpAzo-DC** is coded yellow. The color code in the column 'Default rank' are basically adapted from the column defining the surface area of the as-synthesized COFs. The color code in the column 'Rank after discussion' are defined based on the overall assessment of the solvent properties as well as the COFs features. As per classification mentioned in the table S12, the column basically provides the information on the efficiency of the respective green solvent in the synthesis of crystalline and porous COFs. For example, the GBL, PC, and MP solvents, which are coded green in the "Overall green assessment" column, are efficient in delivering the crystalline (this information is deduced from relative crystallinity plot) and porous COFs (this information is deduced from SA_{BET} column). Therefore, the GBL solvent in the "Rank after discussion" column is coded green. It is worth mentioning that the **TpAzo** COFs synthesized in the GBL, PC, and MP solvents exhibit improved SA_{BET} values when

compare to those synthesized in a conventional organic solvent DMAc : *o*-DCB mixture reported in the literature.[12] This clearly suggests high efficiency of the green solvents over conventional organic solvents in delivering crystalline and porous COFs.

Table S 18. Assessment of the green solvents used in the synthesis of TpAnq COFs. The color coding is adapted from Venturi et al.[18]

Classification	Solvent	Overall green assessment	Boiling point (°C)	Viscosity (η, mPa s)	COF	Presence of characteristic peak (100) plane	BET surface area ($m^2\ g^{-1}$)	Default rank	Ranking after discussion
Carbonate	DC		90	0.7	TpAnq–DC	NR	-		
	PC		242	5.4	TpAnq–PC	Yes	785		
Ester	GBL		204	1.8	TpAnq–GBL	NR	-		
Sulfite	ES		159.1	1.6	TpAnq–ES	NR	-		
	PS		211-217	1.5	TpAnq–PS	NR	-		
Ether	Cyr		226	3.4	TpAnq–Cyr	NR	-		
	IDE		93-95	2.8	TpAnq–IDE	Yes	717		
	DF		93.5	0.7	TpAnq–DF	Yes	573		
Alcohol	MP		108	1.2	TpAnq–MP	NR	-		
	Tn		214-217	4.8	TpAnq–Tn	NR	-		
Aromatic	Cym		177	1.2	TpAnq–Cym	Yes	1033		
Aprotic	PCl		281.9	24.2	TpAnq–PCl	Yes	1000		
	DMAc*[15]					Yes	435		
	Water[20]		100	9.1		Yes	489		

*DMAc = *N*,*N*-Dimethylacetamide

According to the results shown in table S14, nine out of the twelve green solvents employed in the synthesis resulted in the formation of **TpAnq** COFs, suggesting the compatibility of the solvents with the reaction conditions. The resulting COFs were characterized by their PXRD patterns. Analysis of the PXRD patterns indicates the presence of the characteristic peak corresponding to the diffraction from (100) planes; hence, the COFs exhibiting this property are coded green. Formation of no COFs or amorphous polymers are coded red. The SA_{BET} values of COFs are color-coded as described earlier. For example, the highest surface area of 1033 $m^2\ g^{-1}$ observed for **TpAnq–Cym** is coded green, whereas the lowest one (573 $m^2\ g^{-1}$) observed for **TpAnq–DF** is coded yellow. The color code in the column 'Default rank' are basically adapted from the column defining the surface area of the as-synthesized COFs. The color code in the column 'Rank after discussion' are defined according to the overall assessment of the solvent properties as well as the COFs features. As per classification mentioned in the table S12, the column basically provides the information on the efficiency of the respective green solvent in the synthesis of crystalline and porous COFs. As-synthesized **TpAnq** COFs exhibit improved surface areas when compared those synthesized in DMAc[15] or water.[20] This clearly suggests high efficiency of the green solvents over conventional organic solvents in delivering crystalline and porous COFs.

Table S19. Assessment of the green solvents used in the synthesis of TpTab COFs. The color coding is adapted from Venturi et al.[18]

Classification	Solvent	Overall green assessment	Boiling point (°C)	Viscosity (η, mPa s)	COF	Presence of characteristic peak (100) plane	BET surface area (m^2 g^{-1})	Default rank	Ranking after discussion
Carbonate	DC		90	0.7	TpTab–DC	Yes	77		
	PC		242	5.4	TpTab–PC	Yes	102		
Ester	GBL		204	1.8	TpTab–GBL	Yes	288		
Sulfite	ES		159.1	1.6	TpTab–ES	Yes	144		
	PS		211-217	1.5	TpTab–PS	Yes	217		
Ether	Cyr		226	3.4	TpTab–Cyr	Yes	166		
	IDE		93-95	2.8	TpTab–IDE	Yes	190		
	DF		93.5	0.7	TpTab–DF	Yes	42		
Alcohol	MP		108	1.2	TpTab–MP	Yes	84		
	Tn		214-217	4.8	TpTab–Tn	Yes	63		
Aromatic	Cym		177	1.2	TpTab–Cym	Yes	30		
Aprotic	PCl		281.9	24.2	TpTab–PCl	Yes	1036		
	M/D*[16]					Yes	567		

*M = Mesitylene, and D = 1,4-Dioxane

According to the results shown in table S14, all twelve green solvents used in the synthesis produced **TpTab** COFs, suggesting that the solvents are compatible with the reaction conditions. The resulting COFs were characterized by PXRD measurements. Analysis of the PXRD patterns indicates the presence of characteristic diffraction peaks corresponding to diffraction from (100) planes; hence, the COFs exhibiting these peaks are coded green. No COF or amorphous polymer formations are red-coded. The eighth column of the table displays the values of the SA_{BET} of the COFs, which suggest their high porous nature. This property of COFs is color-coded accordingly. For example, the BET surface of **TpTab-PCl** (1036 m^2 g^{-1}) is the highest; hence, it is green-coded in the table. Accordingly, the lowest BET surface (30 m^2 g^{-1}) is observed for **TpTab-Cym**, and thus it is red-coded in the table. The color code in the column 'Default rank' are basically adapted from the column defining the surface area of the as-synthesized COFs. The color code criteria in the column 'Rank after discussion' are defined based on the overall assessment of the solvent properties as well as the COFs features. As per the classification mentioned in table S12, the column basically provides an information on the efficiency of the respective green solvent in the synthesis of crystalline and porous COFs. Among the green solvents used in this study, PCl is efficient in forming crystalline (this information is deduced from relative crystallinity plot) and porous COFs (this information is deduced from SA_{BET} values). Therefore, PCl in the "Rank after discussion" column is green-coded. It is worth mentioning that **TpTab-PCl** synthesized in the PCl solvent exhibits an improved SA_{BET} value compared to that synthesized in conventional organic solvent (mesitylene : dioxane mixture) as reported in a previous study[16]. On the contrary, the rest of the solvents exhibited low surface area, and thus were found

incompetent. This clearly suggests that PCl is highly efficient over other green solvents as well as conventional organic solvents in delivering crystalline and porous COFs.

To rationalize the role of the solvents in the synthesis of crystalline and porous COFs, various solvent parameters, such as boiling point, viscosity, and dispersion, were plotted against the surface area of the resulting COFs.

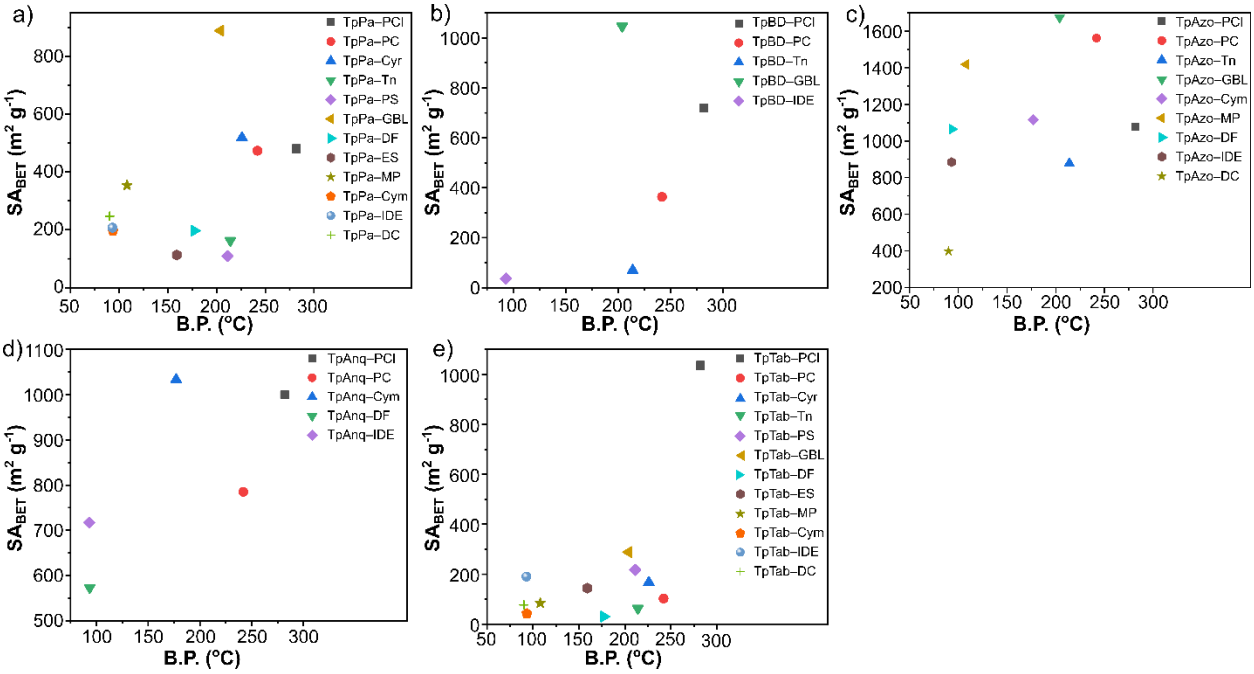

Figure S51. Plots of solvent boiling point vs BET surface area for series of a) **TpPa**, b) **TpBD**, c) **TpAzo**, d) **TpAnq**, and e) **TpTab**.

As shown in figure S50, the boiling point of the solvents were plotted against the surface area of the resulting COFs. High boiling point solvents are capable of distributing sufficient energy supplied among the reactants to cross the energy barrier, which ultimately governs the reversible covalent bond formation and its contribution in the formation of crystalline frameworks. However, in this study, except the **TpTab** COF series, the other COFs such as **TpPa**, **TpBD**, **TpAzo**, and **TpAnq** exhibit wide distribution of points, which indicates no direct correlation between the boiling point of the solvents and the surface area of the resulting COFs. Therefore, considering only the boiling point is insufficient for determining the suitability of the solvents in the preparation of crystalline and porous COFs.

We explored solvent viscosity for better rationalization of the solvent effects. The viscosity value of the green solvents were calculated using the HSPiP software. In general, low-viscosity solvents should effectively distribute heat energy among the reactant molecules compared to high-viscosity solvents. As shown in the figure S51, for all the COFs, except **TpTab**, the points are widely distributed with no direct

correlation among them. Thus, solvent viscosity of the green solvents could not be considered as a reliable parameter to depict suitability of a solvent for the preparation of a crystalline and porous COF.

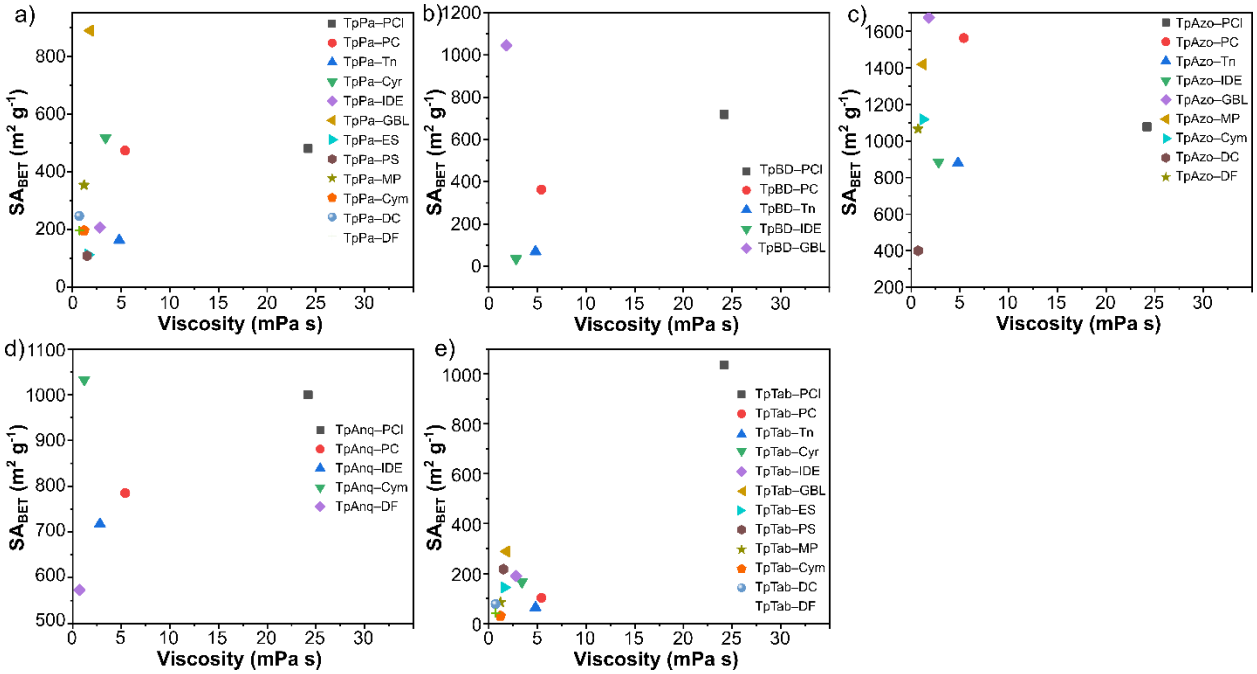

Figure S52. Plots of solvent viscosity vs BET surface area for series of a) **TpPa**, b) **TpBD**, c) **TpAzo**, d) **TpAnq**, and e) **TpTab.**

The dispersion parameter (δD) of precursors utilized in the synthesis of the COFs in green solvents were calculated using the HSPiP software. Analysis of the dispersion (δD) parameter plotted against the BET surface area shows the efficiency of GBL in delivering highly porous **TpPa**, **TpBD**, and **TpAzo** COFs; para-Cymene for **TpAnq**, and PolarClean for **TpTab** COFs.

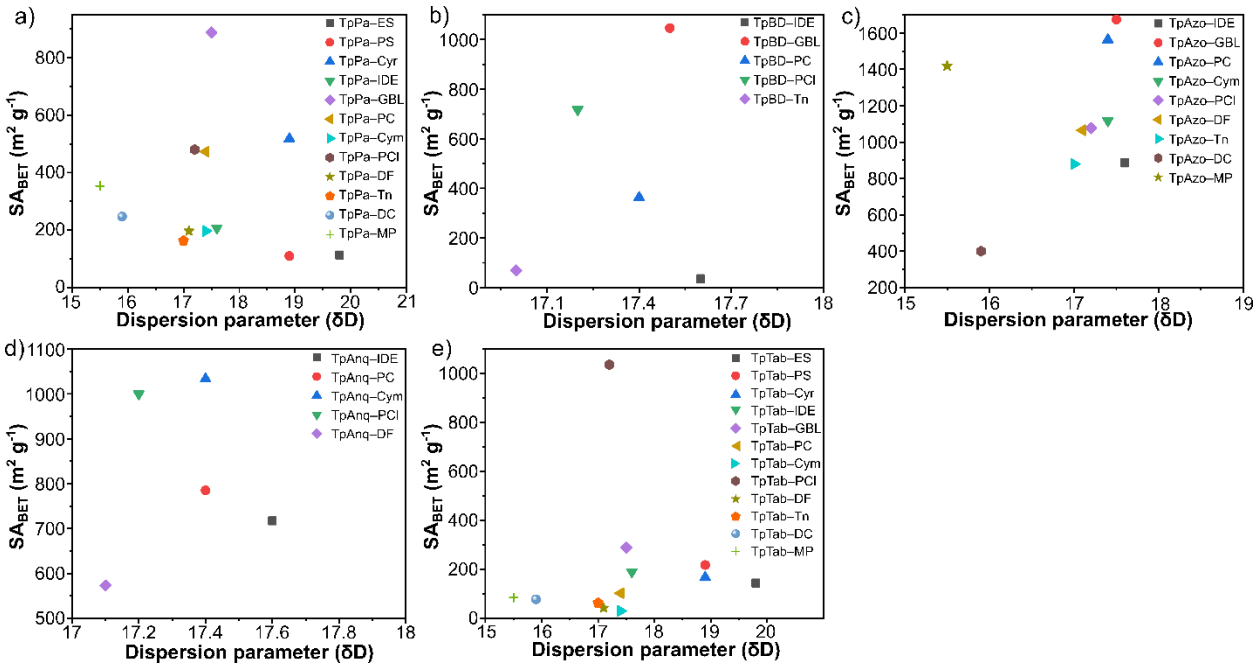

Figure S53. Plots of solvent HSPiP dispersion (δD) parameter vs BET surface area for a series of a) **TpPa**, b) **TpBD**, c) **TpAzo**, d) **TpAnq**, and e) **TpTab.**

Section S15. QSAR data

S15.1 Partial Least Squares Regression Analysis

VIP-scoring list as a MATLAB list:

[163-164 182-184 188-189 197 218 229 238 248 260 269 278 284 293 308 314 316 328 330 332 339 344 350 357 383 385 399 401 405 410 417-418 425 429 432-433 442 449 453 455 457 597 711 730 809 856 858 885 918 924 930 941-942 954 983 985-986 996 1261 1282 1327 1390-1393 1397 1405 1421-1426 1429-1433 1437-1442 1463-1465 1472-1473 1475 1500-1503 1509-1512 1516-1519 1521 1525 1527-1529 1534-1535 1537 1543-1544 1546 1552-1553 1555 1562-1564 1566-1567 1573 1577-1578 1597 1617-1618 1625 1628-1629 1633 1635 1637 1641 1645 1649-1651 1657 1659 1668 1672 1689 1707 1714 1717 1721 1724 1728 1731 1736 1742-1743 1750 1752 1756-1757 1759 1765 1771 1773 1780 1787 1794 1796 1798-1802 1805 1808 1812-1816 1819 1822 1829 1834-1835 1841-1842 1844 1846-1847 1849 1851 1854-1856 1864 1877 1890 1903 1916 1929 1955 1966 1976 2030-2031 2036 2048-2050 2099 2106 2174 2178 2185 2237-2238 2240 2245 2268 2274-2276 2278-2280 2282 2286-2287 2291-2294 2306-2310 2312-2316 2319-2324 2341 2344 2346 2349 2357 2359 2362-2363 2370 2376-2377 2379 2382 2386-2387 2393 2396 2399-2400 2402-2403 2417 2584 2592 2595 2599-2600].

where each integer refers to the corresponding molecular descriptors.

S15.2 SSQ Table

Table S20. Percentage variation captured by the regression model.

	X-block		Y-block	
Comp	This	Total	This	Total
1	39.86	39.86	69.26	69.26
2	11.24	51.09	19.56	88.82
3	12.73	63.83	2.95	91.77

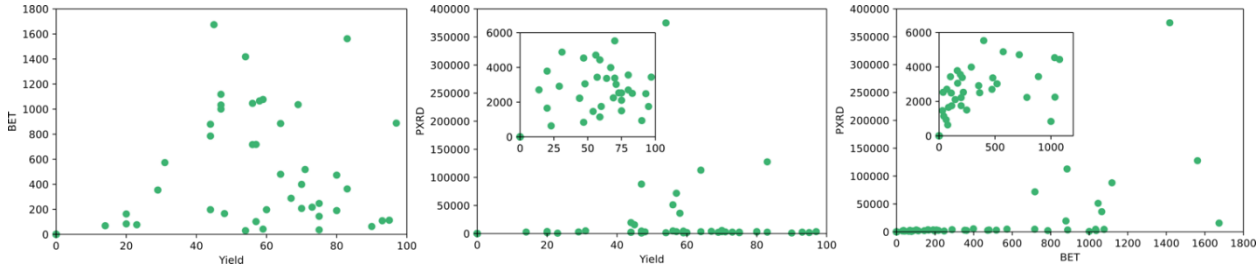

Figure S54. a) Cross-correlation between the yield and BET surface area of as-synthesized COFs. b) Cross-correlation between the yield and intensity value of the first peak (corresponds to diffraction from 100 plane) in the PXRD patterns of the as-synthesized COFs. c) Cross-correlation between the BET and intensity value of the first peak in the PXRD patterns of the as-synthesized COFs. Based on the uniform distribution of the points, the results show no cross-correlation between each measurement. At point (0,0), the failed experiments are shown.

S15.3 Model statistics:

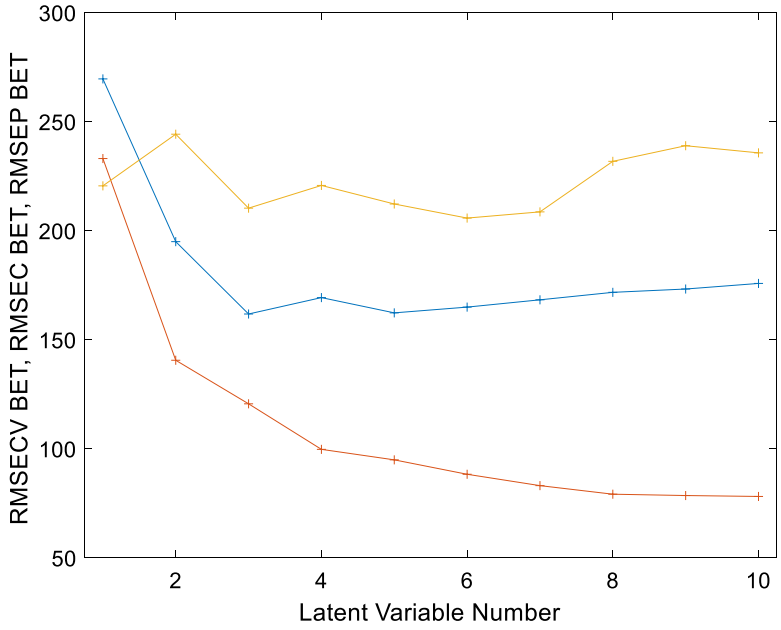

Figure S55. RMSECV (blue), RMSEC (orange), and RMSEP (yellow) values as functions of latent variable (LV) number. The optimal point, where the difference between the RMSECV and RMSEC is the smallest, can be found at LV = 3. With increasing LVs, the model tends to overfit, and RMSECV and RMSEC diverge.

Table S21. Model parameters and corresponding results for the train, cross-validation, and test sets (depicted on figure 4). Results of the final Y-scrambling parameters.

Model	**BET surface area ($m^2 g^{-1}$)**
Preprocessing	Autoscale
Cross-validation	Seven-fold with blink thickness of 1
Number of latent variables (LVs)	3
RMESC	120
RMSECV	161
RMSEP	210
R^2 train	0.92
R^2 cross-validation	0.84
R^2 test	0.83
Y-Scrambling results	
R^2 train	0.92
R^2 cross-validation	0.83
R^2 test	0.83
RMESC	119
RMESCV	174
RMEP	199

Section S16. Characterization data of TpPa2 and TpTta COFs

Four new COFs, *i.e.* **TpPa2-PCl** and **TpPa2-GBL**, and **TpTta-PCl** and **TpTta-GBL** were synthesized by Schiff-condensation reaction of **Tp** with corresponding amines, *i.e.* 2,5-dimethylphenylenediamine (**Pa2**), and 1,3,5-tris(4-aminophenyl)triazine (**Tta**) using solvothermal method. To serve the purpose, the reaction was performed in two different green solvents *i.e.* γ-butyrolactone (**GBL**) and polarclean (**PCl**). All four COFs are crystalline and porous in nature. Both the binary classification and the PLZ regression model showed the excellent predictive power for the COFs.

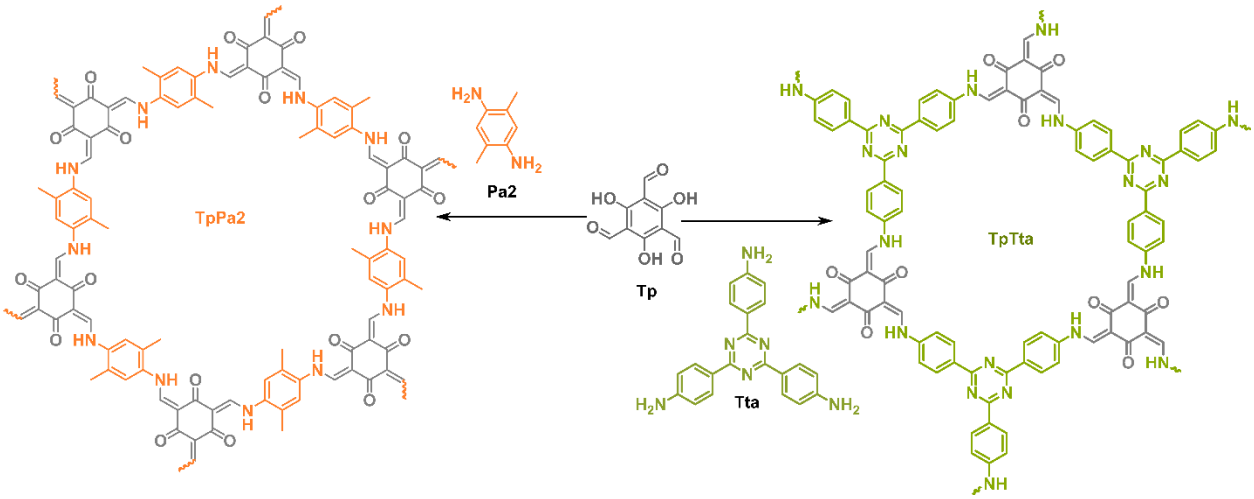

Figure S56. Schematic representation of the synthesis of TpPa2 and TpTta COFs.

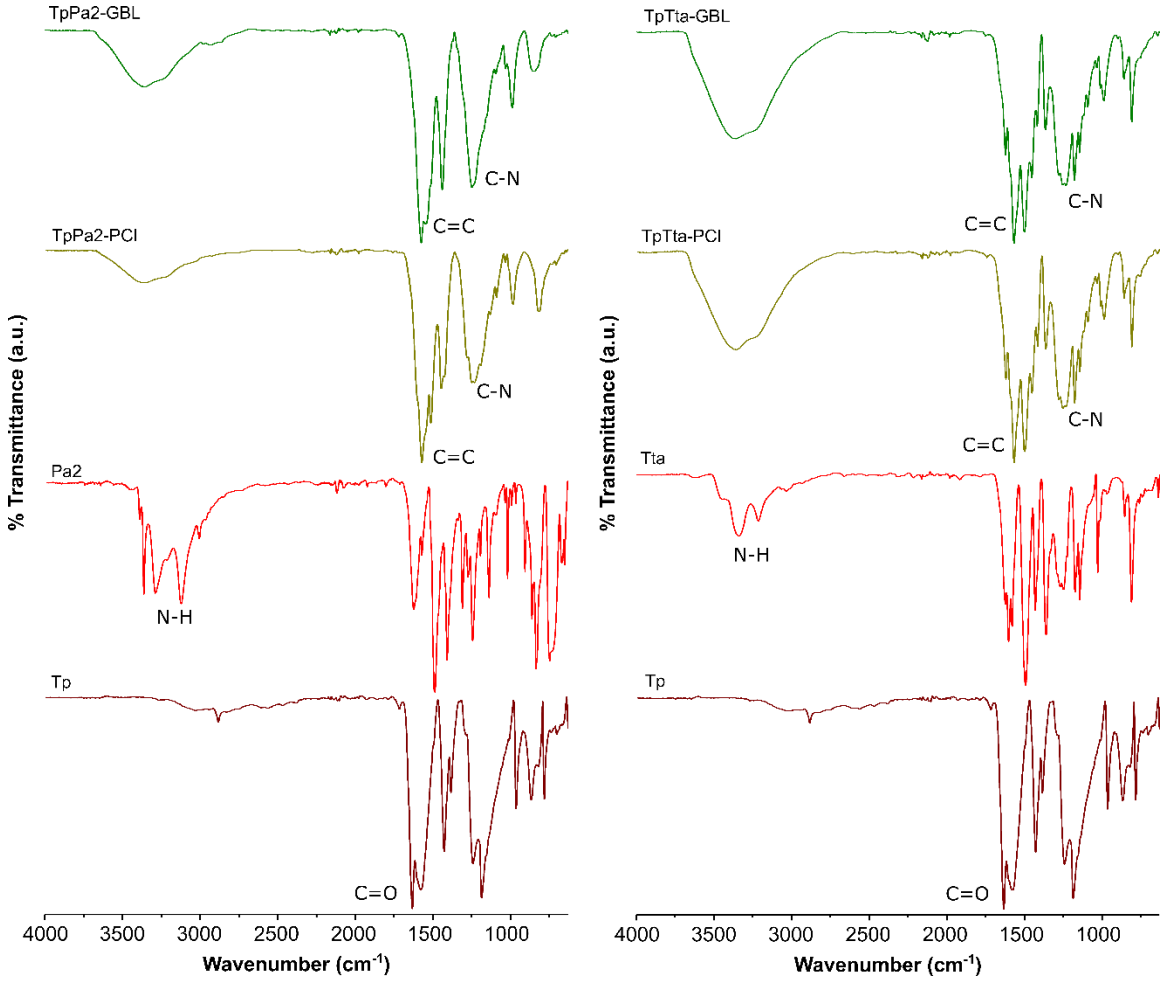

Figure S57. Comparative FTIR spectra of as-synthesized **TpPa2** and **TpTta** COFs with **Tp** and corresponding diamines (**Pa2** and **Tta**). FTIR spectra of the as-synthesized COFs exhibit characteristic C=C and C–N stretches corresponding to the β-ketoenamine linked framework.

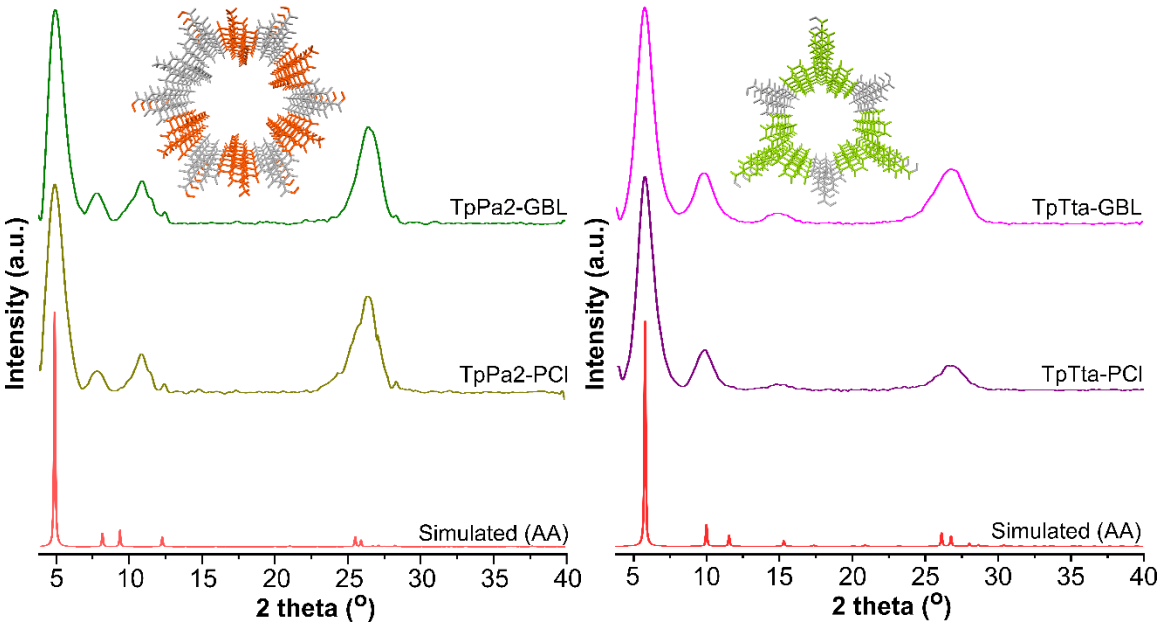

Figure S58. PXRD patterns for as-synthesized TpPa2 and TpTta COFs. The COFs were synthesized in two green solvents i.e. PCl and GBL. Experimental PXRD patterns were compared with the simulated PXRD patterns. The first peak corresponds to the [100] plane, where the peak at 2theta = 27° is assigned to the diffraction from [001] plane.

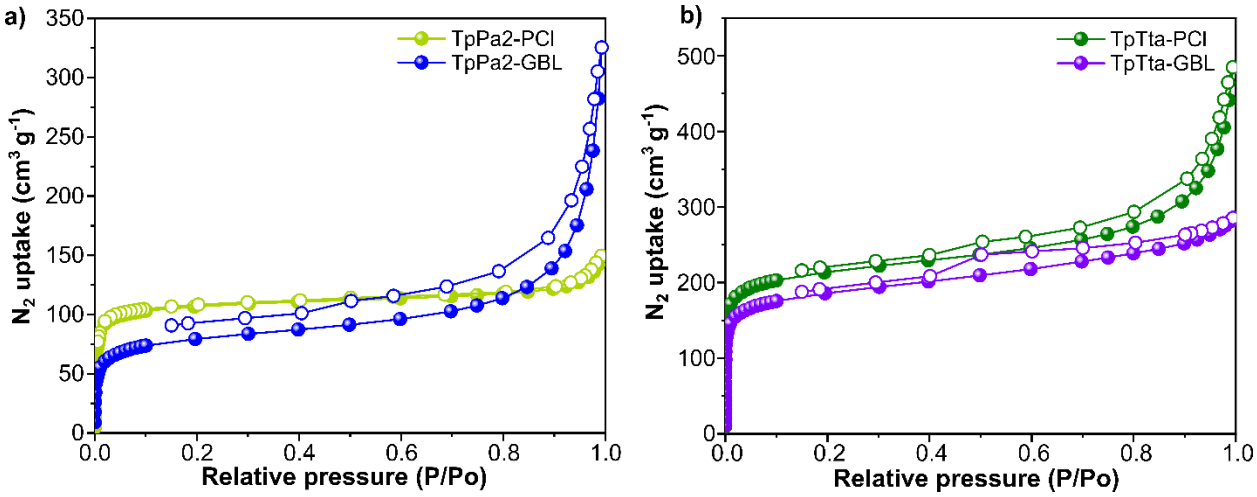

Figure S 59. Nitrogen uptake BET isotherm of a) **TpPa2-PCl** and **TpPa2-GBL**, and b) **TpTta-PCl** and **TpTta-GBL** recorded at 77 K.

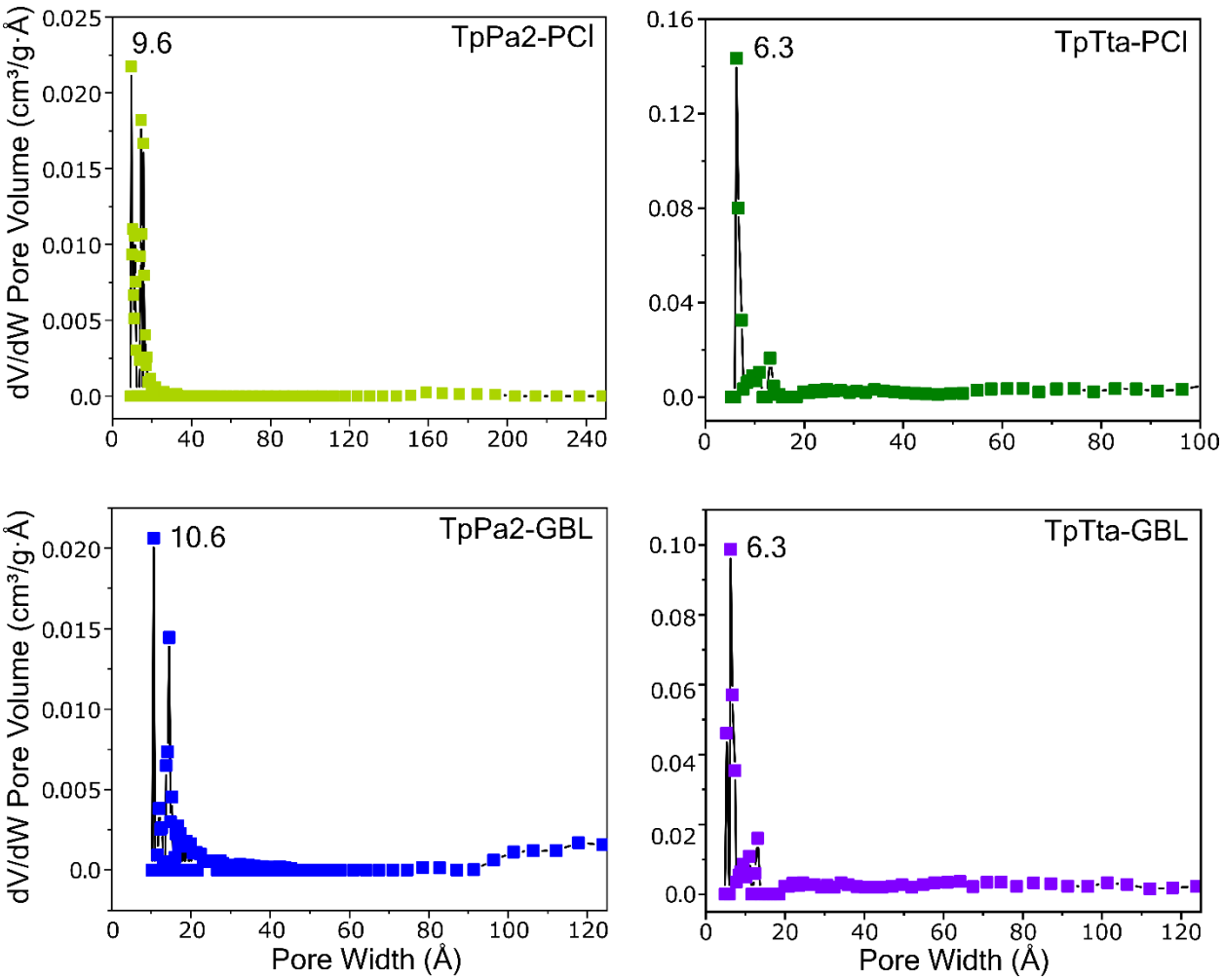

Figure S60. Pore size distribution of **TpPa2-PCl, TpPa2-GBL, TpTta-PCl, and TpTta-GBL** calculated using non-local density functional theory (NL-DFT) model.

Section S17: References

(1) Chong, J. H.; Sauer, M.; Patrick, B. O.; MacLachlan, M. J. Highly Stable Keto-Enamine Salicylideneanilines. *Org. Lett.* **2003**, *5* (21), 3823–3826. https://doi.org/10.1021/ol0352714.

(2) Fabian Pedregosa, Gael Varoquaux, Alexandre Gramfort, Vincent Michel, Bertrand Thirion, Olivier Grisel, Mathieu Blondel, Peter Prettenhofer, Ron Weiss, Vincent Dubourg, Jake Vanderplas, Alexandre Passos, David Cournapeau, Matthieu Brucher, Matthieu Perrot, E. D. Scikit-Learn: Machine Learning in Python. *J. Mach. Learn. Res.* **2011**, *12*, 2825–2830.

(3) Ari N, U. M. Matplotlib in Python. 2014 11th International Conference on Electronics, Computer and Computation (ICECCO); 2014.

(4) Zheng W, T. A. Novel Variable Selection Quantitative Structure−Property Relationship Approach Based on the K-Nearest-Neighbor Principle. *J. Chem. Inf. Comput. Sci.* **2000**, *40* (1), 185–194.

(5) Czermiński, R.; Yasri, A.; Hartsough, D. Use of Support Vector Machine in Pattern Classification: Application to QSAR Studies. *Quant. Struct. Relationships* **2001**, *20* (3), 227–240. https://doi.org/https://doi.org/10.1002/1521-3838(200110)20:3<227::AID-QSAR227>3.0.CO;2-Y.

(6) Obrezanova, O.; Csányi, G.; Gola, J. M. R.; Segall, M. D. Gaussian Processes: A Method for Automatic QSAR Modeling of ADME Properties. *J. Chem. Inf. Model.* **2007**, *47* (5), 1847–1857. https://doi.org/10.1021/ci7000633.

(7) Svetnik, V.; Liaw, A.; Tong, C.; Culberson, J. C.; Sheridan, R. P.; Feuston, B. P. Random Forest: A Classification and Regression Tool for Compound Classification and QSAR Modeling. *J. Chem. Inf. Comput. Sci.* **2003**, *43* (6), 1947–1958. https://doi.org/10.1021/ci034160g.

(8) Neural Networks in QSAR and Drug Design. *Neural Networks in QSAR and Drug Design*. 1996. https://doi.org/10.1016/b978-0-12-213815-7.x5000-6.

(9) Svetnik, V.; Wang, T.; Tong, C.; Liaw, A.; Sheridan, R. P.; Song, Q. Boosting: An Ensemble Learning Tool for Compound Classification and QSAR Modeling. *J. Chem. Inf. Model.* **2005**, *45* (3), 786–799. https://doi.org/10.1021/ci0500379.

(10) Chen, B.; Sheridan, R. P.; Hornak, V.; Voigt, J. H. Comparison of Random Forest and Pipeline Pilot Naïve Bayes in Prospective QSAR Predictions. *J. Chem. Inf. Model.* **2012**, *52* (3), 792–803. https://doi.org/10.1021/ci200615h.

(11) Contrera, J.; MacLaughlin, P.; Hall, L.; Kier, L. QSAR Modeling of Carcinogenic Risk Using Discriminant Analysis and Topological Molecular Descriptors. *Current Drug Discovery Technologies*. 2005, pp 55–67. https://doi.org/10.2174/1570163054064684.

(12) Chandra, S.; Kundu, T.; Kandambeth, S.; BabaRao, R.; Marathe, Y.; Kunjir, S. M.; Banerjee, R. Phosphoric Acid Loaded Azo (−N═N−) Based Covalent Organic Framework for Proton Conduction. *J. Am. Chem. Soc.* **2014**, *136* (18), 6570–6573. https://doi.org/10.1021/ja502212v.

(13) Hardian, R.; Liang, Z.; Zhang, X.; Szekely, G. Artificial Intelligence: The Silver Bullet for Sustainable Materials Development. *Green Chem.* **2020**, *22* (21), 7521–7528. https://doi.org/10.1039/D0GC02956D.

(14) Chandra, S.; Kandambeth, S.; Biswal, B. P.; Lukose, B.; Kunjir, S. M.; Chaudhary, M.; Babarao, R.; Heine, T.; Banerjee, R. Chemically Stable Multilayered Covalent Organic Nanosheets from Covalent Organic Frameworks via Mechanical Delamination. *J. Am. Chem. Soc.* **2013**, *135* (47), 17853–17861. https://doi.org/10.1021/ja408121p.

(15) DeBlase, C. R.; Silberstein, K. E.; Truong, T.-T.; Abruña, H. D.; Dichtel, W. R. β-Ketoenamine-Linked Covalent Organic Frameworks Capable of Pseudocapacitive Energy Storage. *J. Am. Chem. Soc.* **2013**, *135* (45), 16821–16824. https://doi.org/10.1021/ja409421d.

(16) Kaleeswaran, D.; Vishnoi, P.; Murugavel, R. [3+3] Imine and β-Ketoenamine Tethered Fluorescent Covalent-Organic Frameworks for CO2 Uptake and Nitroaromatic Sensing. *J. Mater. Chem. C* **2015**, *3* (27), 7159–7171. https://doi.org/10.1039/C5TC00670H.

(17) Geng, K.; He, T.; Liu, R.; Dalapati, S.; Tan, K. T.; Li, Z.; Tao, S.; Gong, Y.; Jiang, Q.; Jiang, D. Covalent Organic Frameworks: Design, Synthesis, and Functions. *Chem. Rev.* **2020**, *120* (16), 8814–8933. https://doi.org/10.1021/acs.chemrev.9b00550.

(18) Morelli Venturi, D.; Campana, F.; Marmottini, F.; Costantino, F.; Vaccaro, L. Extensive Screening of Green Solvents for Safe and Sustainable UiO-66 Synthesis. *ACS Sustain. Chem. Eng.* **2020**, *8* (46), 17154–17164. https://doi.org/10.1021/acssuschemeng.0c05587.

(19) Kandambeth, S.; Dey, K.; Banerjee, R. Covalent Organic Frameworks: Chemistry beyond the Structure. *J. Am. Chem. Soc.* **2019**, *141* (5), 1807–1822. https://doi.org/10.1021/jacs.8b10334.

(20) Thote, J.; Barike Aiyappa, H.; Rahul Kumar, R.; Kandambeth, S.; Biswal, B. P.; Balaji Shinde, D.;

Chaki Roy, N.; Banerjee, R. Constructing Covalent Organic Frameworks in Water via Dynamic Covalent Bonding. *IUCrJ* **2016**, *3*, 402–407. https://doi.org/10.1107/S2052252516013762.